EFFECTS OF THE LOADING DIRECTION AND CONTACT GEOMETRY ON THE HIGH STRAIN RATE BEHAVIOR OF WOVEN GRAPHITE/EPOXY COMPOSITES

by

Fatih Turan

Bachelor of Science, Celal Bayar University, 2006

Submitted to the Graduate Faculty of

Swanson School of Engineering in partial fulfillment

of the requirements for the degree of

Master of Science

University of Pittsburgh

2010

UNIVERSITY OF PITTSBURGH

SWANSON SCHOOL OF ENGINEERING

This thesis was presented

by

Fatih Turan

It was defended on

November 22, 2010

and approved by

Jeffrey S. Vipperman, Associate Professor, Department of Mechanical Engineering and Material Science

Lisa Mauck Weiland, Assistant Professor, Department of Mechanical Engineering and Material Science

Thesis Director: Sylvanus N. Wosu, Associate Professor, Department of Mechanical Engineering and Material Science

EFFECTS OF THE LOADING DIRECTION AND CONTACT GEOMETRY ON THE HIGH STRAIN RATE BEHAVIOR OF WOVEN GRAPHITE/EPOXY COMPOSITES

Fatih Turan, M.S

University of Pittsburgh, 2010

High strain compressive impact testing was carried out using Split Hopkinson Pressure Bar for woven graphite/epoxy composites transversely and diametrically loaded at the impact energies of 67 J, 113 J, 163 J, and 263 J. As it is hypothesized, the results show that thicker specimens exhibit better elastic modulus and lower strain rate deformation. However, no thickness effect was observed on the energy absorption history for transversely loaded specimens even though energy absorption increases with increasing thickness for diametrically loaded specimens. The results show that energy absorption, elastic modulus, ultimate strength, and the strain rate increase with increasing applied energy as it is hypothesized. Most of the expendable energy for specimen damage returns to the system in the transverse loading case, with no visible incipient damage, while some portion of the energy absorption is consumed in the deformation process for the diametrical loading case. Smaller contact area gives larger deformation to the transversely loaded specimens resulting in lower elastic modulus, lower ultimate strength, higher energy absorption because of the energy release, and higher strain rate for the same thickness and impact energy.

TABLE OF CONTENTS

LIST OF TABLES

LIST OF FIGURES

ACKNOWLEDGEMENT

I would first like to express my deepest appreciation to Prof. Sylvanus N. Wosu, my advisor, for all the support, patience, and guidance he has given me throughout my thesis and graduate study.

I am grateful to my committee members, Prof Jeffrey S. Vipperman and Lisa Mauck Weiland, for their time to evaluate my thesis and invaluable suggestions.

I want to express my gratitude to Dr. Tan for providing access to the Raman Spectroscopy and guiding me in the completion of the work. Albert Stewart assisted me in the Scanning Electron Microscopy experiments and I am very grateful for his assistance. I also would like to express my appreciation to Mr. Reza, Mr. Keith, and people who work in the machine shop for their patient fully help to setup the all Dynamic Characterization Laboratory. I am grateful to Ms. Cook for reviewing my thesis with her busy schedule.

Lastly, I want to thank my wife for her support and patience in the most difficult times during my thesis research and completion of my graduate studies.

1.0 BACKGROUND INTRODUCTION

Composite materials consist of at least two different materials on a macroscoping or microscopic scale resulting in a completely new material and having better mechanical and physical properties than their constituent materials. Composite materials have been widely used in many applications in which high strength to weight ratio is required. Most common natural composite is wood. Modern composites imitate the wood such that they consist of strong fibers embedded in softer supporting material called matrix. The advantage of composite materials is that they usually exhibit the best qualities of their components or constituents and often some qualities that neither constituent possesses. Some of the properties that can be improved by forming a composite material are strength, stiffness, weight, wear resistance, and corrosion resistance [1]. In some cases such as automobile accidents, bird strikes on aircraft structures, and ballistic loading on impact loading, composite materials are exposed to the dynamic loading and therefore it is vital to understand the mechanical behavior of the fiber reinforced polymer matrix composites to high strain rate loading. Thus, much work has been done to understand the response of the fiber reinforced composites exposed to impact loading so far. Based on the type of constituent material, composite materials can be classified as ceramic, metallic, and polymer composites and based on the more traditional method they can be classified as particulate, flake, fiber reinforced, and laminated composites.

Fiber - reinforced polymer matrix composite materials consist of fibers of high strength and modulus embedded in or bonded to a polymer matrix with distinct interfaces between them. In general, fibers work as load carrying members while the surrounding matrix gives an environment to the fibers with desired orientation and location, transfers the load to the fibers, and protects them from environmental damage such as humidity, and temperature. As a result of having high strength – weight ratios and modulus – weight ratios, these composites are markedly superior in weight and strength critical structures, to those of metallic materials as shown in Table 1.1. Moreover, fatigue strength and fatigue damage tolerance of these composites are excellent. Thus, fiber reinforced polymers have been widely used in weight and strength critical structures such as aircrafts, automobiles, armored vehicles, and space shuttles [2 – 4].

Table 1.1 Mechanical properties of some composites and metals [2].

Material	Density (g/cm^3)	Modulus (GPa)	Tensile strength (MPa)	Ratio of modulus to weight (10^6 m)	Ratio of tensile strength to weight (10^3 m)
SAE 1010 steel (Cold -worked)	7.87	207	365	2.68	4.72
6061 - T6 aluminum alloy	2.7	68.9	310	2.6	11.7
Ti - 6A1 - 4V Titanium alloy (aged)	4.43	110	1171	2.53	26.9
17 - 7 PH Stainless steel (aged)	7.87	196	1619	2.54	21
High strength carbon fiber - epoxy matrix (unidirectional)	1.55	137.8	1550	9.06	101.9
High modulus carbon fiber - epoxy matrix (unidirectional)	1.63	215	1240	13.55	77.5
E glass fiber - epoxy matrix (unidirectional)	1.85	39.3	965	2.16	53.2
Kevlar 49 fiber - epoxy matrix (unidirectional)	1.38	75.8	1378	5.6	101.8

Unlike traditional materials such as steel and aluminium alloys, the properties of fiber reinforced composites depend strongly on the direction of measurement and, therefore, they are not isotropic materials. This non – isotropic nature of a fiber reinforced composite material provides a unique opportunity of tailoring its properties according to the design requirements. This opportunity can be used to selectively reinforce a structure in the directions of major stresess, increase its stiffness in prefferred direction, or produce structures with zero coefficients of thermal expansion. For example, for a lamina containing undirectional fibers, the composite material has the highest strength and the modulus in the longitudinal direction of the fibers although its strength and modulus are very low in the transverse direction. For a balanced lamina, these properties are the same in both direction [2].

It has been found that strength and stiffness of the various types of composite systems increase with increasing strain rate [5 – 13]. However, in general, the high strain rate response was found to be material dependent.

Woldenbet and Winson conducted research to understand the effect of specimen geometry and the effect of varying lengths to diameter ratio of graphite/epoxy laminates at high strain rate. The results indicated that there is no significant influence of geometry and length to diameter ratio [5].

A comprehensive study has been done by Nwosu et al. [6] to understand the high strain rate behavior of woven carbon composite materials fabricated by VARIM process, which is low cost process, using Compression Split Hopkinson Bar at high strain rates ranging from 320 s^{-1} to 1149 s^{-1}. In this study, high strain rate behavior of stitched and unstitched woven carbon/epoxy composites have been studied in plane and off plane directions (0^o – 45^o for plain weave and 0^o – 90^o for satin weave at 15^o increments). The results show that the peak stress and modulus tend to

increase with increasing strain rate for woven composites while unstitched composites exhibit higher peak stress and modulus than stitched ones. The study also reveals that satin weave composites display higher peak stress and modulus when compared to plain weave composites and the samples loaded along off axes angles exhibit a large nonlinear response increasing up to 45^{o}. This study enables one to compare low cost woven composite materials produced VARIM process with those produced by traditional high cost woven composites in terms of dynamic compressive behavior and to see the high strain behavior of stitched composites.

H.M. Hsiao et al. [7] carried out a research to study the strain rate effects on the transverse compressive and shear behavior of 72- and 48-ply unidirectional carbon/epoxy composites at strain rates up to 1800 s^{-1} using Split Hopkinson Pressure Bar. The results indicated that transverse compressive strength increases with increasing strain rate even though ultimate strain exhibits no strain rate effect. The stress strain curve stiffens as the strain rate increases until it becomes almost linear at the strain rate of 1800 s^{-1} in transverse direction. In addition, thirty and forty-five degree off axis compression tests showed that shear stress – strain behavior exhibits high nonlinearity as the strain rate increases.

N.K. Naik, and Venkateswara R. K [8] investigated high strain rate compressive behavior of plain weave E-glass/epoxy and plain weave carbon/epoxy composites along all the principal directions (warp, fill, and thickness directions) at the strain rates ranging from 680 s^{-1} to 2890 s^{-1} using Compressive Split Hopkinson Pressure Bar. The authors concluded that compressive strength increases with increasing strain rate in thickness directions. Also the compressive strength and failure strain are higher in the thickness direction compared with those along warp and fill directions while compressive modulus is lower along thickness directions compared with

those along warp and fill directions. This study is useful to gain an understanding of effects of different loading directions on compressive behavior of carbon/epoxy composites.

S. Sivashanker et al [9] have conducted research to examine compressive failure of a unidirectional carbon/epoxy composite at high strain rates up to 3500 s^{-1} using Split Hopkinson Pressure Bar. The specimen used was not cylindrical shaped as usual but rectangular shaped which is short enough to avoid macrobuckling. It was found that there is almost no strain dependency on peak failure stress. And also the fracture examination by SEM in this study suggests that failure is by microbuckling with attendant splitting and delamination that is similar behavior observed in quasi static compression. While this experiment can be regarded educative for unidirectional fiber reinforced type composites and one enables to compare the effect of the specimen geometry on high strain rate behavior of polymer composite materials, it does not give knowledge regarding the woven fabric reinforced composites that also needs to be examined.

I.W. Hall and M. Guden [10] carried out research to determine the mechanical properties and failure mechanisms of unidirectional reinforced graphite/epoxy composites using a compression Split Hopkinson Pressure Bar. The results showed that there is a strong rate dependency on the strength properties in the transverse direction although no similar dependence is observed longitudinally. This behavior is attributed to fracture surfaces. Authors concluded that since failure of the epoxy matrix is observed in the transverse direction, this must be the source of the strain rate sensitivity.

1.1 APPLICATION OF CARBON FIBER POLYMER COMPOSITES

Carbon fiber polymer composites, especially carbon fiber epoxy composites, have been commonly used in the aerospace, automobile, marine, and sports industry. Table 1.2 summarizes the use of carbon/epoxy in military aircraft applications. Carbon fiber epoxy composites have widely been used in automobiles for saving weight in body panels, structural members, bumpers, wheels, drive shaft, engine components, and suspension systems.

Carbon fiber polymer composites have been used in space applications due to its light weight. Carbon fiber polymer composites account for 80 % of the weight of the structure of a satellite due to their high specific mechanical properties.

Carbon fiber polymer composites are suitable in order to be used for static dissipation which requires an electrical resistivity of $10^4 - 10^6$ Ω.cm and functional elements in high impedance circuits which require $10^2 - 10^3$ Ω.cm since they are electrically conductive.

Their high thermal conductivity and low thermal expansion of continuous carbon fiber polymer composites in the direction of the fibers make them good candidate to be used in heat sinks in electronics. Since they have low density compared to copper, they have been preferred in aerospace electronics.

Carbon fiber polymer composites are replacing steel for reinforcing concrete structures because they are lightweight, mechanically strong, and do not rust as steel does.

Continuous carbon fiber polymer composites are also used as acoustic diaphragms in speakers and microphones since they have low weight, high elasticity, fast sound transmission velocity, and excellent rigidity.

Woven fabric carbon fiber – reinforced polymer matrix composites, have an important place in defense and aerospace applications since they have high strain ratio to failure in tension,

and compression due to interlacing of the fiber bundles. Although the crack initiation can easily traverse the fibers in the case of unidirectional composites, the crack initiation has to overcome fibers both in the warp direction and fill direction in the case of woven fabric reinforced composites. Hence, the main advantage of using woven fabric laminates are that they provide properties that are more balanced in the 0^{o} and 90^{o} directions than unidirectional laminates [2] and they have better resistance to impact damage than the unidirectional continuous fibers [1]. In addition to their excellent quasi – static mechanical properties, understanding the impact behavior of these composites is essential since they are exposed to extensive impact damage while they are in the service conditions in the aircrafts, automobiles, armored vehicles, and space shuttles.

Table 1.2 Applications of fiber – reinforced composites in aircraft [2].

Aircraft	Component	Material	Overall weight saving over metal (%)
F - 11	Under wing fairings	Carbon - epoxy	25
F - 15	Fin, stabilizer skins	Boron - epoxy	25
F - 16	Skins on vertrical fin box, fin leading edge	Carbon - epoxy	23
F/A - 18	Wing skins, horizontal and vertical tailboxes, wing and tail control surface	Carbon - epoxy	35
AV - 8B	Flaps, horizontal stabilizers, wing skins and sub structure	Carbon - epoxy	25

1.2 FIBER PROPERTIES

1.2.1 Woven Fibers

Fiber reinforced composite structures consist of many laminates. A lamina is formed by incorporating large number of fibers into a matrix. The thickness of a lamina usually in the range of 0.1 – 1 mm. If fibers in the lamina are continuous, then they may be arranged either in unidirectional orientation, in a bidirectional orientation, or in a multidirectional orientation as shown in Figure 1.1. The bi- or multidirectional orientation fiber are used for woven composites [2, 14].

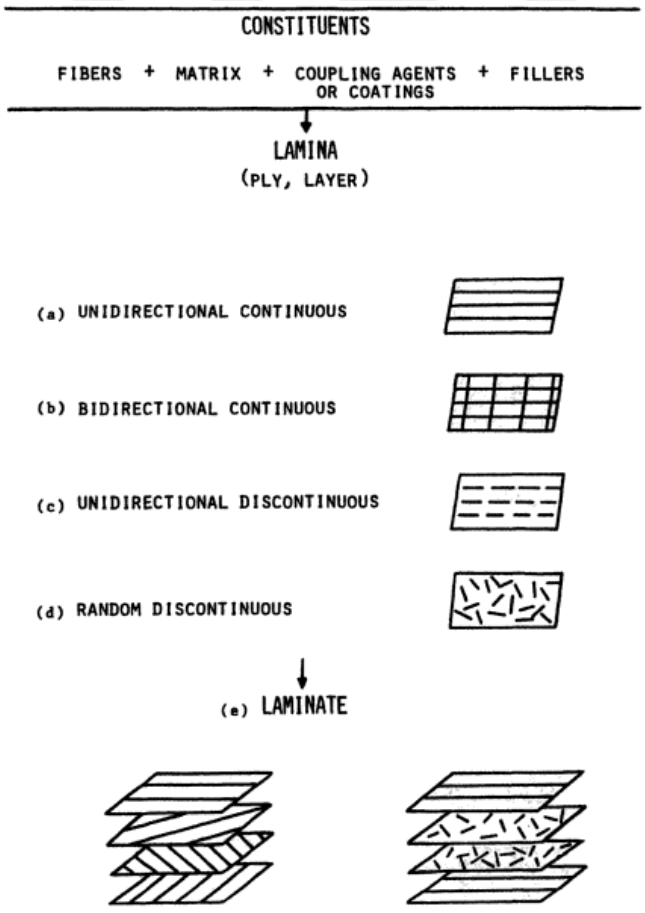

Figure 1.1 Basic building blocks in fiber reinforced composites [2].

Woven reinforcement is produced by interlacing two sets of unidirectional long fibers: fill and warp yarns. Common weave styles are as following:

a) **Plain Weave:** Warp and fill yarns are interlaced over and under each other in various combinations.
b) **Basket Weave:** A group of two or more warp yarns are interlaced with a group of two or more fill yarns in a various combination
c) **Satin Weave:** Each warp yarn weaves over several fill yarns and under one fill yarn. Common satin weaves are four – harness satin (over three, under one), five – harness satin (over four, under one), and eight – harness satin (over seven, under one).

Plain weave style, the schematic representation of a ply, and warp and fill directions are shown in Figure 1.2, 1.3, and 1.4, respectively [15, 16].

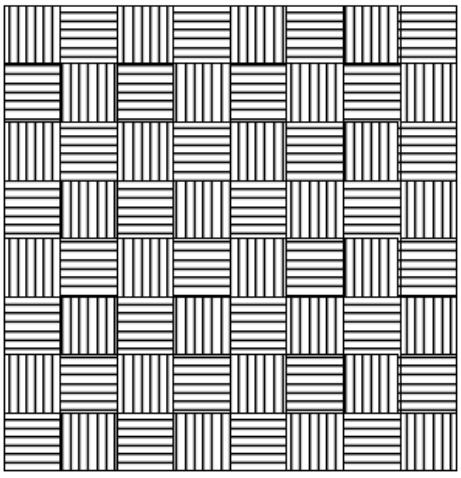

Figure 1.2 Typical 2D plain weave pattern [15].

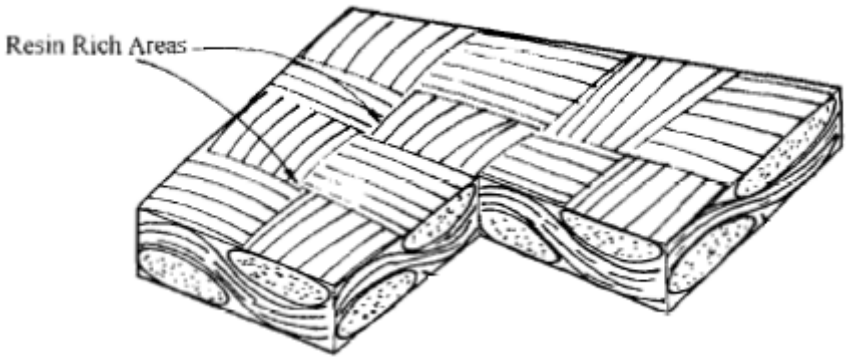

Figure 1.3 Schematic representation of the ply [16].

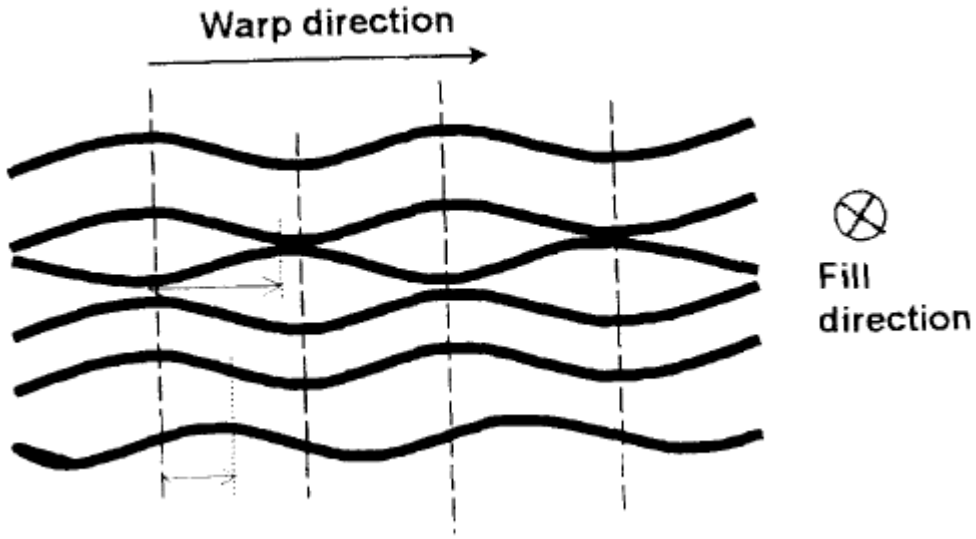

Figure 1.4 The warp and fill direction in a woven fabric [16].

The proper selection of fiber type, fiber volume fraction, fiber length, and fiber orientation is very important since it effetcs the following properties of composite laminate:

- Density
- Tensile strength and modulus
- Compressive strength and modulus
- Fatigue strength and failure mechanism
- Electrical and thermal conductivities
- Cost

1.2.2 Carbon Fibers

Carbon is the sixth lightest element and the carbon – carbon covalent bond is the strongest in nature (4000 kj/mole). However, the arrrangements of the bonds and the distances between the carbon atoms can vary, resulting in different types of carbon, including graphite, diamond and amorphous form. Carbon fibers contain at least 92 wt.% carbon in composition. Their structure can be crsytalline, amorphous, or partly crystalline. One of its crystalline forms is graphite. Graphite has a high modulus of elasticity parallel to the plane and a low modulus perpendicular to the plane due to the fact that graphite is highly anisotropic.

The proportion of graphite in a carbon fiber can range from 0 to 100%. The fiber is called graphite fiber when the graphite content is high. There are numerous types of carbon fibers. Among the fibers, high – strength carbon fibers exhibit the highest strength, whereas high modulus carbon fibers exhibit the highest modulus of elasicity as shown in Table 1.3. The specific modulus of high strength carbon fibers is significantly high since their density is very low. Thus, carbon fibers have been widely used in military, automative, and aerospace

applications, especially in polymer – matrix composites for aircraft applications in which light weight is required [2 – 4].

Table 1.3 Properties of various fibers and whiskers [4].

Material	Density (g/cm^3)	Tensile Strength (GPa)	Modulus of Elasticity (GPa)	Ductility (%)	Melting Temperature (°C)	Specific Modulus (10^6 m)	Specific Strength (10^4 m)
E - glass	2.55	3.4	72.4	4.7	<1725	2.9	14
S - glass	2.5	4.5	86.9	5.2	<1725	3.56	18
SiO_2	2.19	5.9	72.4	8.1	1728	3.38	27.4
Al_2O_3	3.95	2.1	380	0.55	2015	9.86	5.3
Boron	2.36	3.4	380	0.89	2030	16.4	12
SiC	4.09	2.1	480	0.44	2700	12	5.1
Carbon (high strength)	1.5	5.7	280	2	3700	18.9	19
Carbon (high modulus)	1.5	1.9	530	0.36	3700	36.3	13

1.3 MATRIX PROPERTIES

The roles of the matrix in fiber reinforced composites are as following:

a) keeping the fibers in place

b) transferring the stresses between fibers

c) providing a barrier against an adverse environment such as moisture and temperature

d) protecting the surface of the fibers from mechanical degradation

The effect of matrix on tensile load carrying capacity of a composite is negligible while it has important influence on the compressive, interlaminar shear, and in plane shear properties.

The polymers used as a matrix system in fiber reinforced polymer composite are thermoset and thermoplastic polymers. The reason why polymers are desired materials for composite materials is as following [14]:

a) They are light in weight with a density little more than that of water.

b) They do not require high pressure and temperature to impregnate the fibers

c) They are highly resistant to corrosive environments which gives useful properties for the composite material

d) Having low elastic moduli allows load transfer between fibers by shear of the matrix materials.

One of the unique characteristics of polymeric solids is that their mechanical properties depend on the loading rate. At low loading rates, the polymer exhibit ductile behavior while it exhibits brittle behavior at high loading rates.

In practice, the glass transition temperature of the matrix material should be higher than the maximum service temperature otherwise the matrix material may melt causing catastrophic deformation in composites.

1.3.1 Epoxy

Epoxy has been widely used for carbon fiber composites since epoxy has an excellent combination of mechanical properties and corrosion resistance, is dimensionally stable, and exhibits good adhesion. In addition, the low molecular weight of uncured epoxy resins in the liquid state turns into high molecular mobility during the curing processing which enables the resin to quickly wet the surface of a carbon fiber. Even though the polyester represents 80% of

the matrix system used in all composites, epoxy represent 90% of the matrix system used in high performance composites because they are tougher and shrink less than the polyester polymers.

The polymerization (curing) reaction to transform the liquid resin to the solid state is initiated by adding small amounts of a reactive curing agent just before incorporating fibers into the liquid mix. Curing time and temperature in polymerization reaction process depends on the type and amount of curing agent. The properties of a cured epoxy resin depend on the crosslink density. In general, the tensile modulus, glass transition temperature, and thermal stability as well as chemical resistance are improved with increasing crosslink density while the strains to failure and fracture toughness are reduced [2 – 4, 14].

1.4 FABRICATION OF THE POLYMER COMPOSITES

In order to fabricate polymer composites, the polymer matrix material, for example polyester or epoxy resins, has to be polymerized incorporating with the fibers. During this solidification process, the resin passes from the liquid state to solid state by copolymerization with the help of heating and pressure. High pressure helps the highly viscous resin material to mix with fiber well in the mold and high temperature is necessary for the chemical reaction through which liquid resin transforms into cured solid. The Figure 1.5 [17] shows the fundamental steps in the fabrication process of polymer composite materials.

The hand layup technique is the early manufacturing technique but it requires labor work and is a slow process, especially for automotive and aerospace industries. The compression molding, pultrusion, and filament winding methods have been widely used to manufacture polymer composites. The graphite/epoxy composites used in this study were manufactured with

vacuum assisted resin infusion technique (VARIM).Vacuum assisted resin infusion technique has been widely used for both aerospace and automotive industries for its ability to produce composite parts with complex shapes at relatively high production rates.

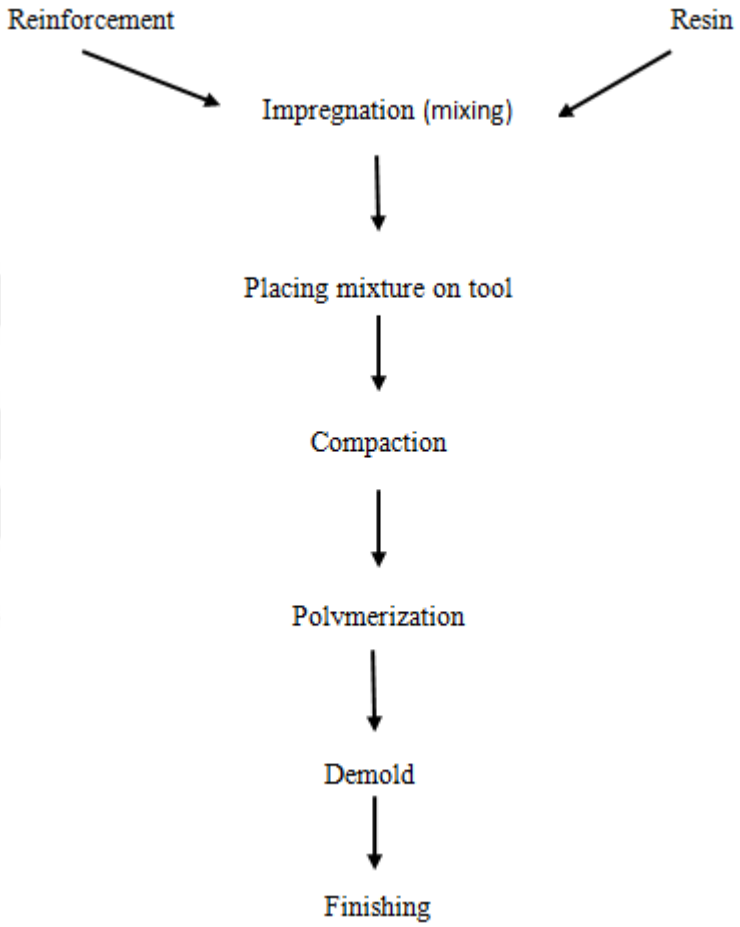

Figure 1.5 Steps in the fabrication process of polymer composite materials [17].

1.5 IMPACT TESTING OF COMPOSITE MATERIALS

Impact loads created by the collision of two solid bodies occur in a short time period. The impact properties of a material give information about its capability to absorb and dissipate energies exposed by impact loading. The understanding of the impact response of polymer composites is

important since in some cases such as automobile accidents, bird strikes on aircraft structures and ballistic loading on impact loading, these polymer composites are exposed to the dynamic loading extensively. Thus, some testing techniques such as drop – weight and pendulum testing techniques have been developed to understand the mechanical behavior of polymer composites at dynamic loading. The effect of the stress wave propagation, which is a source of damage initiation, cannot be examined using drop weight or pendulum testing techniques since in these techniques, energy absorption is the difference of residual energy and initial energy. Moreover, the energy absorption during the penetration process and the projectile's velocity, contact force, and duration of impact are difficult to be obtained by these testing techniques. Hopkinson bar testing used in this study eliminates these drawbacks allowing correct examination of penetration process.

1.5.1 Split Hopkinson Pressure Bar

One of the most widely used tests for determining dynamic response of materials in various modes of testing such as compression, tension, and shear at high strain rates is the Hopkinson pressure bar test. The strain rate sensitivity, dynamic yield strength, damage propagation, and fracture mechanism can be obtained using Hopkinson pressure bar test. Although there is no universal standard design for split Hopkinson pressure bar apparatus (SHPB), a typical SHPB has some common elements as following:

a) Two long symmetrical pressure bars made from same material such as maraging steel, or titanium, with a uniform cross section of length to diameter ratio in the range of 20 to 100 and with bar ends orthogonal to the bar axis to ensure good contact between specimen and bar, and between bar and striker.

b) A bearing and alignment fixture for correct alignment to satisfy 1 D wave propagation conditions.

c) A compressed gas launcher/gun to propel the striker bars made from same pressure bar material. Thus, upon impact a pressure pulse of approximately constant amplitude and finite duration is obtained.

d) Strain gages mounted on both bars with equidistance form the specimen to measure the stress wave propagation in the bars.

e) Associated instrumentation and data acquisition system to control, record, and analyze the stress – wave data in the bars.

Figure 1.6 [18] shows the schematic of SHPB test assembly.

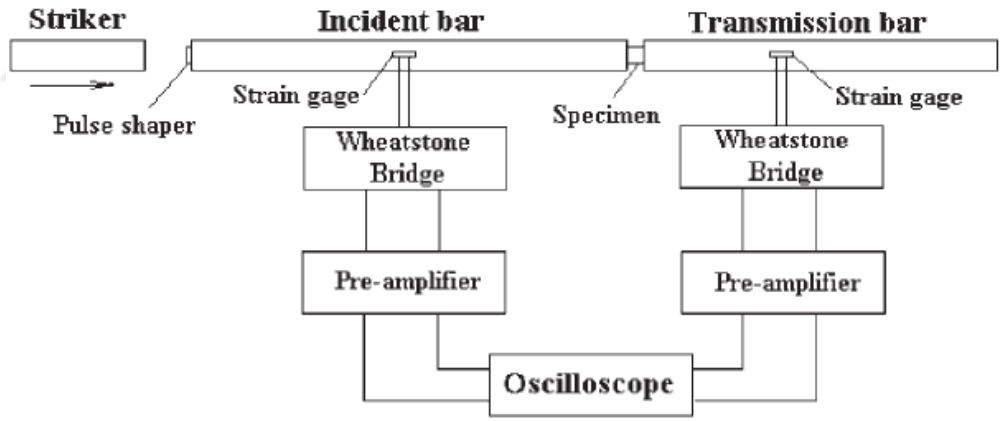

Figure 1.6 Schematic of SHPB test setup [18].

1.5.1.1 Operating Principle of split Hopkinson Bar Pressure

In a compression SHPB test, a specimen is sandwiched between the incident/input bar, and the transmitter/output bar. The striker bar is accelerated by the compressor air pressure. When the striker bar hits the incident bar, a compressive stress/strain pulse is produced on the impact end of the incident bar. This compressive pulse traveling through the impact the striker bar reflects at

the free surface as a tensile pulse and returns to the impact face. Thus, the pulse in the incident pressure bar is twice the length of the striker bar. The shape of this compressive pulse in stress – time coordinates is almost rectangular depending on the geometrical shape of the striker and the amplitude is proportional to the impact velocity of the striker bar [19]. This pulse travels through the incident bar toward the incident bar – specimen interface and is recorded by the strain gage and is termed incident pulse. This incident pulse is picked up by the strain gage after some microsecond. In the present study, it is picked up after 395 μs. Once the incident pulse reaches the interface of the incident bar and specimen at 790 μs, a part of the incident pulse is reflected back to the incident bar as a tensile pulse and a part is transmitted to the transmitter bar as a compressive pulse and they are termed as reflected pulse and transmitted pulse, respectively. The transmitted wave is so small compared to the incident and reflected waves in the case of diametrical loading. This is because significant amount of plastic deformation occurs on the surface of the diametrically loaded specimens making the transmitted waves weak. It should be noted that reflected pulse starts a little earlier than the transmitted pulse. This short delaying time occurs due to the finite thickness of the specimen. During the period of stress wave propagation through the specimen, the specimen undergoes deformation until its dynamic limit is reached. The relative magnitudes of these pulses depend on the physical properties of the specimen. The properties of the bar materials such as density, bar wave velocity, and diameter and the specimen dimensions are known prior to the data analysis from a SHPB test. Since the strain gage signals are recorded as volt vs. time, the signals must be converted to stress/strain in the bar. Figure 1.7 shows the Langrangian diagram for the SHPB [20].

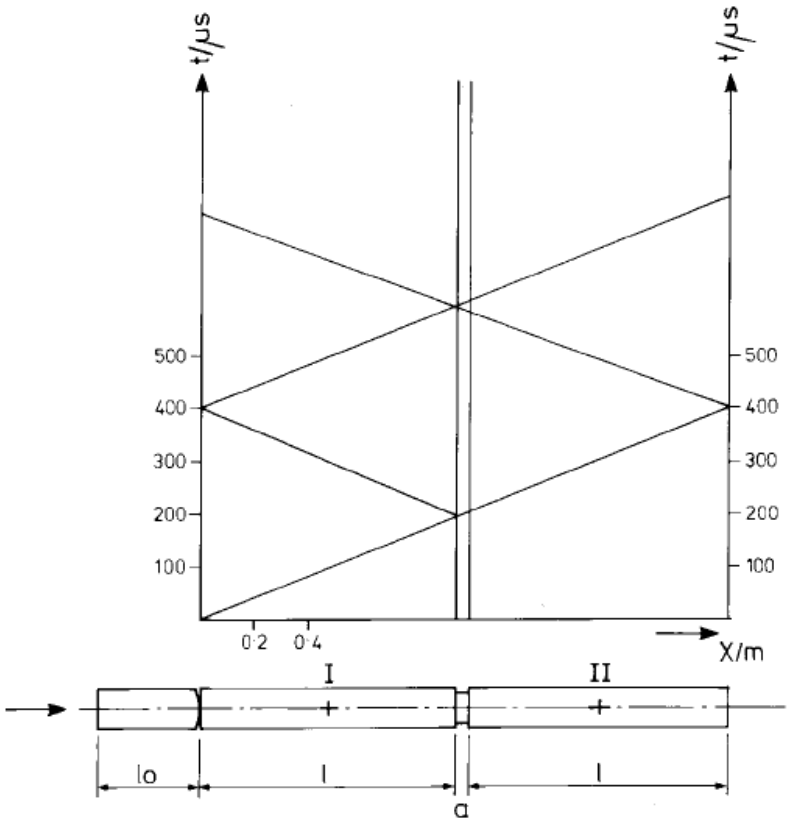

Figure 1.7 Langrangian diagram of SHPB [20].

1.6 THE GOALS OF THE STUDY

A significant amount of work has been done so far in studying high strain response of glass and graphite fiber reinforced polymer composites concluding that there is a tendency for fiber reinforced polymer composites subjected to the high strain rate loading that peak stress, strength, and modulus increase with increasing strain rate. The deformation mechanism of these composites has been observed using SEM or optical microscopy to identify the failure characteristic of the deformed composites.

Thus, with the light of the knowledge given about Raman Spectroscopy, the purpose of this study is to investigate the characterization of the surface micro – structure of the

carbon/epoxy polymer composites subjected to the high strain rate loading by split Hopkinson pressure bar using micro – Raman spectroscopy and to compare the results with SEM results.

1.6.1 Research Goals

In this study, Raman spectroscopy will be used as a nondestructive tool to investigate the effect of the compressive impact loading on the surface morphology of woven carbon/epoxy composites subjected to high strain rate loading in transverse and diametrical directions. The primary goals of the research are to:

1. Investigate the effect of the thickness on the damage parameters.
2. Investigate the effect of the impact energy on the damage parameters.
3. Investigate the effect of the loading direction on the damage parameters.
4. Investigate the effect of the contact geometry on the damage parameters.
5. Investigate the characterization of surface morphology of the woven graphite/epoxy polymer composites subjected to high strain rate loading in transverse and diametrical directions.

1.6.2 Research Questions and Hypotheses

The following research questions served as a guide for the investigations and research goals. Several predictions and hypotheses are generated in initial attempts to answer the research questions for the stated goals:

Goal 1: Investigate the effect of thickness on the damage parameters.

Research Questions

1. Does the variation of thickness affect the energy absorption history?
2. Does the variation of thickness affect the stress – strain and strain rate – strain behaviors?

Hypotheses

1. For the same loading conditions, the level of energy absorbed by the woven composite materials depends on the thickness of the specimen; a thicker specimen provides higher damage threshold than the thinner specimen
2. The stress – strain behavior of woven composite materials depends on thickness; a thinner specimen will undergo greater plastic deformation than a thinner specimen with different stress-strain history.
3. Strain rate – strain behavior of woven composite materials depends on the thickness; for the same loading conditions, the thinner specimens will show more deformation rate than thicker specimens.

Goal 2: Investigate the effect of the impact energy on the damage parameters.

Research Questions

1. Does the variation of impact energy affect the energy absorption history?
2. Does the variation of impact energy affect the stress – strain and strain rate – strain behaviors?
3. Does the variation of impact energy affect the Raman spectrum of graphite fibers?

Hypotheses

1. The level of energy absorbed by the woven composite materials depends on the incident impact energy and compressive wave produced in the incident bar; a higher impact energy will result in higher energy absorption.
2. Strain rate – strain behavior of woven composite materials depends on the impact energy since the greater energy means the higher strain in the specimen.

Goal 3: Investigate the effect of the loading direction on the compressive damage behaviors

Research Questions

1. Does the loading direction affect the energy absorption history?
2. Does the loading direction affect the stress – strain and strain rate – strain behavior?
3. Does the loading direction affect the Raman spectrum of graphite fibers?

Hypotheses

1. The level of energy absorbed by the woven composite materials depends on the loading configuration and direction with transversely loaded specimen showing less energy absorption than diametrically loaded.

2. The stress – strain behavior of woven composite materials depends on loading direction due to differences in the amplitude transmitted compressive wave for diametrically and transversely loaded specimens
3. Strain rate – strain behavior of woven composite materials depends on the loading direction due to differences the amplitude and level of dispersion of reflected compressive wave for diametrically and transversely loaded specimens.

Goal 4: Investigate the effect of the contact geometry on the compressive damage behavior of the woven graphite/epoxy composites subjected to high strain rate loading in transverse and diametrical directions.

Research Questions

1. Does the contact geometry affect the energy absorption history?
2. Does the contact geometry affect the stress – strain and strain rate – strain behavior?

Hypotheses

1. The level of energy absorbed by the woven composite materials depends on the contact geometry due to the fact that different contact areas generate different amounts of surface deformation and reflected waves which affects the energy absorption.
2. The stress – strain behavior of woven composite materials depends on contact geometry and it is expected that the specimens loaded using smaller contact areas will exhibit more deformation resulting in lower strength than the specimens loaded larger contact areas.

3. Strain rate – strain behavior of woven composite materials depends on contact geometry due to the fact that smaller contact areas give larger local deformation resulting in higher strain rate in the specimen.

Goal 5: Investigate the characterization of the surface micro – structure of the woven graphite/epoxy polymer composites subjected to the high strain rate loading in transverse and diametrical directions.

Research Questions

1. Is there a correlation between SEM and Raman surface morphologies of deformed region of loaded specimen?
2. Can SEM and Raman results differentiate between matrix and fiber dominated failures; and transverse and diametrical compressive failures?

Hypotheses

1. Raman peak for graphite will give higher value for the impacted woven composite materials due to decreasing bond length.
2. Raman peak for graphite will give different value for the transversely and diametrically loaded specimens because the atom vibration also depends on the fiber orientation.
3. It is expected that surface micro – structure of SEM images will exhibit higher damage density with increasing applied energy for both transversely and diametrically loaded specimens.

1.7 TOPICS COVERED IN THESIS

Chapter 2 introduces theoretical formulation and data reduction process including assumptions for SHBP to be valid, the calculation of the stress, strain, and energy absorbed by the specimen.

The purpose of Chapter 3 is to introduce the experimental methods in Hopkinson bar, the components of the Hopkinson bar, data acquisition system, and analyzing method as well as the material parameters.

Chapter 4 introduces the results of the study analyzing the stress – strain, stress – strain rate, and energy absorbed – time history of the all types of specimens using equations derived in Chapter 2.

Chapter 5 gives the surface morphology of impacted specimens obtained by SEM images and Raman spectrum and compares these two methods.

Chapter 6 presents the discussions in reference to the stated goals and hypotheses.

Chapter 7 gives the conclusion of this thesis interpreting data from Chapter 4 and 5.

2.0 THEORETICAL FORMULATION AND DATA REDUCTION PROCESS

2.1 ASSUMPTIONS FOR A VALID SHPB TEST

The determination of the stress – strain behavior of a material being tested in a split Hopkinson pressure bar is based on the principle of 1 D wave propagation. According to 1D wave propagation method, there are some assumptions [19 – 21] for validation of the experiment as following;

a) Stress wave propagation in the cross sectional area of the bars is one dimensional and uniaxial.

b) The pressure bars are elastic and their properties remain unchanged by the impact.

c) The wave is non – dispersive.

d) The specimen is in stress equilibrium after an initial ringing up period.

e) Transverse strain, friction, lateral inertia effects, and body forces are negligible.

Assumption a) is satisfied if the bars are homogeneous, isotropic, and uniform in cross section over the entire length, and under a linear elastic state of stress and the length to diameter ratio of the bars *d/L* is less than 1/50 [Zukas et al]. The test apparatus used in this study has a ratio of 1/144.

Assumption b) is satisfied based on the elementary wave theory. According to the elementary wave theory, Poisson's effects are negligible and for validation of elementary wave theory, the wavelength (λ) of the propagating wave must be ten times the diameter (d) of the bar [21]. In the current set – up, the wavelength of the incident pulse is 610 mm compared to 25.4 mm of the rod diameter.

It is possible for a wave to be dispersive during transmission through the specimen due to the fact that composite materials undergo elastic deformation under loading conditions. Then assumption c) is satisfied if the stress wave rise time, which is the time required for stress to increase from 10% to 90% of its final value, is two or three times greater than the time required for the pulse to traverse the diameter of the rod. For the current set – up, the rise time is 15 μs compared to 5 μs to traverse the diameter of the rod.

Assumption d) is satisfied by using longer bars and short specimens. Equilibrium within the specimen is satisfied by multiple reflections because the time to traverse the specimen is short compared to the duration of the wave. Hence, the stress will be homogenous within the specimen.

2.2 DATA REDUCTION PROCESS

Deriving equations used for SHPB test are based on 1 D wave theory and assumptions have been presented by other researchers [19 - 21]. Since the operation principle of SHPB has already been presented in the previous chapter, the derivation of equations will be represented in this section.

2.2.1 Impact Velocity and Incident Stress Pulse Measurements

Once the striker bar impacts to the stationary incident bar, the longitudinal impact load F_0 of the striker acts on the interface cross sectional area A for a time *dt* on a section *dx* of mass *m* and some of the particles at the interface will be reflected back into the striker bar with a velocity V_r relative to the interface and some transmitted with a velocity V_t into the incident bar. Hence, the resultant relative velocity of the particle at the compressed region of the striker bar is given as

$$V_p = V_0 - V_r = V_t \quad \textbf{(2.1)}$$

V_0 = Striker bar Velocity determined by infrared beam sensors

The impulse delivered to an initial stationary particle in the bar by the striker impact is given as

$$F_0 dt = mV_p = (\rho A dx)V_p \quad \textbf{(2.2)}$$

Then the uniaxial stress pulse transmitted to the incident bar is expressed by

$$\sigma(t) = \frac{F_0}{A} = (\rho C)V_p(t) \quad \textbf{(2.3)}$$

where $C = {}^{dx}/_{dt} = \sqrt{{}^{E_0}/_{\rho}}$ = The bar wave velocity

$F_0 =$ Longitudinal load of the striker bar for time interval dt

ρ = Density of the rod

A= Cross sectional area of the bar

$$V_p(t) = {}^{du}/_{dt} \quad \textbf{(2.4)}$$

From the equation (2.3), it can be said that the amplitude of the initial compressive uniaxial stress depends on the bar material, impact wave velocity, which is also function of the applied pressure), and the striker bar's stroke.

Substituting particle displacement velocity $V_p(t)$ into the equation (2.3), the particle displacement is expressed as

$$u(t) = \int_0^t V_p(t)dt = \frac{1}{\rho C}\int_0^t \sigma(t)dt \qquad \textbf{(2.5)}$$

Once the compressive incident pulse reaches the interface of the bar and specimen, some part of the pulse is reflected back to the incident bar due to the impedance mismatch at the interface and some part is transmitted through the specimen to the transmitter bar as shown in Figure 2.1. Therefore, the amplitude of the reflected wave depends on interface and specimen properties and suggests mechanical information about materials defining the interface.

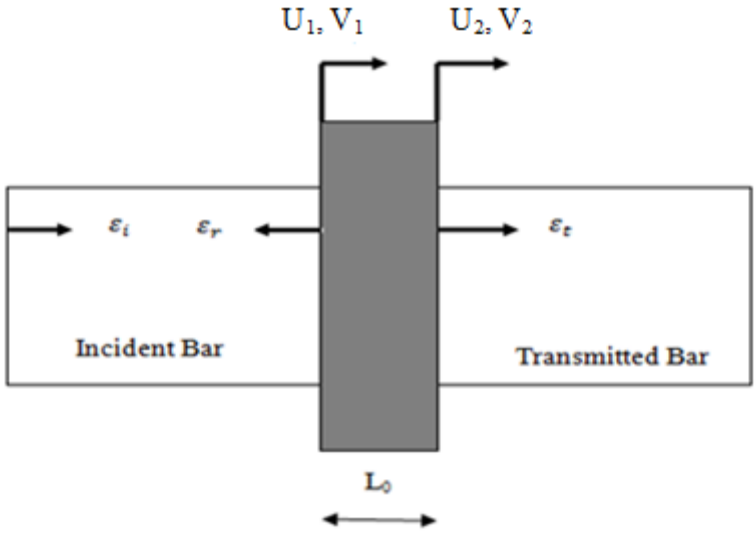

Figure 2.1 Traditional 1 D Hopkinson bar analysis.

The displacement functions at the incident and transmitter bar interfaces of the specimen can be written as

$$u_i = \frac{C_0}{E_0}\int_0^t \sigma_i(t)dt \qquad \textbf{(2.6)}$$

$$u_t = \frac{C_0}{E_0}\int_0^t \sigma_t(t)dt \quad \textbf{(2.7)}$$

where C_0 and E_0 are the bar velocity and Young's modulus, respectively, and σ_i and σ_t are the incident and reflected stress pulses, respectively.

Then, the net displacement at the incident and transmitter bar interfaces of the specimen can be written as

$$U_1(t) = u_i - u_r = \frac{C_0}{E_0}\int_0^t [\sigma_i(t) - \sigma_r(t)]dt \quad \textbf{(2.8)}$$

$$U_2(t) = u_t = \frac{C_0}{E_0}\int_0^t \sigma_t(t)dt \quad \textbf{(2.9)}$$

Finally, the net displacement in the specimen which represents the specimen deformation due to the interaction of compressive and tensile waves in the specimen can be approximately expressed as

$$U_1(t) - U_2(t) = u_n(t) = \frac{C_0}{E_0}\int_0^t [\sigma_i(t) - \sigma_r(t) - \sigma_t]dt \quad \textbf{(2.10)}$$

The specimen's strain and the strain rate in the specimen using the equation (2.10) can be written as

$$\varepsilon_s(t) = \frac{u_n(t)}{L_0} = \frac{C_0}{L_0}\int_0^t [\varepsilon_i(t) - \varepsilon_r(t) - \varepsilon_t(t)]dt \quad \textbf{(2.11)}$$

$$\frac{\partial \varepsilon_s(t)}{\partial t} = \frac{\dot{u_n}(t)}{L_0} = \frac{C_0}{L_0}[\varepsilon_i(t) - \varepsilon_r(t) - \varepsilon_t(t)] \quad \textbf{(2.12)}$$

where L_0 is the initial length of the specimen.

From the equilibrium condition in a short specimen ($\varepsilon_t = \varepsilon_i + \varepsilon_r$), equation (2.11) and (2.12) reduce to

$$\varepsilon_s(t) = -\frac{2C_0}{L_0}\int_0^t [\varepsilon_r(t)]dt \quad \textbf{(2.13)}$$

$$\dot{\varepsilon_s}(t) = -\frac{2C_0}{L_0}\varepsilon_r(t) \quad \textbf{(2.14)}$$

2.2.2 Stress, Particle Velocity, and Force Measurement

Assuming that the specimen is in force equilibrium, and the specimen is deforming uniformly which implies that friction and inertia effects are negligible yield that the forces on each side of the specimen bone by the bars are equal *(F_1=F_2)*. From the force equilibrium in the specimen requires that

$$F_1 = (\sigma_i + \sigma_r)A_b = F_2 = (\sigma_t)A_s \quad \textbf{(2.15)}$$

the continuity of velocity at the interface implies that

$$V_1 = V_i - V_r = V_s \quad \textbf{(2.16)}$$

where from equation (2.3)

$$V_i = \frac{\sigma_i}{(\rho C)_b}$$

$$V_r = \frac{\sigma_r}{(\rho C)_b} \quad \textbf{(2.17)}$$

$$V_t = \frac{\sigma_t}{(\rho C)_b}$$

V_i = The velocity of the incident wave

V_r= The velocity of the reflected wave

V_t= The velocity of the transmitted wave

Substituting equation 2.17 into equation 2.16, the particle velocity can be expressed in terms of the stress by

$$V_s = \frac{C_0}{E_0}(\sigma_i - \sigma_r) \quad \textbf{(2.18)}$$

Then the transmitted and reflected stress pulses can be expressed in terms of incident wave and mechanical impedance Z by

$$\sigma_t = \left(\frac{2Z_s(A_b/A_s)}{Z_s+Z_b}\right)\sigma_i \quad \textbf{(2.19)}$$

$$\sigma_r = \left(\frac{Z_s-Z_b}{Z_s+Z_b}\right)\sigma_i \quad \textbf{(2.20)}$$

where $Z = \rho CA = E_0 A/C_0$

One can say from equation 2.20 $\sigma_r = 0$ for impedance matching, $(Z_s = Z_b)$.

Since the applied forces on each face of the specimen are given by equation 2.15, the stress on each face of the specimen can be expressed by

$$\sigma_1 = \frac{F_1}{A_s} = \frac{A_b(\sigma_i+\sigma_r)}{A_s} \quad \textbf{(2.21)}$$

$$\sigma_2 = \frac{F_2}{A_s} = \frac{A_b\sigma_t}{A_s}$$

Hence, the average stress in the specimen from equation 2.21 can be expressed by

$$\sigma_s(t) = \frac{1}{2}(\sigma_1 + \sigma_2) = \frac{A_b(\sigma_i+\sigma_r+\sigma_t)}{2A_s} \quad \textbf{(2.22)}$$

From the equilibrium assumption in the specimen $(\sigma_i + \sigma_r = \sigma_t)$ equation 2.22 reduces to

$$\sigma_s(t) = \frac{A_b\sigma_t(t)}{A_s} = \frac{A_b E_0 \varepsilon_t(t)}{A_s} \quad \textbf{(2.23)}$$

The elastic modulus of the specimen is determined as the slope of the straight line portion of the stress – strain curve in the limit of small strain interval while the dynamic modulus of elasticity is determined as the maximum value of ratio of yield strength to the corresponding strain [21]. Thus, combining equation 2.13 and 2.23, the dynamic modulus of elasticity is obtained as:

$$\sigma_Y(t) = -[\frac{A_b/A_s\sigma_t(t)}{2C_0\sum_i \varepsilon_r(t)\Delta t}]L_0 \quad \textbf{(2.24)}$$

Equation 2.24 suggests that the dynamic modulus increase with increasing specimen thickness and decrease with decreasing thickness because thicker specimens will develop smaller strain and greater yield strength than that of thin specimens for the same loading force.

2.2.3 Energy Measurements

The net energy transferred to the composite plate by the propagating compressive wave is expressed by [21]

$$E_p = \int_0^t F_1(t)du_n \quad \textbf{(2.25)}$$

$F_1(t)$ = Compressive loading force given by equation 2.15

du_n = Net plate displacement given by equation 2.10

Substituting equation 2.10 and 2.15 into 2.25, the energy absorbed by the specimen is responsible for the damage in the specimen can be expressed by

$$E_A = (E_i - E_r - E_t) = (\frac{AC_0}{E_0})\int_0^t[\sigma_i(t)^2 - \sigma_r(t)^2 - \sigma_t(t)^2]dt \quad \textbf{(2.26)}$$

Equation 2.26 does not only give the energy absorbed by the composite but also includes the energy lost by vibration, plate deformation, friction, and contact. The above integration is implemented with all shifted to zero as illustrated by Figure 2.2. The maximum energy absorption is also equal to the strain energy release energy when the incident bar experiences tensile force and residual energy which goes to the system.

$$E_p = E_s + E_r \quad \textbf{(2.27)}$$

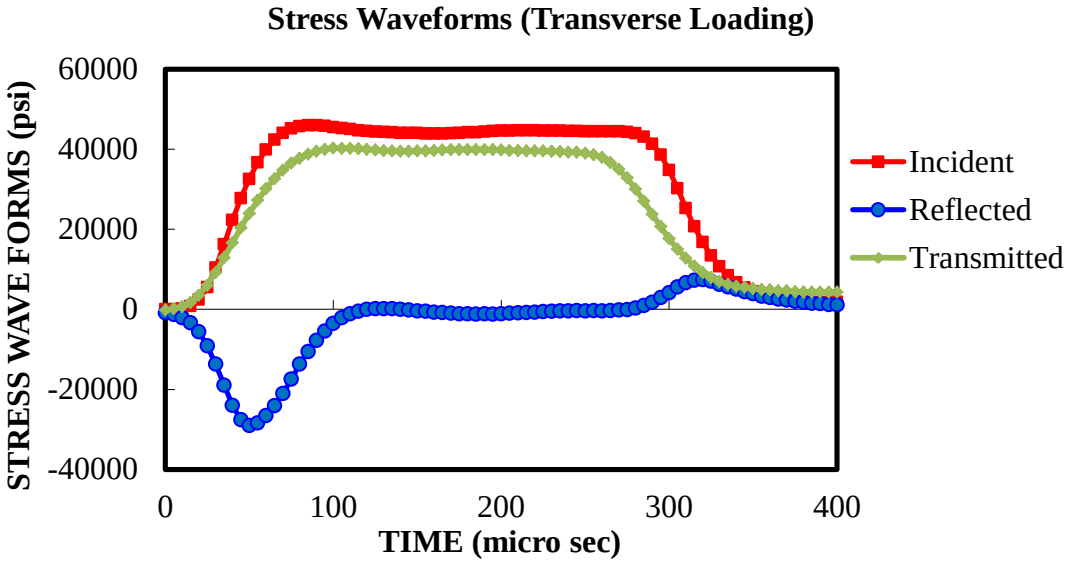

a)

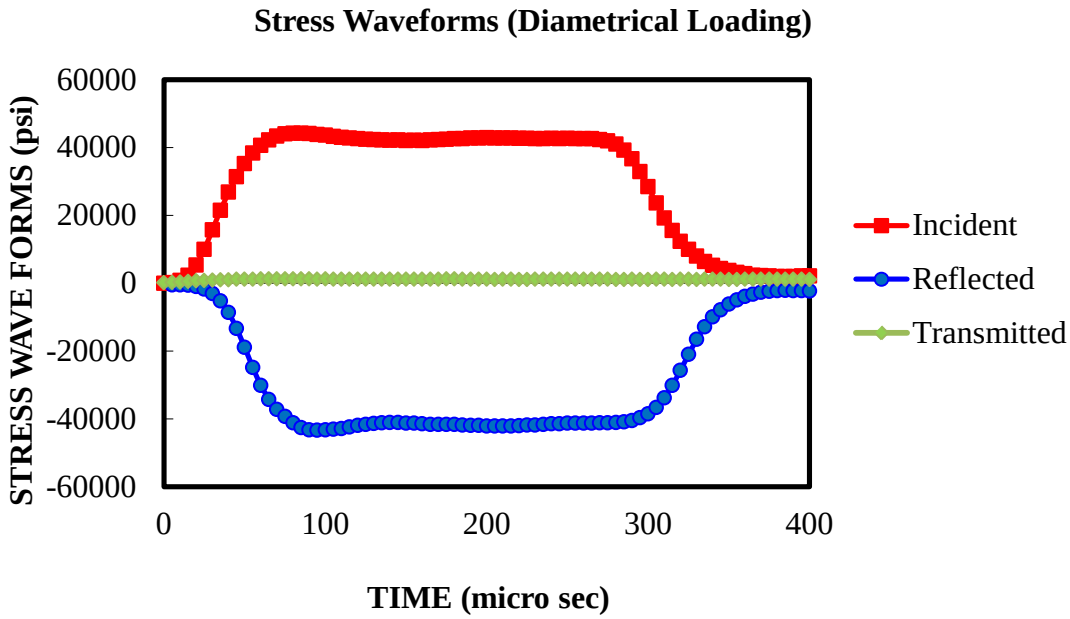

b)

Figure 2.2 Incident, reflected, and transmitted waveforms for a) diametrical loading case and b) transverse loading case.

3.0 TEST SETUP AND MATERIAL SELECTION

This chapter presents a typical experimental setup for the compressive split Hopkinson bar testing. The basic procedure to performing test, sample position between two bars for the conditions of both diametrically and transverse loading, strain transducers used for measuring the strain, and data acquisition and analysis system will be presented.

3.1 THE HOPKINSON BAR SYSTEM

The compression Hopkinson bar apparatus consists of incident, transmitter, and striker bars (300 maraging AMS 6414 steel). The incident and transmitter bars are 3.66 m (144 inches) in length and the striker bar is 0.61 m (24 inches) in length while all bars are 0.0254 m (1 inch) in diameter. Also a retracting rod attached to the striker bar is used to pull back the striker bar to desired ram length then the striker bar has a kinetic energy according to that ram length and. The longer ram length, the greater kinetic energy transferred to the striker bar. Another function of the retracting rod is to complete the triggering circuit between the Hopkinson bar system and the power supply via a cable when the striker bar contacts with the incident bar. Figure 3.1 and 3.2 show the setup of the modified compression Hopkinson bar system and the schematic of the Hopkinson bar used in this experiment, respectively.

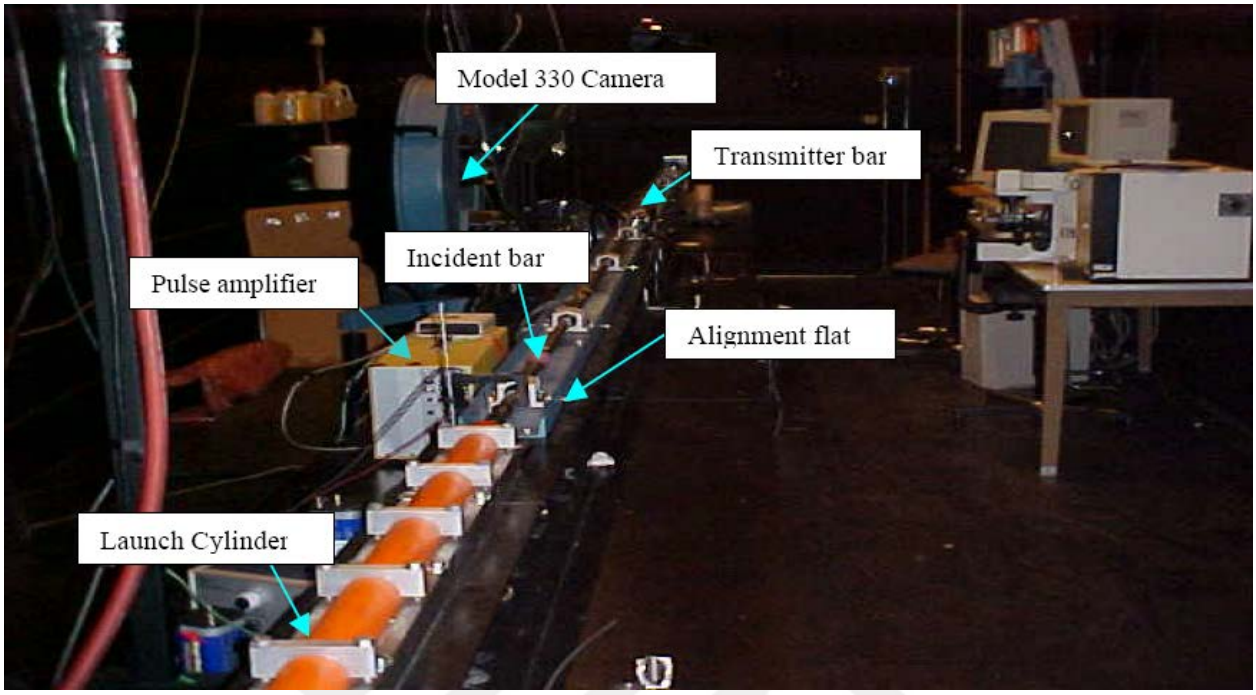

Figure 3.1 The experimental setup of the Hopkinson bar test.

3.1.1 Alignment of the Bars

Alignment of the bars is very important to eliminate possible bending and flexure during an experiment. Proper axial alignment of the bars is determined by vertical and lateral adjustment of the pillow blocks containing low friction Teflon ball bearings. These pillow blocks through which the bars move are supported by a steel channel lying through the below the bars which is supported by an I - beam. The Teflon bearings also need to be adjusted in a way that the bars must move smoothly. The tighter the bearings, the higher the resistance for free movement of the bars.

3.1.2 Stress Generating System

The stress generating system consists of quick acting solenoid valve, retracting rod attached to the striker bar, and striker bar. The striker bar is placed inside a launch cylinder which is 0.305 m (24 inches) in length and 0.0508 m (2 inches) in diameter as shown in Figure 3.2. The desired pressure up to 1.72 MPa (250 psi) to driving the striker bar on each test is manually controlled by an air regulator. The air regulator is connected to a digital pressure reader to obtain exact stored pressure that drives the system. The stored air is released by a switch in the control room activating the quick solenoid valve which allows the compressed air to accelerate into the incident bar to impact it. The impact surface of the striker bar conically shaped with a diameter of 0.0508 m (2 inches) to obtain repeatable longitudinal wave propagation. The venting holes through the launch cylinder keep the low pressure in front of the striker to eliminate the possible multiple impact.

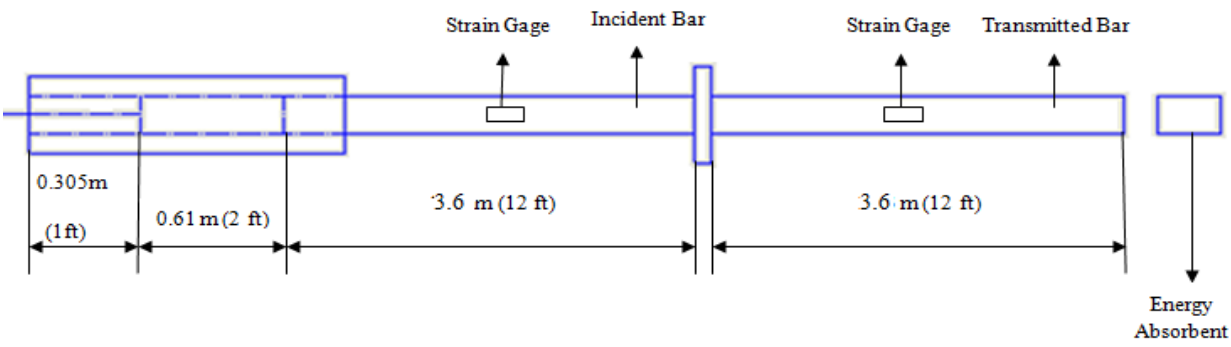

a)

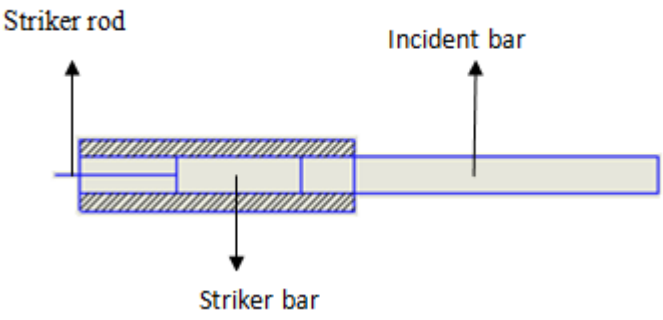

b)

Figure 3.2 Schematic of the Hopkinson bar used in this study a) dimension of the Hopkinson bar and b) cross section of the launch cylinder.

3.2 STRESS MEASUREMENT AND DATA ACQUISITION PROCESS

Stress pulses are measured by two resistive strain gages (supplied by Measurement Group Inc.) mounted diametrically opposing on the midpoint of each bar. The reason to use two diametrically opposing strain gages on each bar is to eliminate the possible bending effect that can be caused by bar misalignment. Strain gages mounted on the bars are connected to a four – arm, full bridge configuration and bridge completion is succeeded by two 350 – ohm resistors. In order to obtain balance on these completed circuits, the bridge completion circuit is connected to

an amplifier (supplied by Measurement Group Inc). In the present study, data acquisition system is Nicolet Pro 42 high speed digital oscilloscope through which waves are recorded at a rate of 20 million samples per second. Data is stored in its memory to be used for analyzing in the Excel later on. The data coming from the incident bar is recorded as Channel 1 providing strain – time history for incident and reflected wave and the data coming from the transmitted bar is recorded as Channel 2 providing strain – time history for only transmitted wave in the oscilloscope. The data format stored in the oscilloscope is converted to excel format to be able to analyze data. Excel gives the data as time versus volt for incident and reflected, and transmitted waves. Then these two waves coming from Channel 1 and Channel 2 are integrated to be analyzed in order to obtain stress versus strain rate plot, stress versus strain plot, and energy absorption versus time plot integrating the incident, reflected, and transmitted waves with all three waves beginning at the same time for the same duration as shown in Figure 2.2. Since the data is stored in the oscilloscope as volts, the data needs to be converted into stress units using conversion factor. In the current study, 1V is equal to 0.000666 strains. Then the volts can be converted to stress unit by

$$\sigma = E \times \varepsilon = 30 \times 10^{6}\ (psi) \times 0.666 \times 10^{-3} (strain) = 20000\ psi \quad \textbf{(3.1)}$$

$$1\ V = 20000\ psi$$

where,

$E = Elastic\ modulus\ of\ the\ Hopkinson\ bars\ (30 \times 10^{6} psi)$

$\varepsilon = Corresponding\ train\ in\ the\ bars\ (1V = 0.000666\ microstrain)$

In this experiment, the data were designed to determine the effect of impact energy, laminate thickness, contact geometry, and loading direction on energy absorption and damage parameters. Data acquisition system and typical wave obtained from oscilloscope and the schematic of the Hopkinson bar integrated with the data acquisition system are shown in Figure 3.3 and 3.4, respectively.

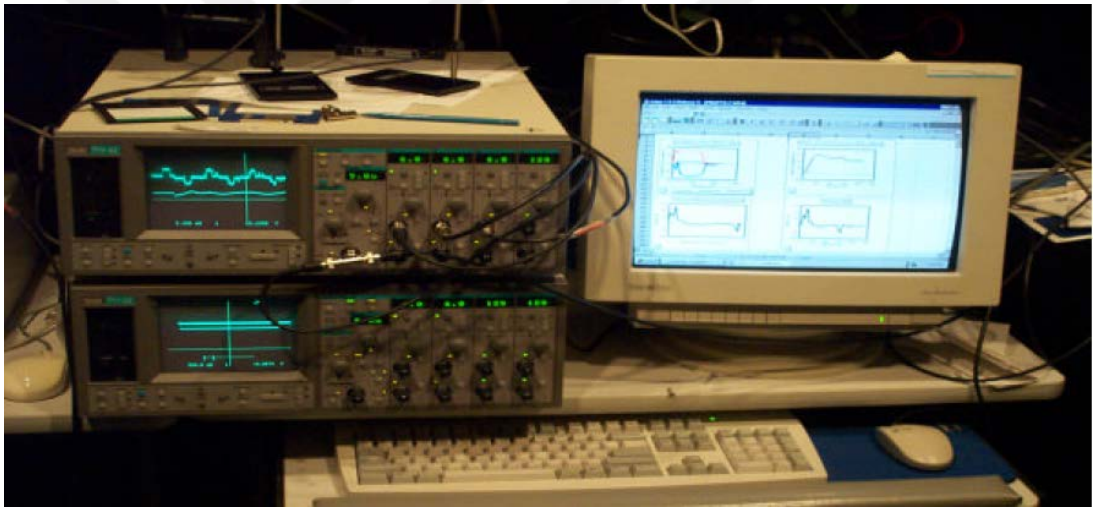

Figure 3.3 Data Acquisition System.

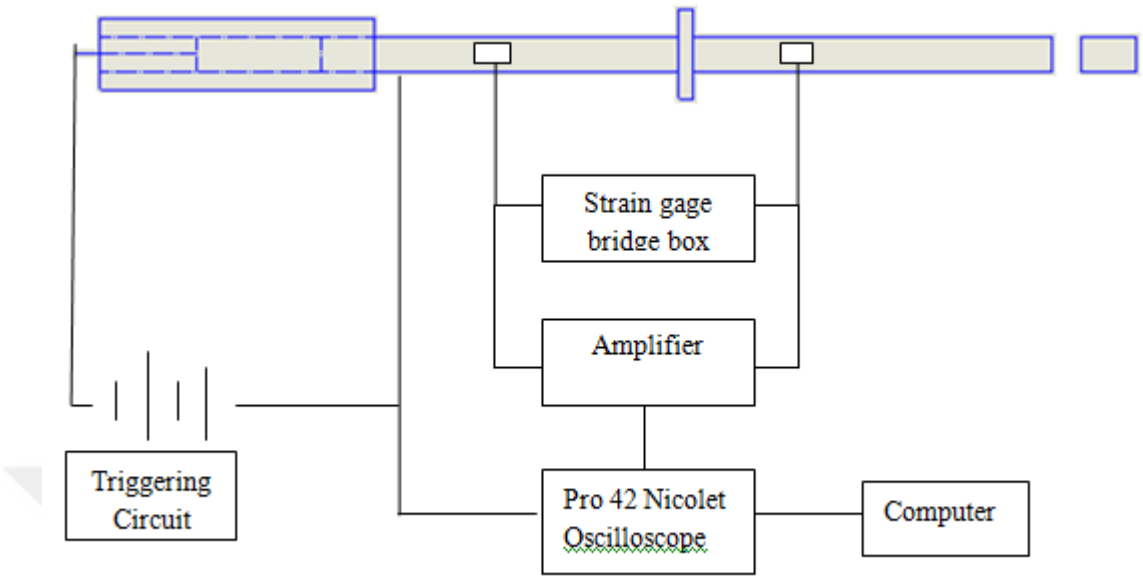

Figure 3.4 The schematic of the modified split Hopkinson bar integrated to the data acquisition system.

3.3 TYPES OF EXPERIMENTS AND MATERIAL SELECTION

In this experiment, two types of experiments have been carried out; transverse loading and diametrically loading.

3.3.1 Transverse Loading Condition

For this type of experiment, the specimen is sandwiched between the bars exposing to the transverse loading as shown in Figure 3.5. $\mathbf{L_0}$ represents the thickness of the specimen used for strain calculation. In transverse loading experiments, the area used in calculations is the area of the surface of the specimen contact with the surface of the incident bar is $\boldsymbol{\pi r^2}$ where *r* is the radius of the specimen.

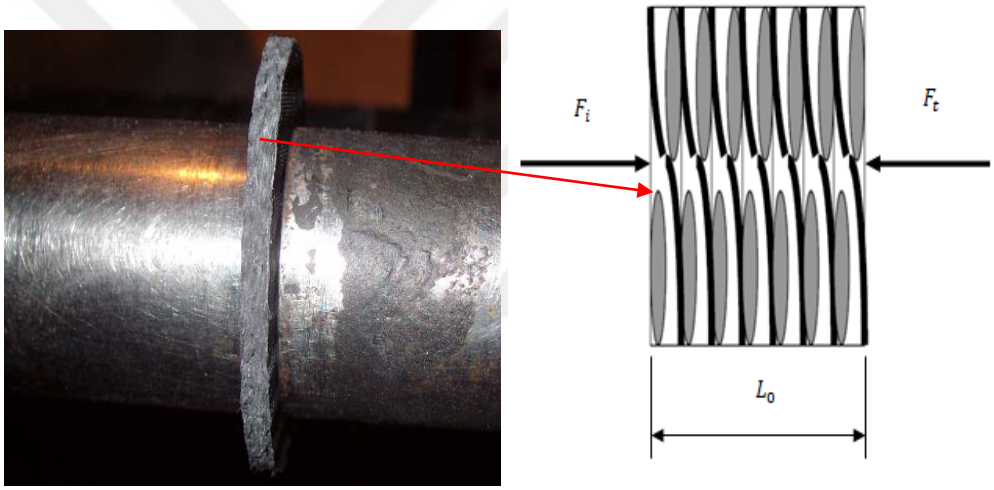

a) b)

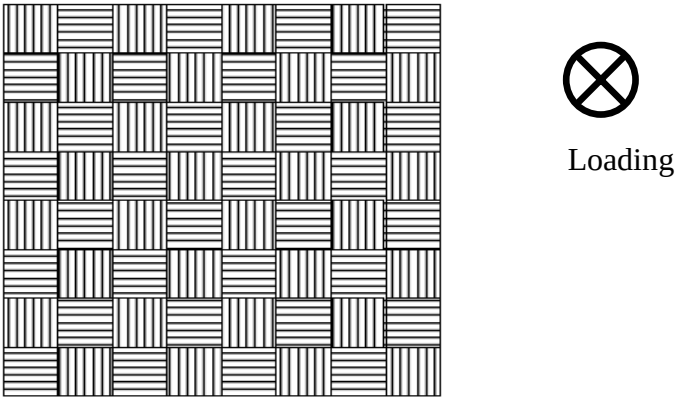

c)

Figure 3.5 Transverse loading in the Hopkinson bar. a) Schematic of the transverse loading case, b) the schematic of the cross – section of the specimen exposing to the transverse loading direction [6], and c) the schematic of the loading surface of the specimen [15].

3.3.2 Diametrical Loading Condition

Figure 3.6 shows the diametrically loading condition. The thickness of the diametrically loaded specimens L_0 is the diameter of the specimen. In this loading configuration, abrupt changes in the cross section area will create non – uniform stress distribution along the specimens as shown in Figure 3.7 – a. The area in this loading case can be expressed as $A_i = t \times x_i$, where t is the thickness of the specimens which is constant and x_i is the length which varies with respect to the cross sectional area of the specimen as shown 3.7 – b . The stress – strain curves of diametrically loaded specimens will be obtained by taking x as 0.15 inch which is close to the contact point to estimate maximum stress in the specimen which occurs in the contact surface.

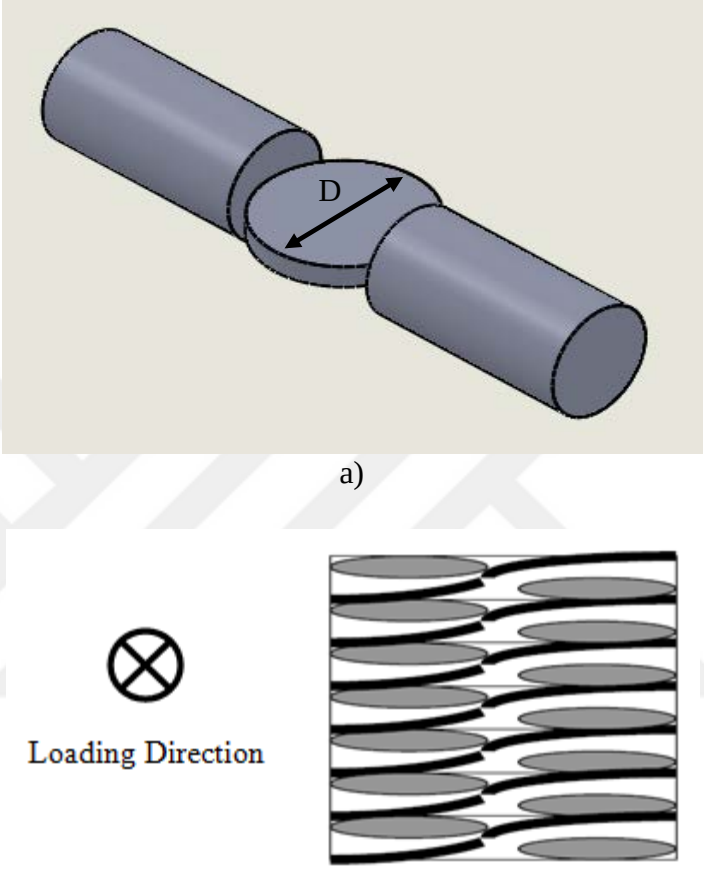

Figure 3.6 Diametrical loading in the Hopkinson bar. a) Schematic of the diametrical loading case and b) the schematic of the loading direction [6].

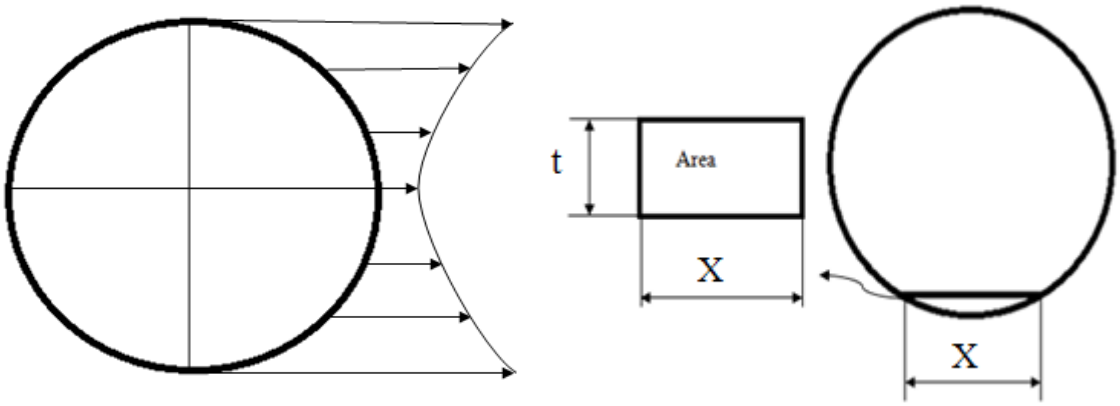

Figure 3.7 Schematic of a) stress concentration and b) unit area in the diametrically loaded specimens.

3.3.3 Transverse Loading Using Different Contact Area

In this type of experiment, instead of sandwiching the specimen between two bars, the specimen is sandwiched between the incident bar and the different contact geometry with the diameter of 0.5 inch attached to the incident bar to investigate the effects of the contact geometry in high strain rate behavior of the specimen as shown in Figure 3.8.

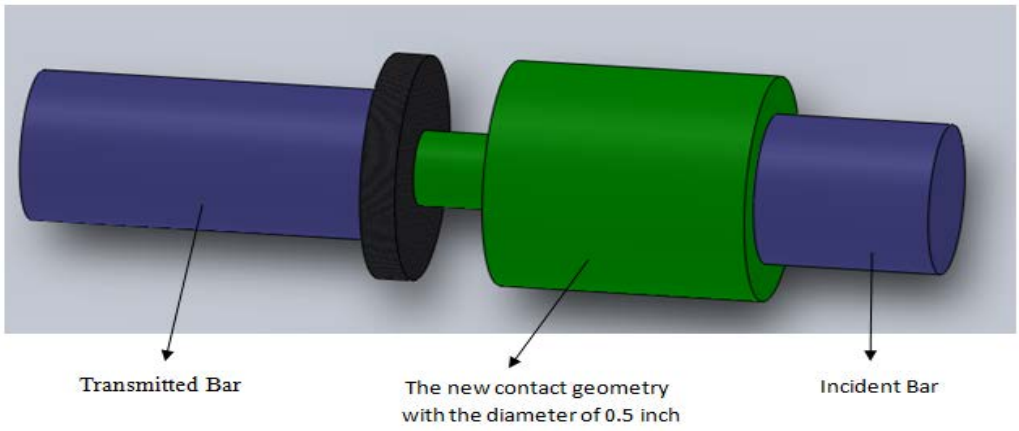

Figure 3.8 The schematic of the different contact geometry with the diameter of 0.5 inch.

Using different contact area in the incident bar does not effect the equation for the stress in the specimen (2.23) due to the equilibrium assumptions in the system as shown below.

From the equilibrium assumption, $F_1 = (\sigma_i + \sigma_r)A_{b'} = (\sigma_t)A_b = F_2$, it can be obtained

$$(\sigma_i + \sigma_r) = \frac{A_b}{A_{b'}}(\sigma_t) \quad \textbf{(3.1)}$$

where A_b and $A_{b'}$ are the contact areas of the transmitted bar and the different geometry with the specimen , respectively.

The average stress in the specimen from equation (2.22),

$$\sigma_s = \frac{(\sigma_i+\sigma_r)A_{b'}+(\sigma_t)A_b}{2A_s} \quad \textbf{(3.2)}$$

Substituting equation (3.1) into (3.2), the average stress in the specimen can be expressed as

$$\sigma_s = \frac{A_b(\sigma_t)}{A_s} \quad \textbf{(3.3)}$$

which is the same with equation 2.3.

3.3.4 Materials Selection

The composite materials used in this study are graphite/epoxy composites and fabricated by VARIM process using plain weave T300B – 40B – 3K – Toray carbon fabric and SC – 14 epoxy resin. The thicknesses of the composite materials are 8 ply (0.078 inch), 12 ply (0.113 inch), and 16 ply (0.140 inch).

3.4 SYSTEM CALIBRATION

The purpose of the system calibration is to obtain a relationship between the compressed pressure applied to the system and the striker velocity delivered to the incident bar and the energy transferred to the incident bar using infrared photo gate detectors just before the impact.

A photo gate detector and a flag with the length of 0.023 m were used to measure the duration of the blocking time in photo gate detectors. The time measured in photo gate detectors is divided to the length of the flags to determine the velocity. The photo gate detector was positioned to the end of the impact bar to measure the impact velocity V_i just before impact. In order to measure the impact bar velocity, the flag was attached to the end of the striker rod. Once the pressure is applied, the rod moves toward the incident bar blocking the infrared beam in photo gate detectors just before the impact. The blocking time is obtained from a software program connected to the photo gate detectors (Data Studio). Then the blocking time is divided to the length of the flag to determine the impact bar velocity just before the impact. The impact energy transferred to the system is equal to the kinetic energy of the impact bar and can be expressed by

$$E_i = \frac{1}{2} m_s V_i^{\,2} \qquad \textbf{(3.2)}$$

where m_s is the mass of the striker bar.

Finally, calibration curve can be obtained plotting striker velocity versus applied pressure and corresponding energy versus applied pressure data. Figure 3.9 gives the calibration curves showing there is a nonlinear relationship between the striker velocity and applied pressure.

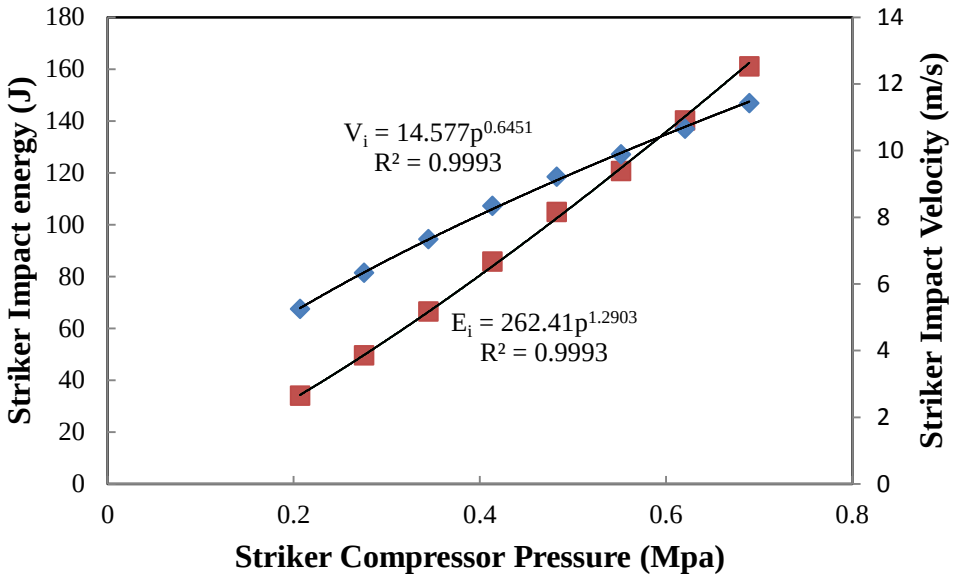

Figure 3.9 Relationship between the impact velocity, impact energy, and compressor pressure.

Incident and Transmitted Bar Parameters

- Young's Modulus of the maraging steel : $2.07 \times 10^5 MPa$ $(30 \times 10^6 psi)$
- Yield Stress of maraging steel : $2.03 \times 10^5 MPa$ $(295 \times 10^5 psi)$
- Wave velocity in the bars : $4633\ m/s$
- Transmitted and incident bar length : $3.6\ m$
- Density of maraging steel : $8000\ kg/m^3$

Impact and Calibration Parameters

- Striker bar length : $0.61\ m$
- Mass of the striker bar : $2.47\ kg$
- Ram displacement : $0.61\ m$
- Impact Energy : $254.76 \times p^{1.4463}$

  (where p is in MPa; 1 MPa = 145psi)

4.0 EXPERIMENTAL RESULTS

High strain rate compression testing was carried out on three different thicknesses of graphite/epoxy composites produced by VARIM process using split Hopkinson bar at four different impact energies of 67 J, 113 J, 163 J, and 263 J. Based on the thickness, the specimens were classified as 8 ply, 12 ply, and 16 ply. Under each energy level, specimens were tested transversely and diametrically. Transverse loading was achieved by sandwiching the specimens between bars as shown in Figure 3.5 and by sandwiching the specimens between the transmitted bar and the 0.5″ indentor attached to the incident bar as shown in Figure 3.6. The transverse loaded specimens have not shown any visible damage while they have exhibited plastic deformation within the specimen due to viscoelastic behavior of the matrix system and the temperature rise during the impact testing and any microscopic damages that might have possibly developed within the samples and on the sample surface without influencing overall integrity of the specimens. Thus, the loading portion of the stress – strain behavior of transversely loaded specimens is different from its unloading portion. Unlike transverse loading, in the case of diametrically loading, the all specimens have displayed visible damage which can be seen in the nature of the graphs. All the data in this study was analyzed with three trials so that experimental errors for the data is shown in peak energy absorbed, peak strain, peak stress, elastic modulus, and Raman spectrum graphs for the reader to understand validation of the experiments.

4.1 EFFECT OF THE THICKNESS ON THE DAMAGE PARAMETERS

4.1.1 Effect of the Thickness on Energy Absorbed

Figures 4.1 shows the plots of energy absorbed and time as a function of thickness at 67 J, 113 J, 163 J, and 263 J impact energies for the specimens exposed to transverse loading without using indentor. It is clear from the results that the specimen thickness has almost no effect on the energy absorbed for the specimens subjected to the transverse loading. The energy absorbed is almost same for 8 ply, 12 ply, and 16 ply specimens for the same impact energy. This indicates that no significant damage occurs on the specimen surface as shown in Figure 4.25. Equation 2.26 shows that for the same impact energy, energy absorption is dependent on the reflected and transmitted wave which depends on the characteristic of the surface specimen. In Figure 4.1, only less than 10, 20 and 24% of the initial impact energy is used for energy for damage initiation and accumulation. Thus, most of the energy stored during loading stage goes to the system within the first 200 microsecond of the damage process as shown in Figure 4.1. This also explains why the tensile release wave in the strain energy release region which occurs after 300 microseconds (Figure 4.2) is completely missing.

Figure 4.2 shows the plots of energy absorbed and time as a function of thickness at 67 J, 113 J, 163 J, and 263 J impact energies for the specimens exposed to transverse loading using 0.5″ indentor to create localized though-the-thickness damage. The results now show the presence of tensile release or strain energy release indicating incipient damage. Figure 4.1 and

4.2 indicate that the specimen thickness has almost no effect on the energy absorbed for the specimens subjected to the transverse loading.

Figure 4.3 shows the relationship between force and energy absorption history for transversely loaded specimens. The energy absorbed increases rapidly with increasing applied load in the loading stage until the applied load begins decreasing in the unloading stage. Flat region on the force curve corresponds to the maximum displacement of the specimen. The curve also shows the absence of tensile release force or strain energy release indicating no damage.

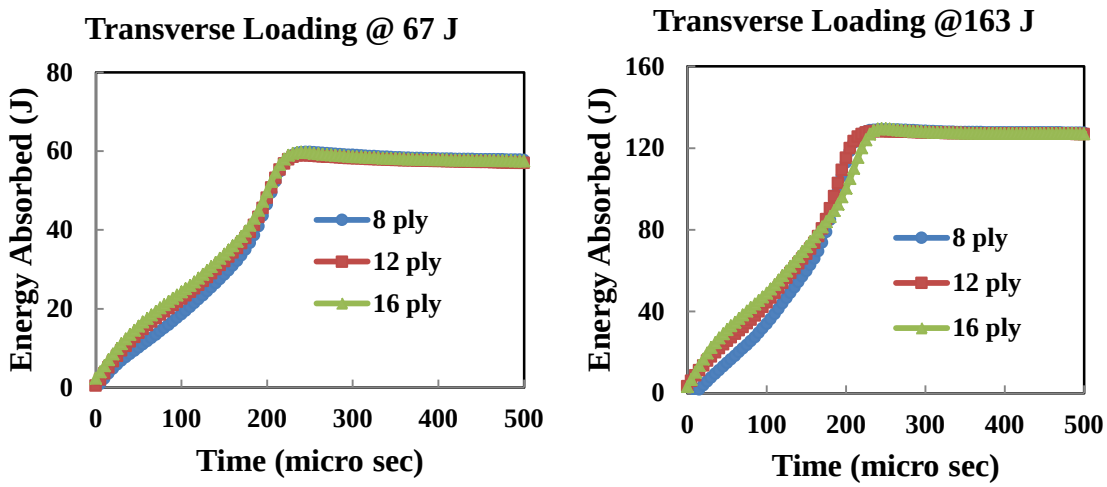

a) b)

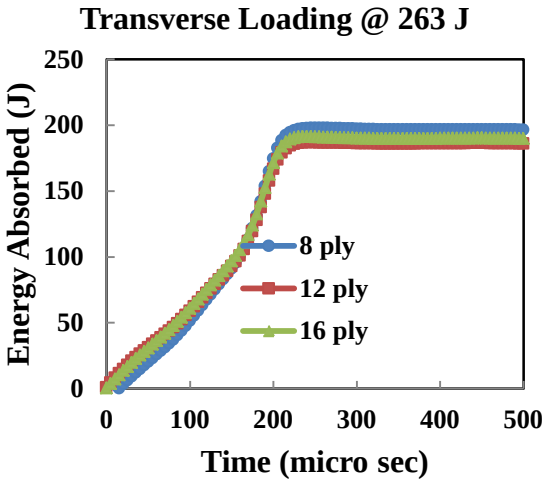

c)

Figure 4.1 Energy absorbed – time plot of transversely loaded specimens for varying specimen thickness at the impact energies of a) 67 J, b) 163 J, and c) 263 J.

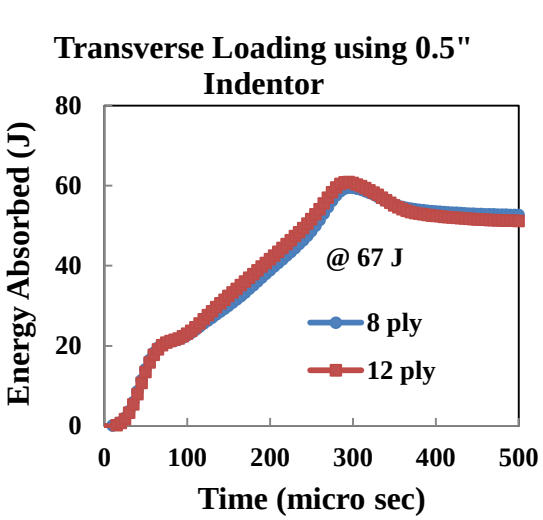

a)

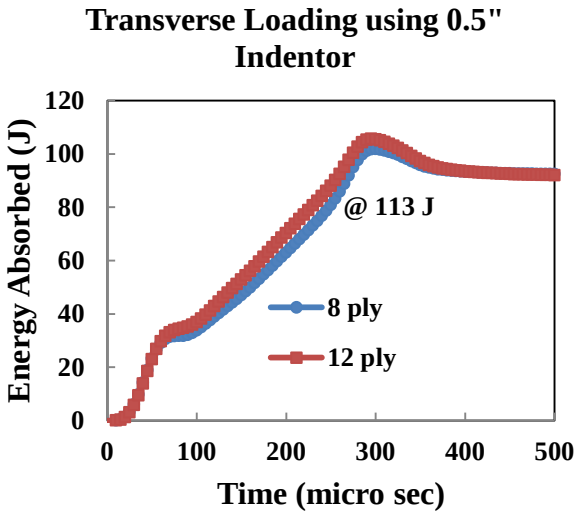

b)

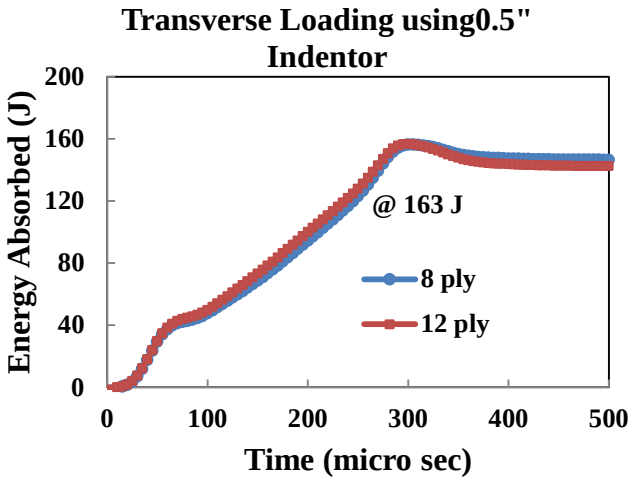

c)

Figure 4.2 Energy absorbed – time plot of transversely loaded specimens using 0.5″ indentor for varying specimen thickness at the impact energies of a) 67 J, b) 113 J, and c) 163 J.

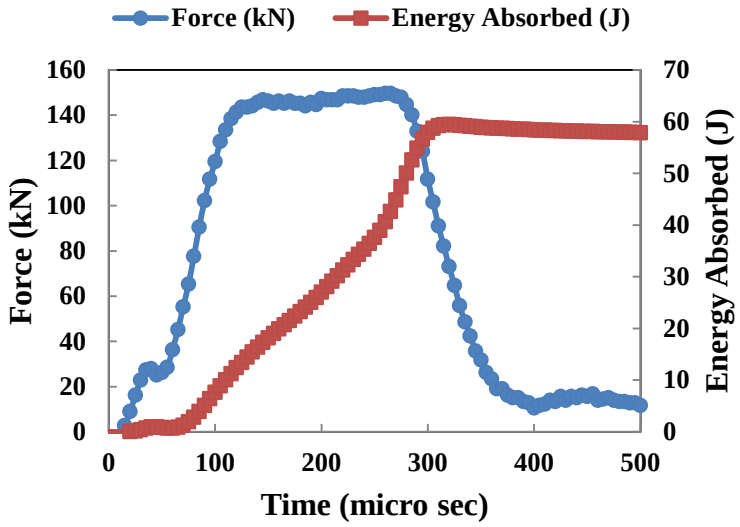

Figure 4.3 The relationship between energy absorbed and applied force for transverse loading case.

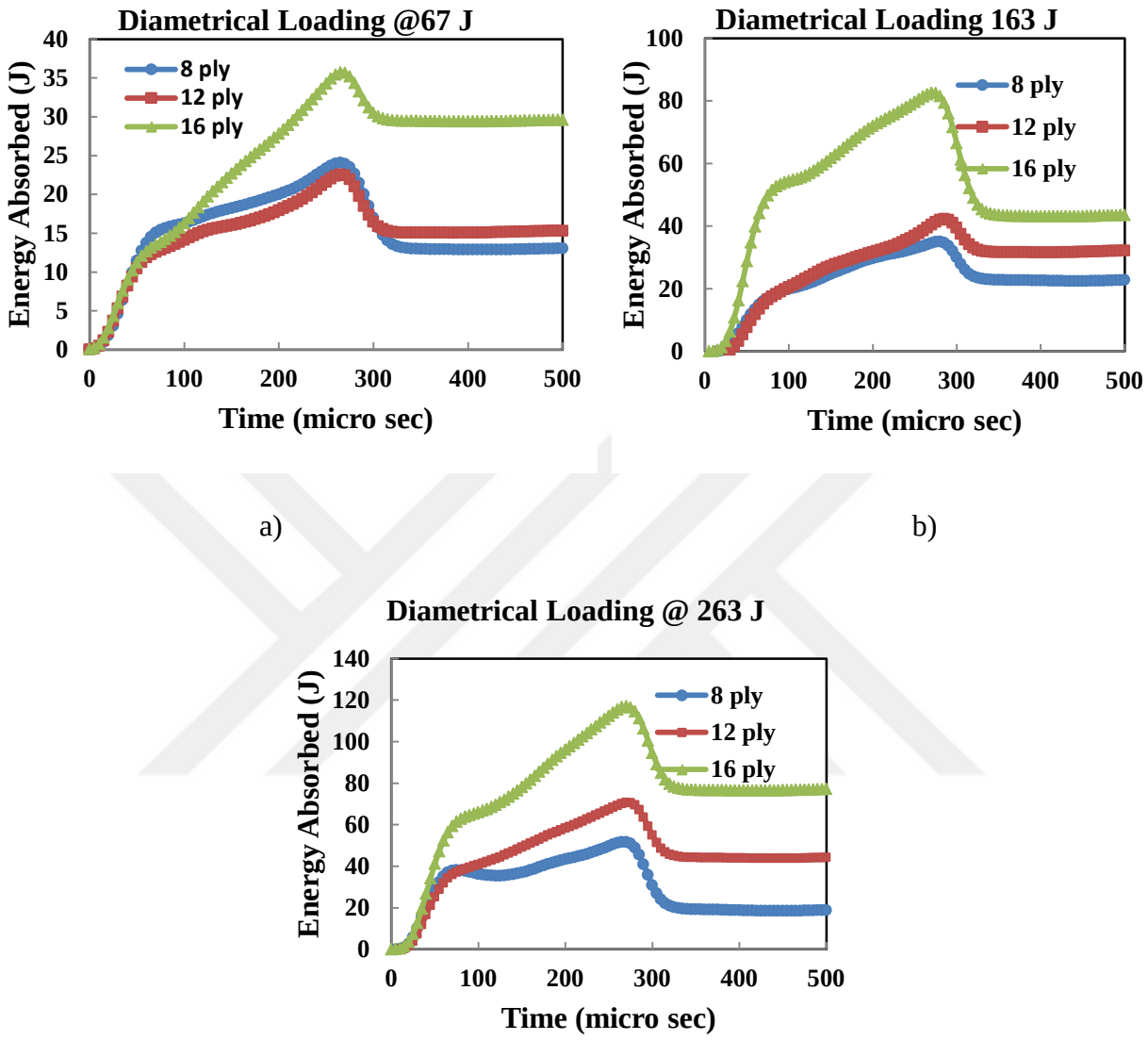

a) b)

c)

Figure 4.4 Energy absorbed – time plot of diametrically loaded specimens for varying specimen thickness at the impact energy of a) 67 J, b) 113 J, and c) 163 J.

Figure 4.4 shows the plot of energy absorbed – time as a function of the thickness at 67 J, 163 J, and 263 J of impact energies for the specimen subjected to the diametrical loading. In this case, the energy absorbed rapidly increases with increasing applied load in the loading and unloading stages in the first 100 microseconds, increases slowing after unloading stage between

100-300 microseconds because of the very little contact force to the specimen as shown in Figure 4.5. Specimen continues to experience damage during this constant strain rate stage. The energy absorbed decreases to a constant residual energy after 300 microseconds. The reduction in the energy absorption after its maximum value is the indication of strain energy release. During this stage, the incident compressive wave is released in tension and a tensile wave as shown in the force curve on the rear surface of the specimen. Thickness effect on the energy absorbed for the diametrical loaded case is seen in Figure 4.4 showing that the specimen damage residual energy is higher in the thicker specimens than the thinner specimens. The higher energy retained means greater strain energy release, and therefore greater material compressive strength. This suggests that the thinner the specimen, the greater the damage the specimen experiences.

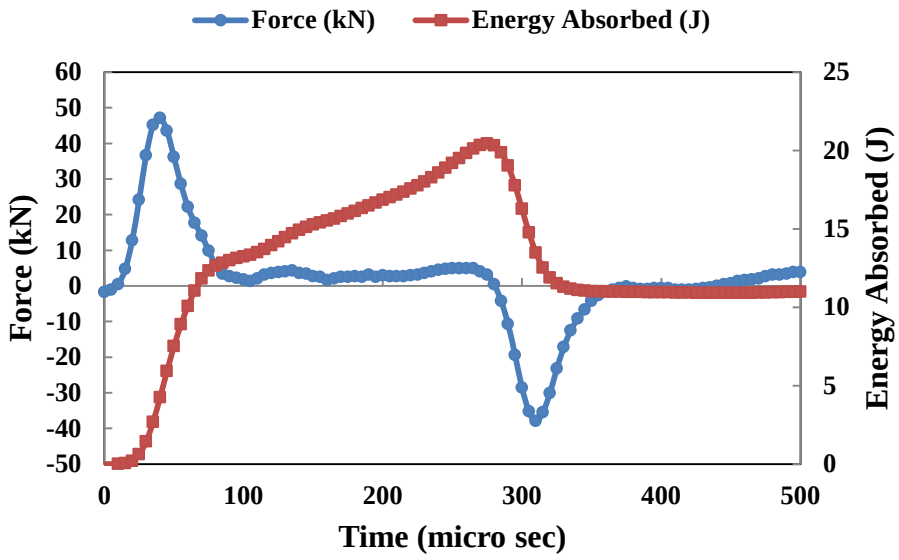

Figure 4.5 The relationship between the energy absorbed and applied force for diametrical loading case.

4.1.2 Effect of Thickness on Stress – Strain Behavior

Figures 4.6 and 4.7 show the effect of the thickness on the stress – strain behavior of the transversely loaded specimen at varying level of impact energies with and without using indentor, respectively. The results show a typical uniaxial-type loading cycle in which the stress increases during the loading stage. The compressive stress wave is purely elastic and increases linearly with strain below 100 J impact energy. As energy increases from 67 J to 163 J and 263 J, the stress-strain curve shows some non-linearity. It is conceivable that the specimen unloads with minimal plastic deformation to strain (residual strain) that is independent of thickness and energy. But the stress intensity in the material is below the ultimate strength. For the same applied energy, or maximum stress on the stress-strain curve reached by specimen is almost the same for the all specimens although the corresponding ultimate strain (maximum strain at the maximum stress) is higher for thinner specimens than for thicker specimens due to the fact that there is larger deformation for thinner specimens. Hence, there is a tendency for a thicker specimen to have a higher modulus than a thinner specimen as shown in Figure 4.8 and 4.9. This independence of peak stress on thickness is due to the fact that applied impact energy is not high enough to pass the ultimate strength of the transversely loaded specimens. In other words, some portion of plastic deformation within the specimen is recoverable which can be understood from the nature of the stress – strain curve.

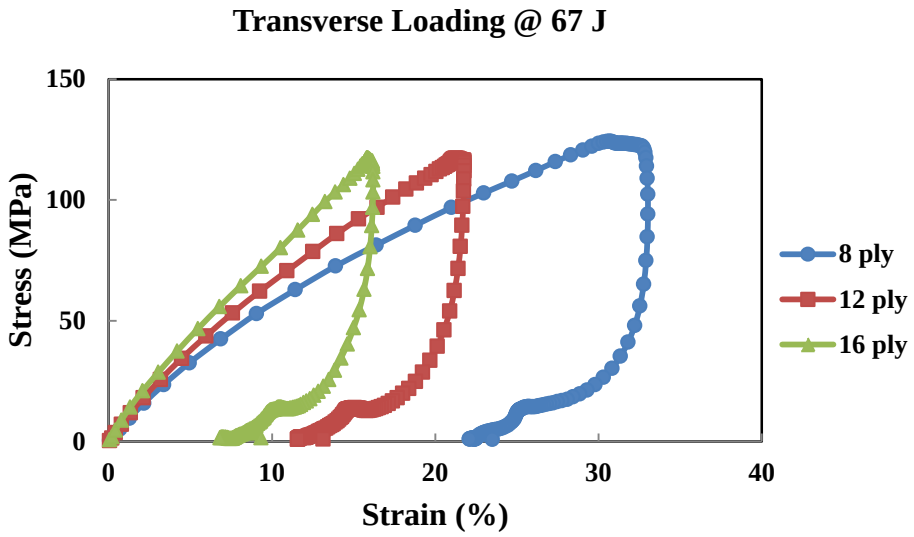
Transverse Loading @ 67 J
Stress (MPa)
150
100
50
0
0
10
20
30
40
Strain (%)
8 ply
12 ply
16 ply

a)

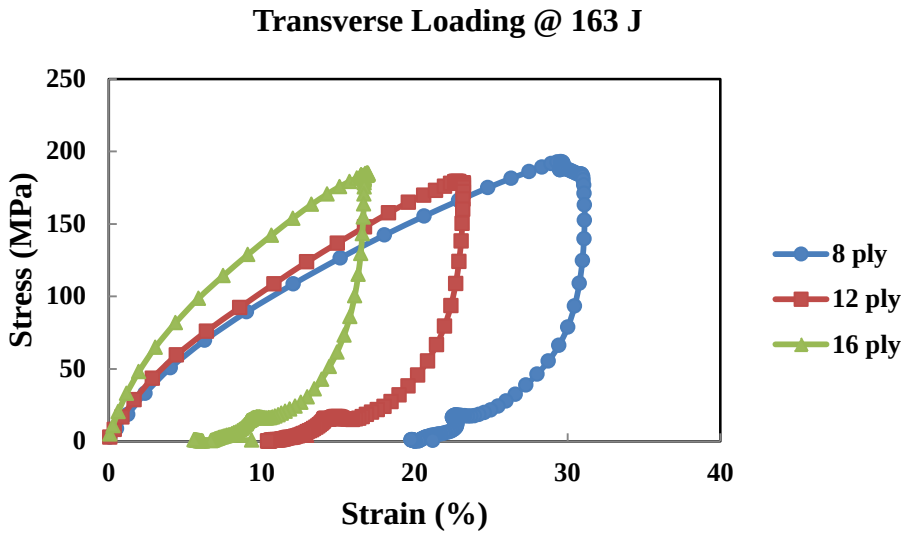
Transverse Loading @ 163 J
Stress (MPa)
250
200
150
100
50
0
0
10
20
30
40
Strain (%)
8 ply
12 ply
16 ply

b)

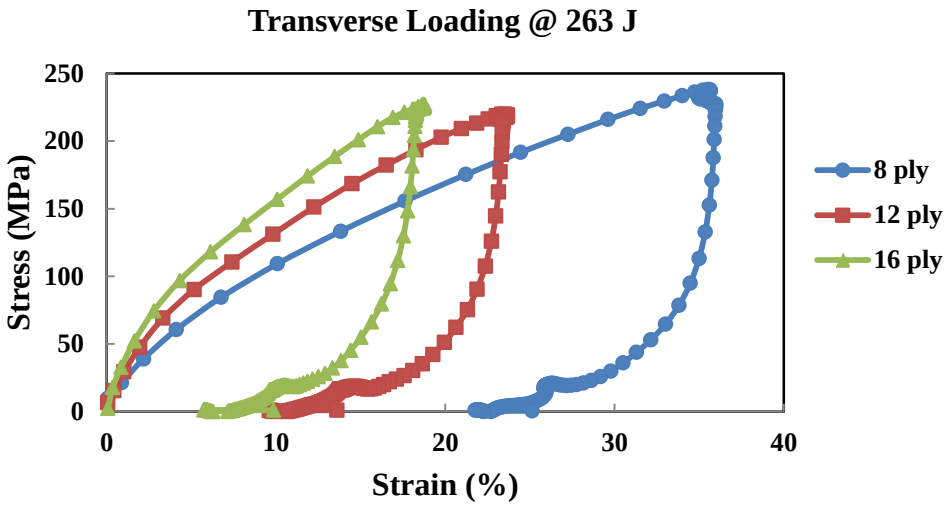

c)

Figure 4.6 Plot of the stress – strain curve of transversely loaded specimens for varying specimen thickness at the impact energy of a) 67 J, b) 163 J, and c) 263 J.

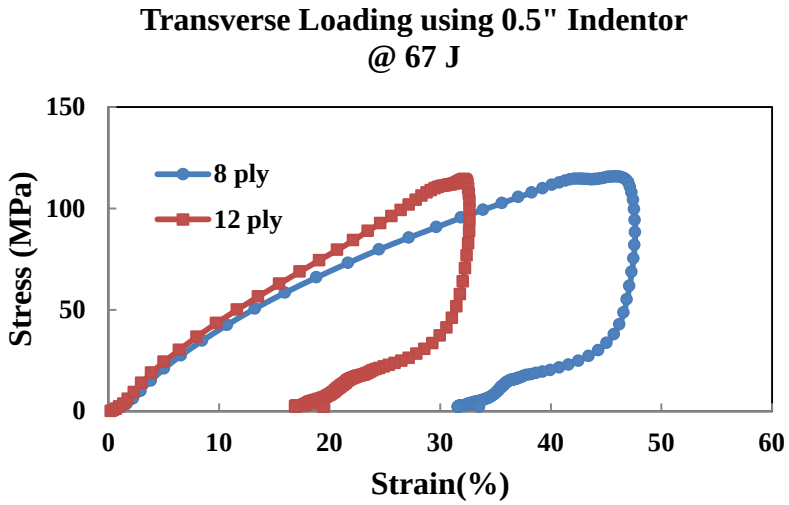

a)

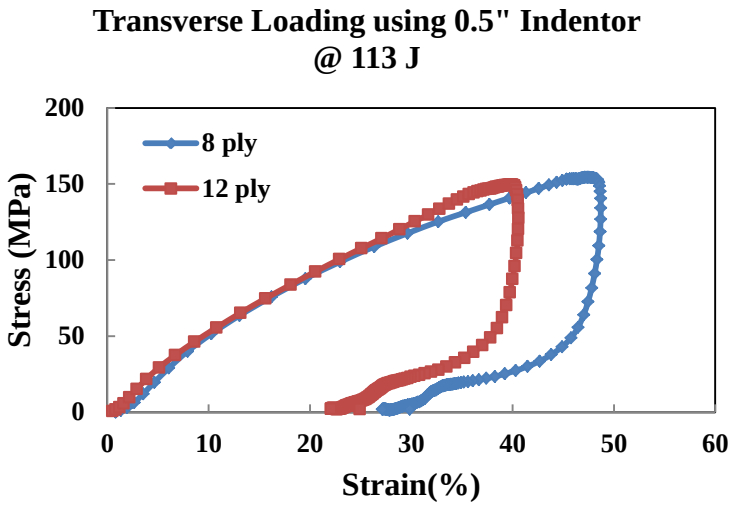

b)

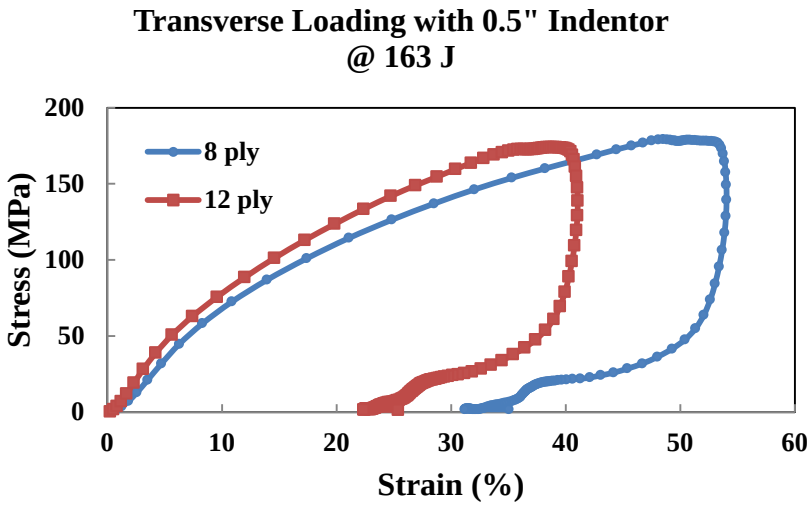

c)

Figure 4.7 Plot of the stress – strain curve of transversely loaded specimens with 0.5″ indentor for varying specimen thickness at the impact energy of a) 67 J, b) 113 J, and c) 163 J.

It should also be noted that the loading portion of stress – strain plots is different from its unloading portion in Figure 4.6 and 4.7. This behavior can be attributed to the viscoelastic

behavior of the matrix system, temperature rise during the experiment, and some microscopic damages that might have developed within the samples without influencing overall integrity.

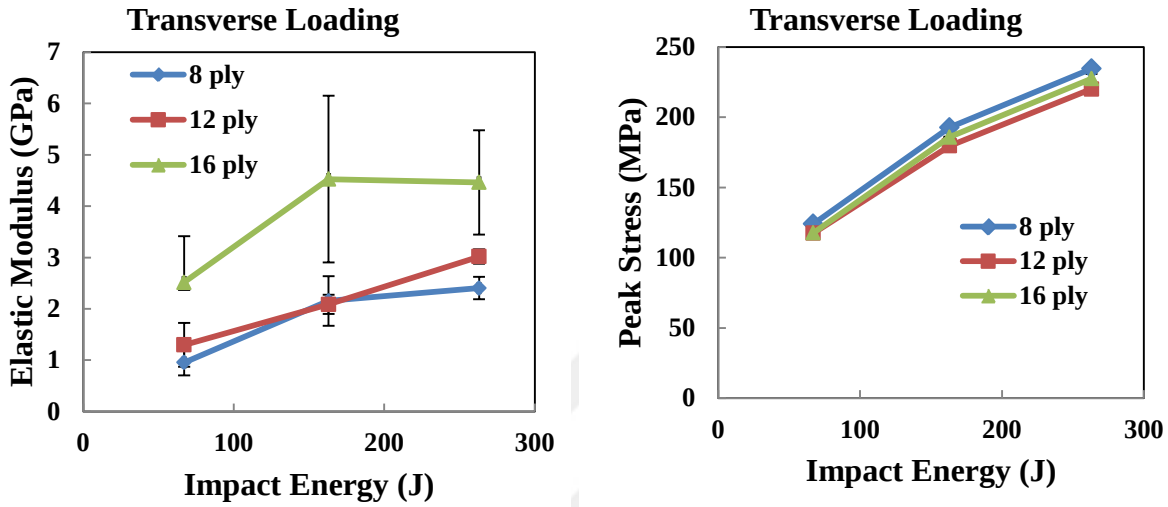

a) b)

Figure 4.8 The effect of the thickness on a) elastic modulus and b) ultimate strength at the same impact energies for transversely loaded specimens.

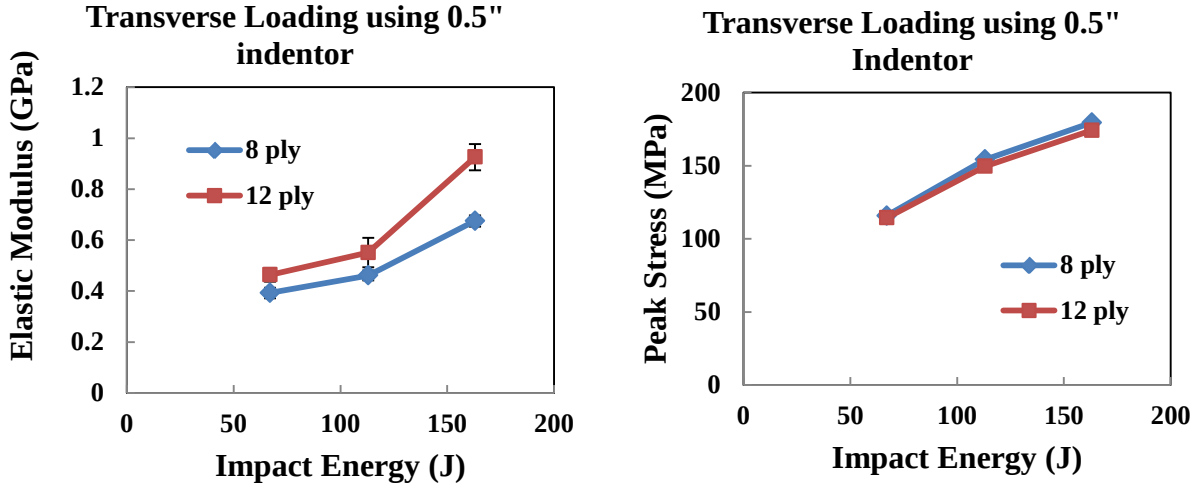

a) b)

Figure 4.9 The effect of the thickness on a) elastic modulus and b) ultimate strength at the same impact energies for transversely loaded specimens using 0.5″ indentor.

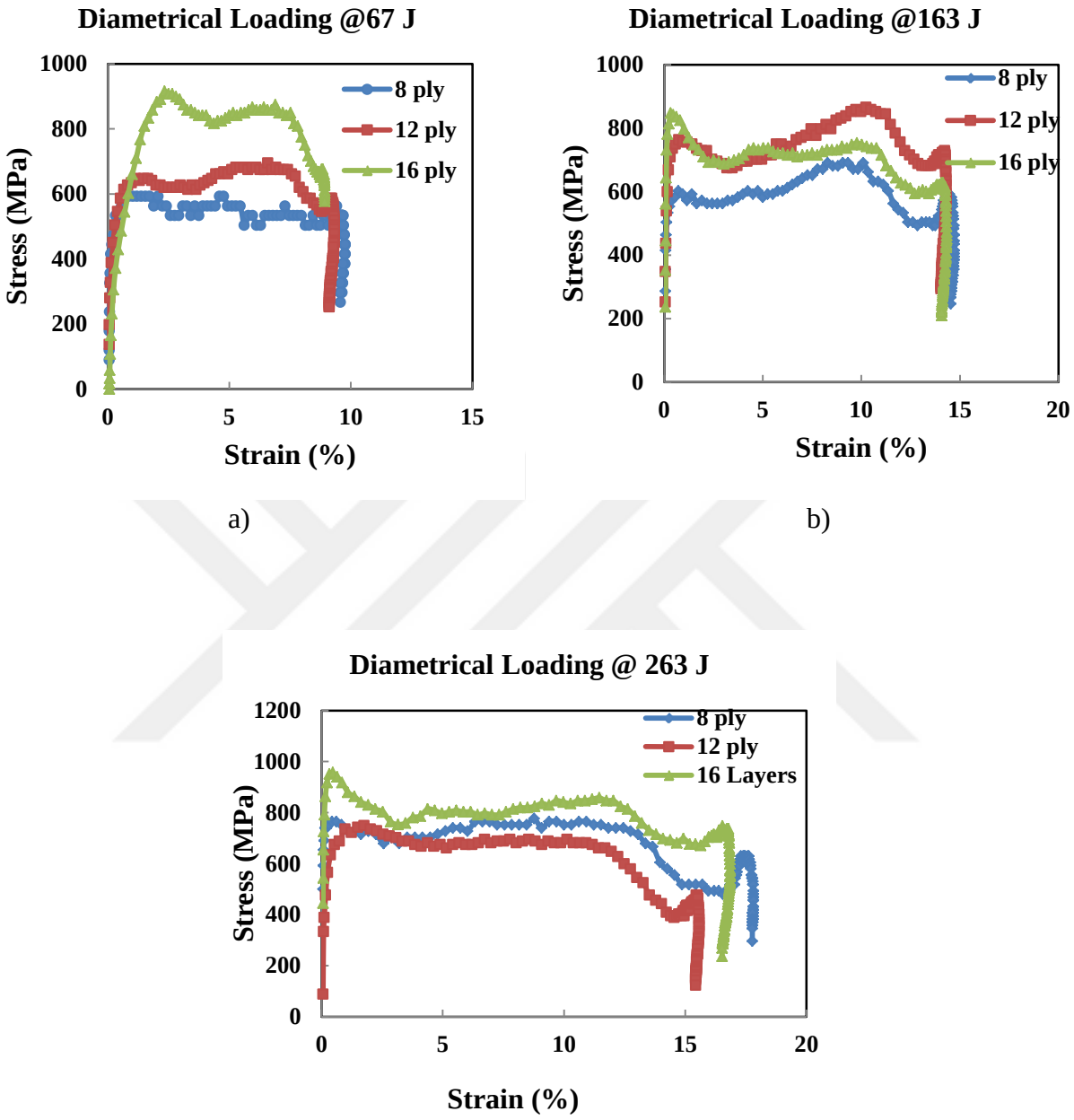

Figure 4.10 Plot of the stress – strain curve of diametrically loaded specimens for varying specimen thickness at the impact energy of a) 67 J, b) 163 J, and c) 263 J.

Figures 4.10 and 4.11 indicate that the stress - strain behavior of the diametrically loaded specimens is strongly dependent on the thickness. Results show typical plastic deformation

behavior without exhibiting any recoverable damage ending up with catastrophic failure in the specimen. It is observed that ultimate stress and elastic modulus are higher at each level of impact energies for the thicker specimens than that of the thinner specimens as it is expected because the greater deformation in the specimen surface allows reflected wave to be greater and transmitted wave to be weaker resulting in lower strength in the specimen (see Equ. 2.23). However, the ultimate failure strain is almost independent of thickness since it depends on the applied impact energy proportionally. As shown in Figure 4.24 diametrically loaded specimens exhibit visible damage which is seen in the nature of the stress – strain plot that there is no recoverable deformation within the specimen.

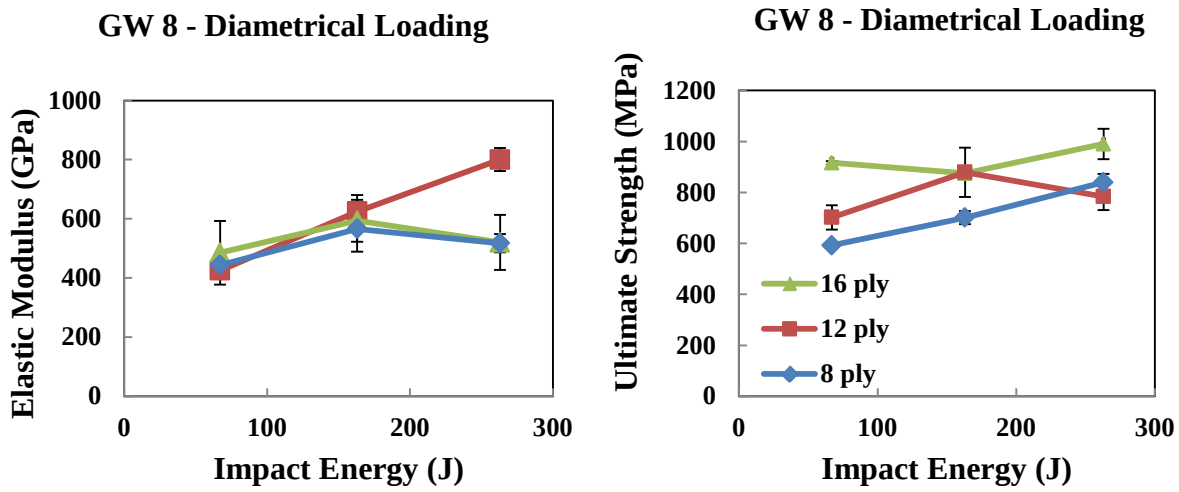

a) b)

Figure 4.11 The effect of the thickness on a) elastic modulus and b) ultimate strength at the same impact energies for diametrically loaded specimens.

4.1.3 Effect of Thickness on Strain Rate

Figures 4.12 and 4.13 show the strain rate – strain plots of transversely loaded specimens. . The strain rate increases to a maximum before sharply decreasing to zero with no region of constant strain rate. This is because the compressive incident wave in the transverse loading configuration did not provide sufficient force and space for the material to flex and deform. It is clear that the results, although thickness and energy dependent as hypothesized, do show the plateau region expected in typical strain-rate data for valid Hopkinson bar experiment because the strain rate is changing too rapidly to allow any degree of stress and strain rate uniformity. Therefore, no constant region is observed in the reflected wave as shown in Figure 2.2 – a.

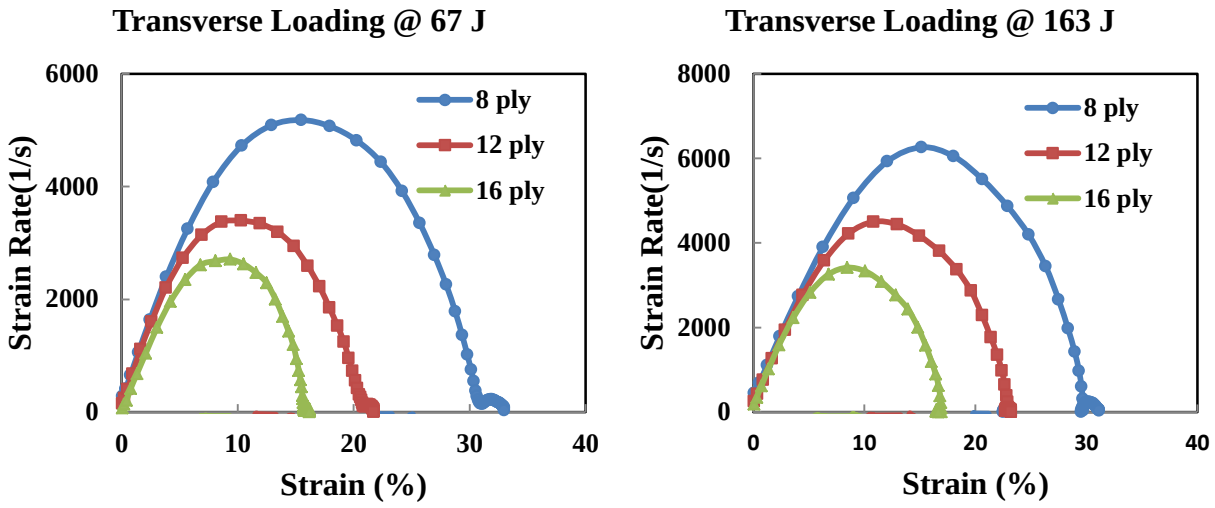

a) b)

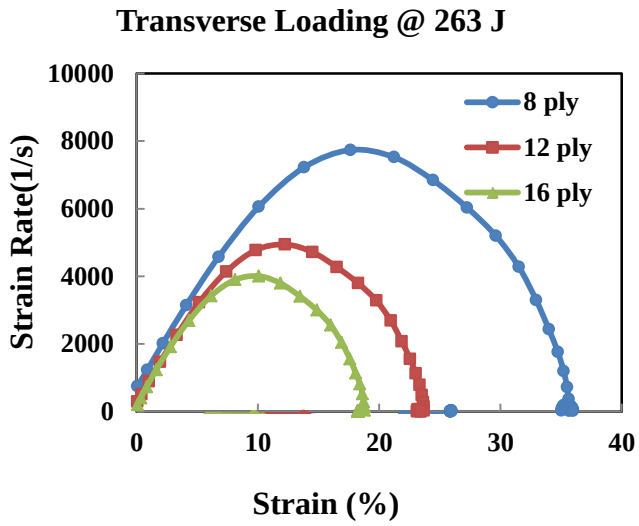

c)

Figure 4.12 Strain rate - strain plot of transversely loaded specimens for varying specimen thickness at the impact energy of a) 67 J, b) 163 J, and c) 263 J.

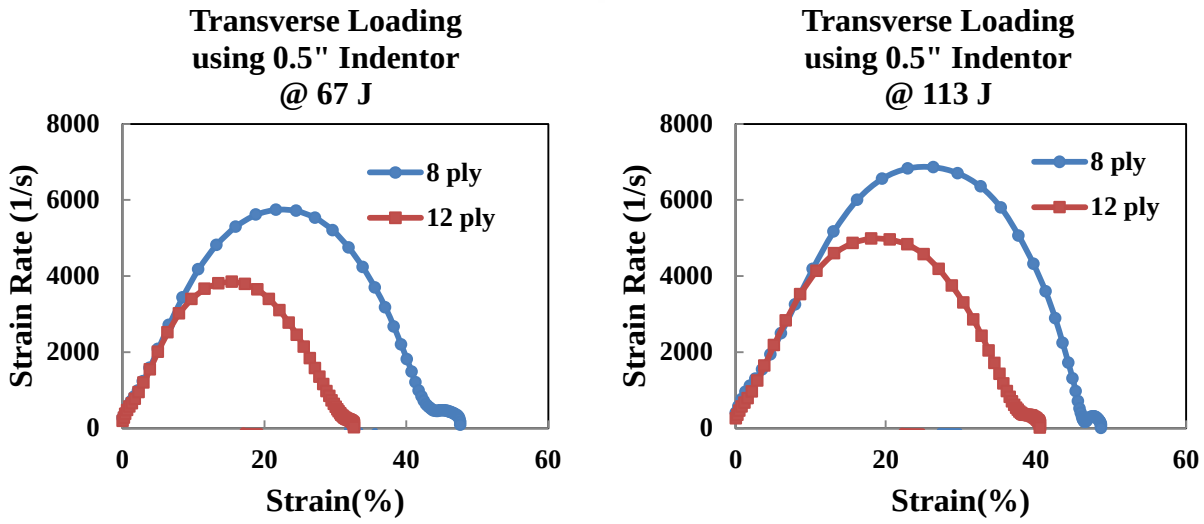

a) b)

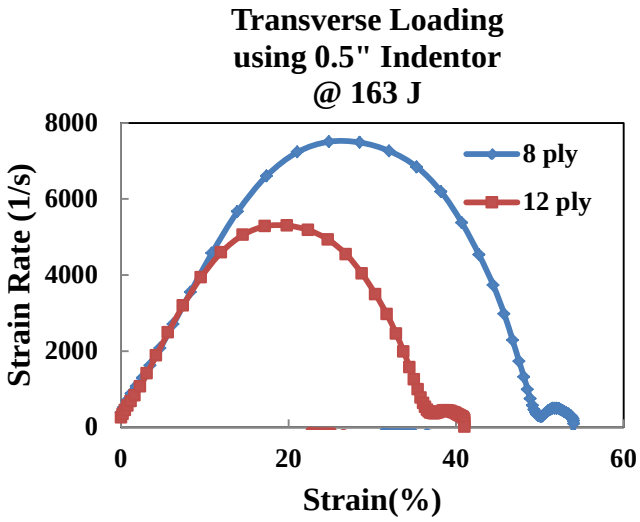

c)

Figure 4.13 Strain rate - strain plot of transversely loaded specimens using 0.5″ indentor for varying specimen thickness at the impact energy of a) 67 J, b) 113 J, and c) 163 J.

Figure 4.14 shows results different from that of transversely loaded specimen. The strain rate is only slightly dependent on the thickness for the specimens exposed to the diametrically loading. This is because the thickness of the specimen sandwiched between the bars is assumed to be the diameter of the specimen (as illustrated in Figure 3.6) and therefore the same for all the 8-, 12-, and 16- ply specimens. The region of constant strain rate suggests that damage is initiated and accumulated during the loading and unloading stages for time duration of 300 microseconds. This is seen in the nature of the reflected wave as a constant region as shown in Figure 2.2 – b making strain rate constant (Equation 2.14).

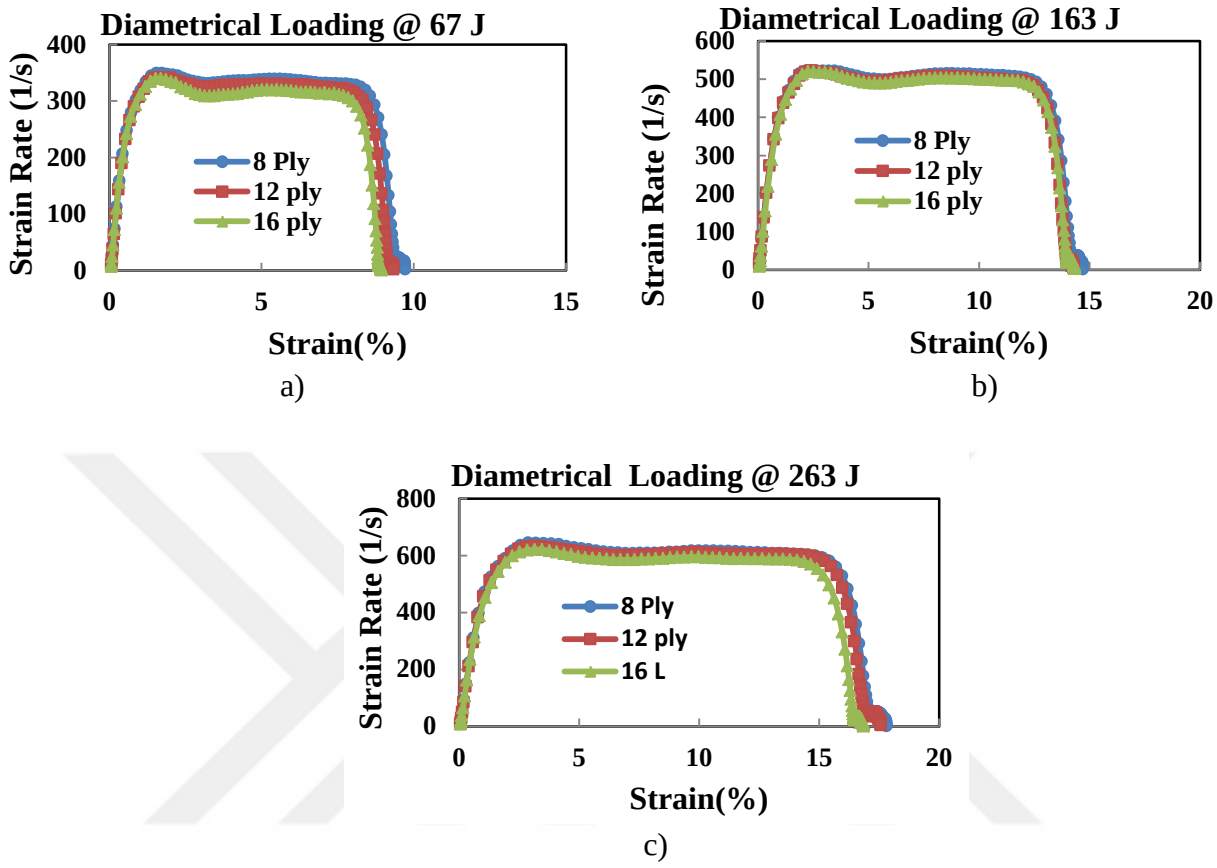

Figure 4.14 Strain rate - strain plot of diametrically loaded specimens for varying specimen thickness at the impact energy of a) 67 J, b) 163 J, and c) 263 J.

4.2 EFFECT OF IMPACT ENERGY ON DAMAGE PARAMETERS

4.2.1 Effect of Impact Energy on Energy Absorbed

Figure 4.15 and 4.16 show the effect of the impact energy on the energy absorbed for the specimens having same thicknesses and subjected to transverse loading with and without a 0.5″

indentor, respectively. The results indicate that the peak energy absorbed and residual energy increases with increasing incident energy since the specimen is exposed to higher compressive stress amplitude at higher impact energies (Equ. 2.26). In this case, most of the incident energy is returned as residual energy before 300 microseconds, indicating minima strain energy release and surface damage. This is further discussed in later sections 4.3.1. Notice a small energy release after 300 microseconds for the 0.5" indent case, indicating small local damage with this indentor. Figure 4.17 and 4.18 show the effect of the impact energy on the peak energy absorbed with experimental error for the specimens having same thicknesses and subjected to transverse loading with and without a 0.5″ indentor, respectively.

Figure 4.19 shows that peak energy absorbed and residual energy increase with increasing impact energy for the same specimens having the same thicknesses and subjected to diametrical loading. The strain energy release is clearly seen at about 300 microseconds. The results also show that the residual energy increases with thickness for the same energy as predicted. Figure 4.20 shows the effect of the impact energy on the peak energy absorbed with experimental error for the specimens having same thicknesses and subjected to transverse loading.

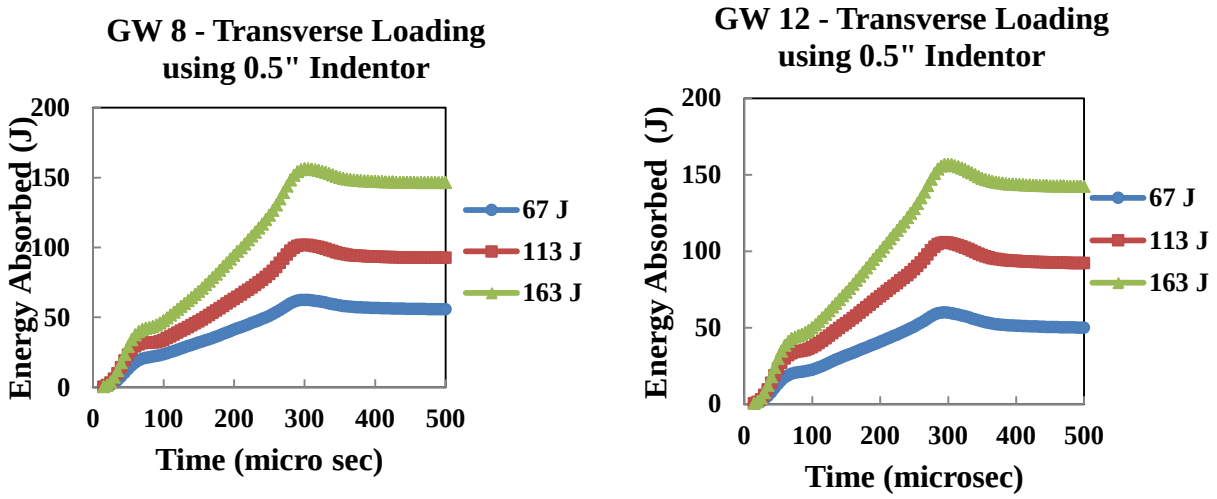

a) b)

Figure 4.15 Energy absorbed – time plot with varying impact energies for transversely loaded a) 8 ply and b) 12 ply specimens using 0.5″ indentor.

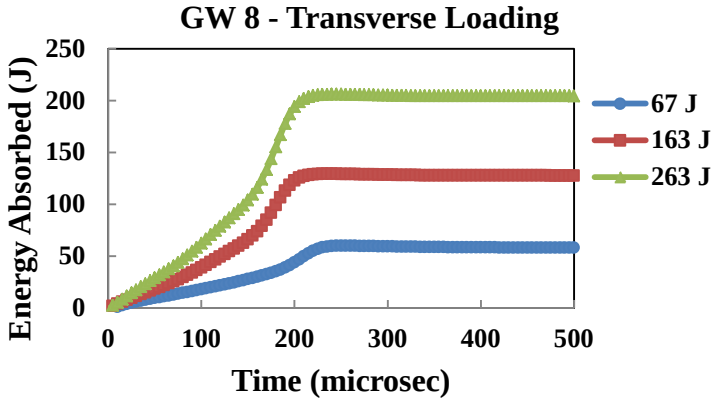

a)

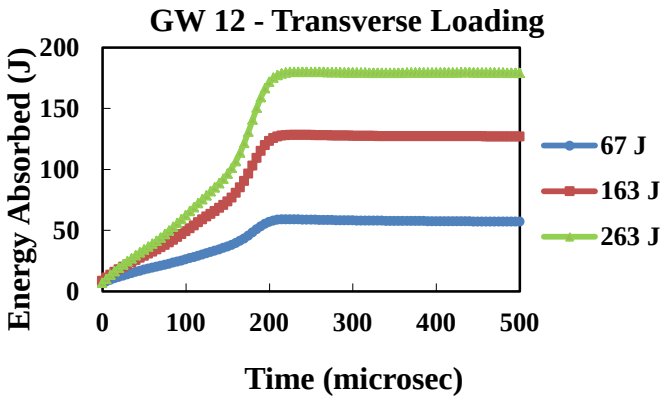

b)

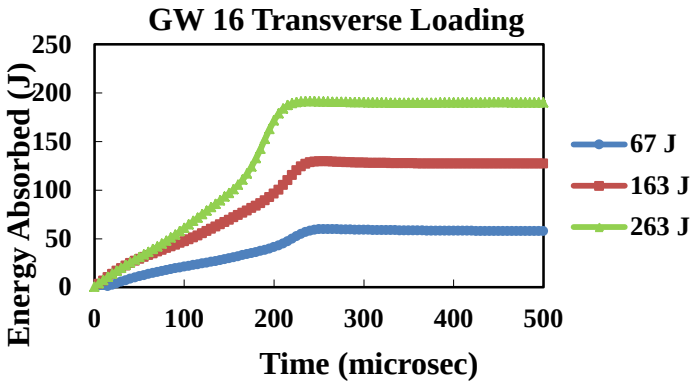

c)

Figure 4.16 Energy absorbed – time plot with varying impact energies for transversely loaded a) 8 ply b) 12 ply and c) 16 ply specimens without indentor.

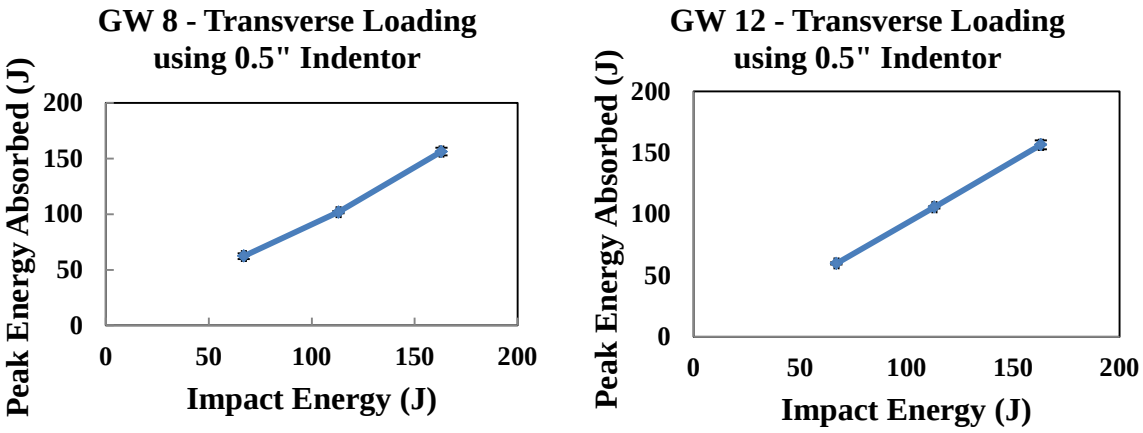

a) b)

Figure 4.17 Effect of the impact energy on the peak energy absorbed with experimental error for the a) 8 ply and b) 12 ply specimens subjected to transverse loading using a 0.5″ indentor.

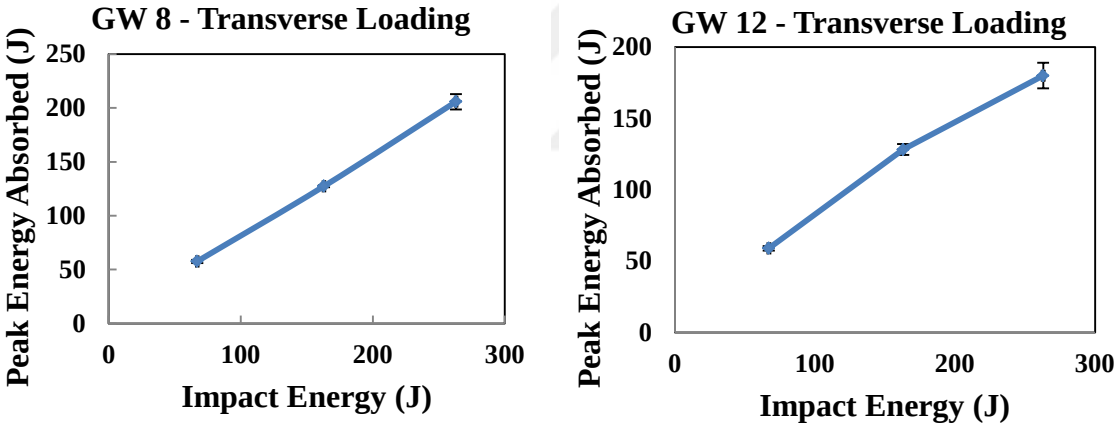

a) b)

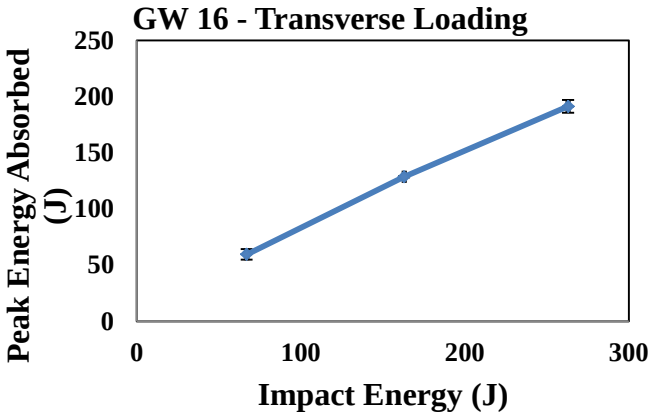

c)

Figure 4.18 Effect of the impact energy on the peak energy absorbed with experimental error for the a) 8 ply, b) 12ply, and c) 16 ply specimens subjected to transverse loading without no indentor.

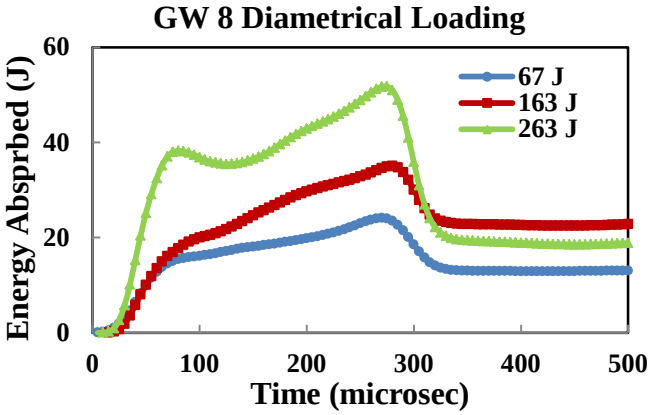

a)

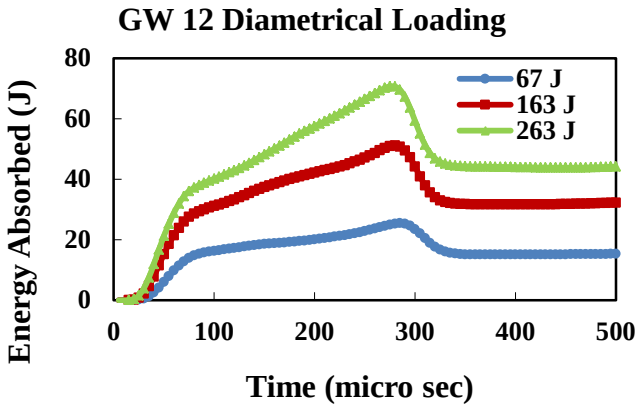

b)

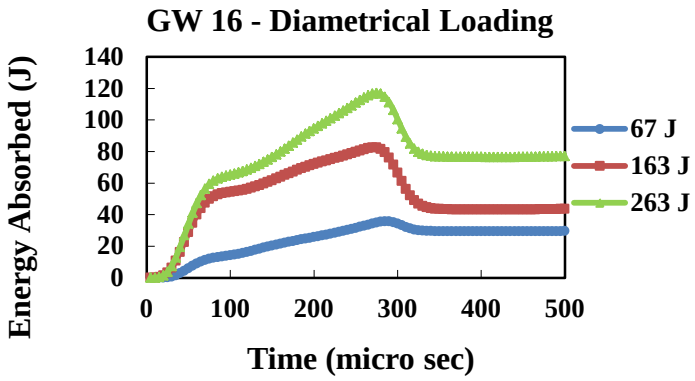

c)

Figure 4.19 Energy absorbed – time plot with varying impact energies for diametrically loaded a) 8 ply, b) 12 ply, and c) 16 ply.

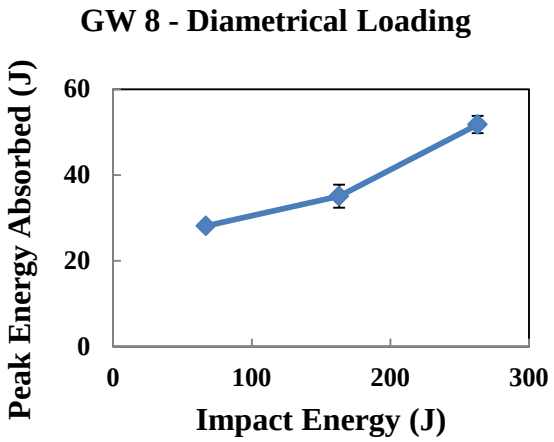

a)

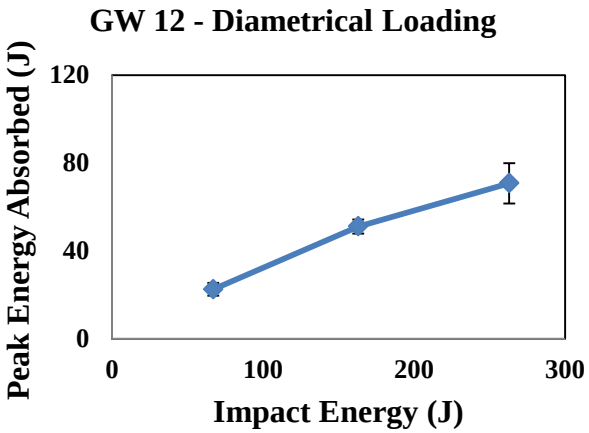

b)

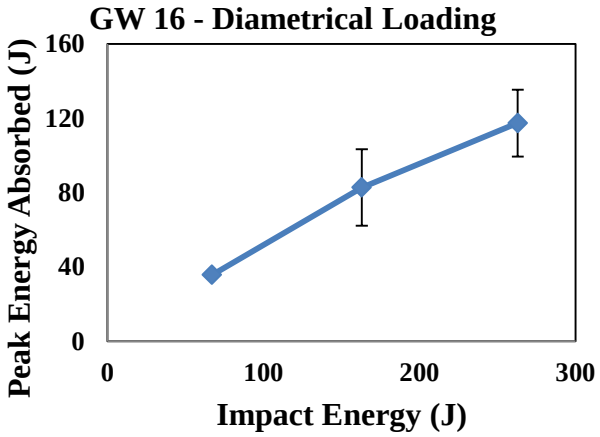

c)

Figure 4.20 Effect of the impact energy on the peak energy absorbed with experimental error for the a) 8 ply, b) 12ply, and c) 16 ply specimens subjected to diametrical loading.

4.2.2 Effect of Impact Energy on Stress – Strain Behavior

Figure 4.21 and 4.22 show the effect of the impact energy on stress – strain behavior for the transversely loaded specimens having same thicknesses without using and with using 0.5″ indentor, respectively. Results indicate that stress – strain rate is dependent on impact energies. This dependence is expected because with increasing impact energy, the contact force and absorbed energy increase (see Figure 4.15 – 4.17) and therefore the stress that specimens experience increases. For transverse loading, peak stress increases with increasing impact energy without exhibiting dependence on thickness as it is also shown in Figure 4.8. Figure 4.23 and 4.24 show the effect of impact energy on the elastic modulus with experimental error for the transversely loaded specimens having same thicknesses without using and with using 0.5″ indentor, respectively.

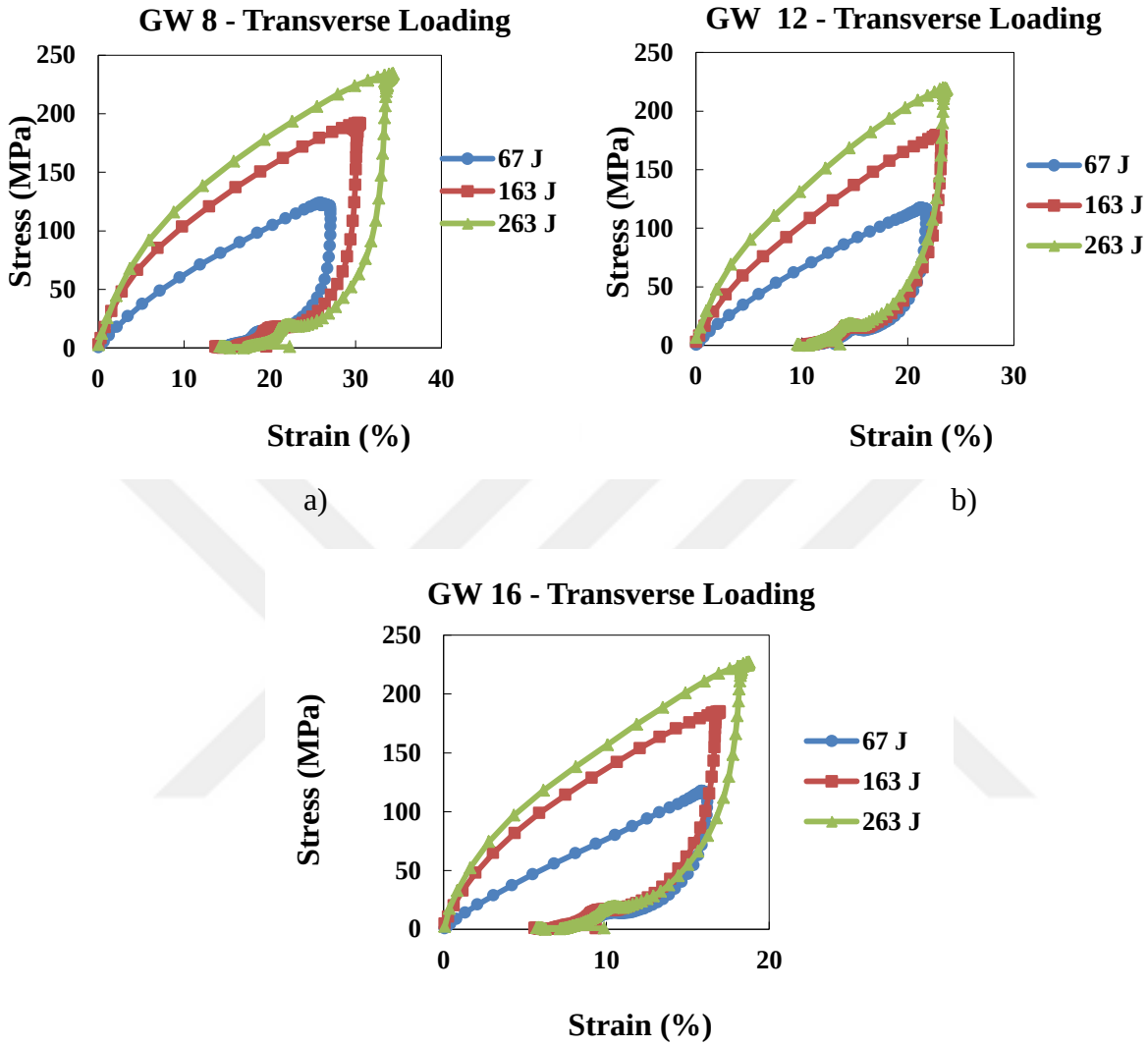

Figure 4.21 Stress - strain plot with varying impact energies for transversely loaded a) 8 ply b) 12 ply and c) 16 ply specimens

c)

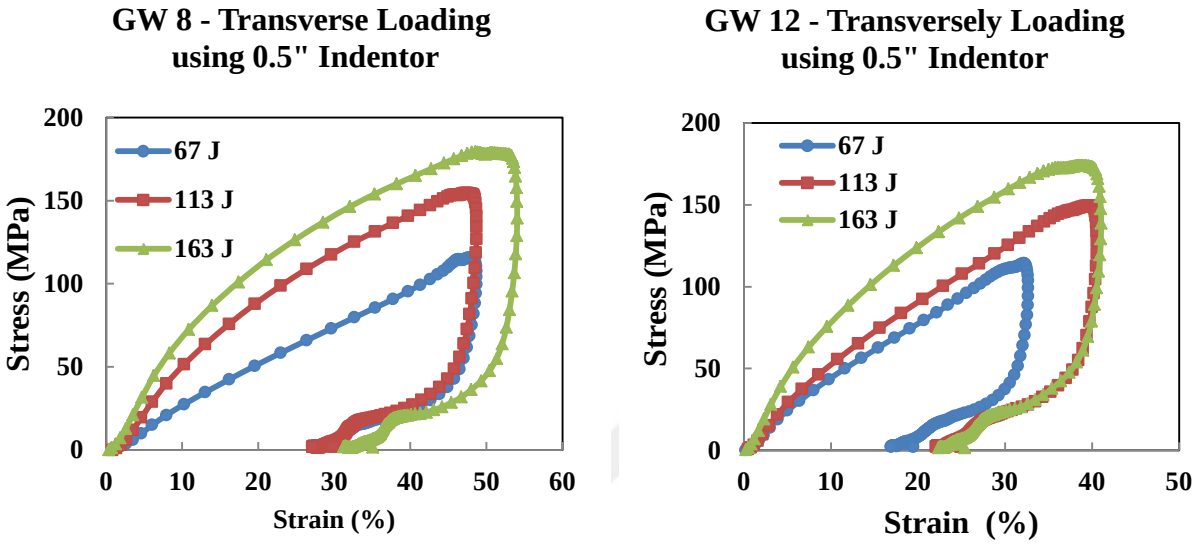

a) b)

Figure 4.22 Stress - strain plot with varying impact energies for transversely loaded a) 8 ply and b) 12 ply specimens using 0.5″ indentor.

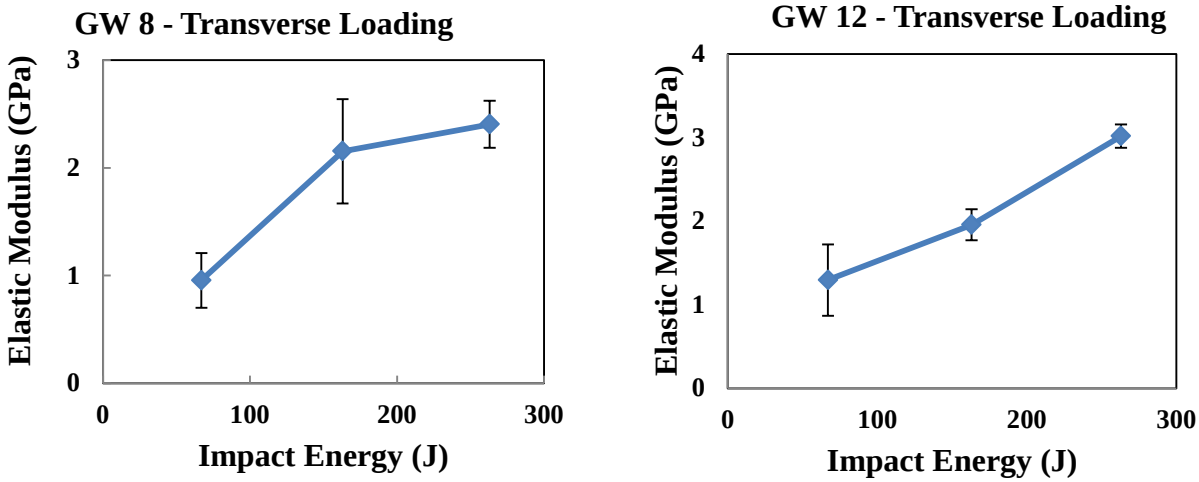

a) b)

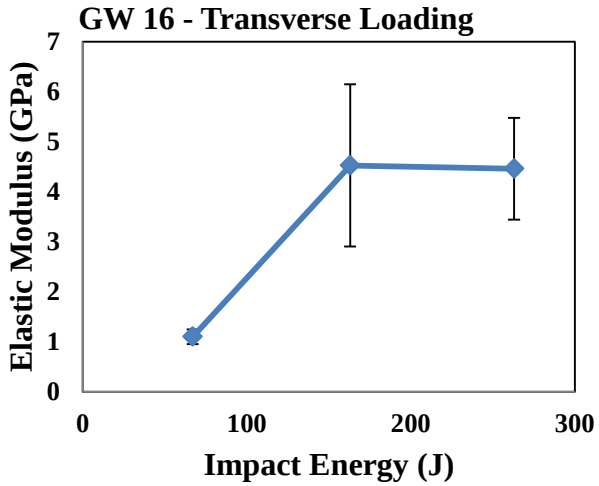

c)

Figure 4.23 Effect of the impact energy on the elastic modulus with experimental error for the a) 8 ply, b) 12 ply, and c) 16 ply specimens subjected to transverse loading.

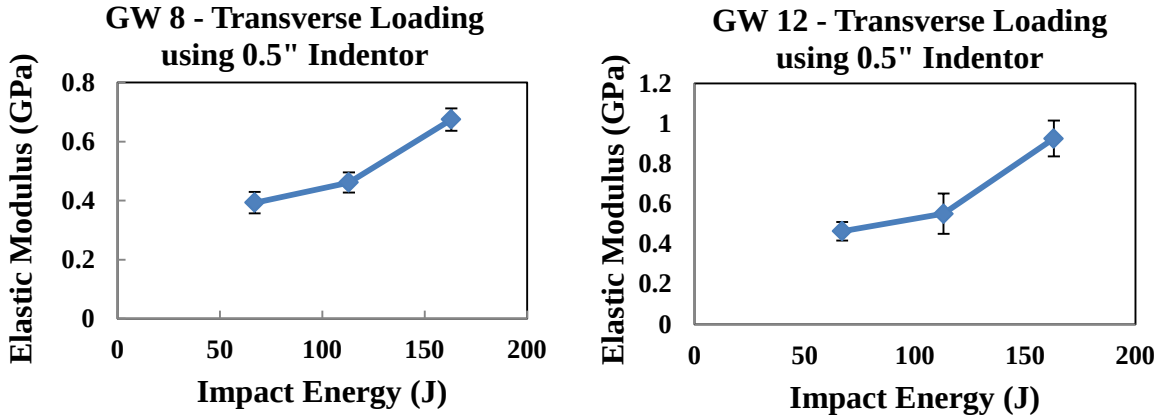

a) b)

Figure 4.24 Effect of the impact energy on the elastic modulus with experimental error for the a) 8 ply and b) 12 ply specimens subjected to transverse loading using a 0.5″ indentor.

Figure 4.25 and 4.26 show the effect of impact energy on the peak stress with experimental error for the transversely loaded specimens having same thicknesses without using and with using 0.5″ indentor, respectively.

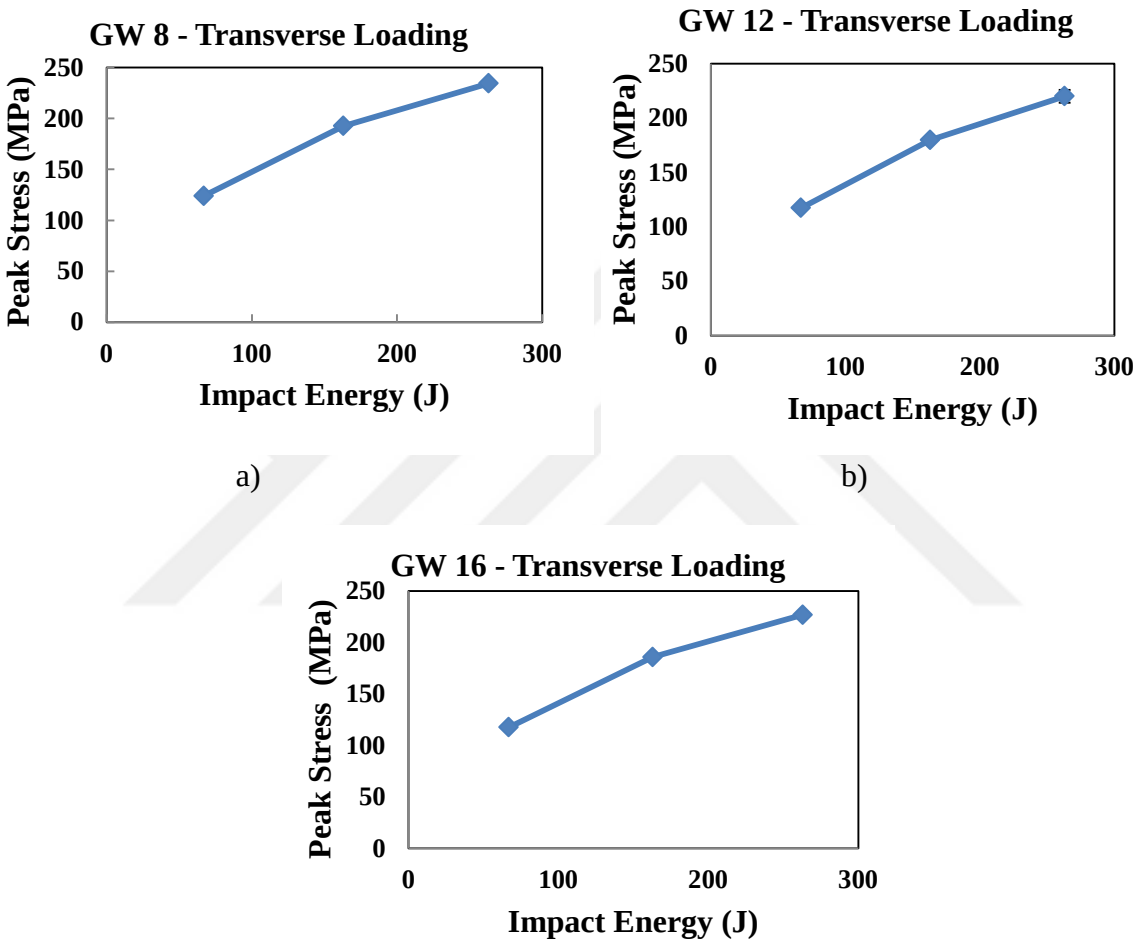

Figure 4.25 Effect of the impact energy on the peak stress with experimental error for the a) 8 ply, b) 12 ply, and c) 16 ply specimens subjected to transverse loading.

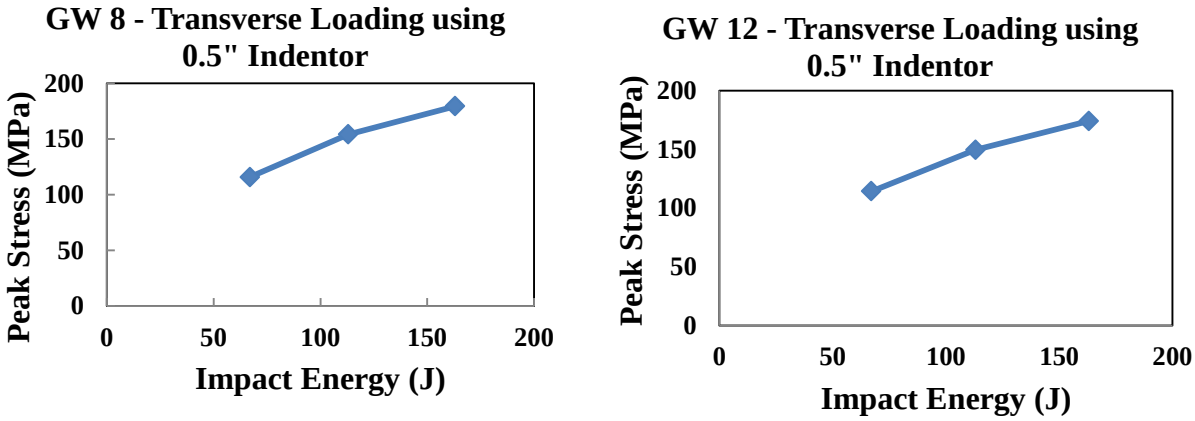

Figure 4.26 Effect of the impact energy on the peak stress with experimental error for the a) 8 ply and b) 12 ply specimens subjected to transverse loading using a 0.5″ indentor.

Figure 4.27 shows the effect of the impact energy on the stress – strain behavior for the specimens having same thicknesses and subjected to diametrical loading. Results indicate that stress – strain is dependent on impact energies. This dependence is expected because with increasing impact energy, the contact force and absorbed energy increase and therefore the stress that specimens experience increases. For transverse loading, peak stress increases with increasing impact energy without exhibiting dependence on thickness as shown in Figure 4.8. It is also important to note that residual strain in the transversely loaded specimens is almost independent of impact energy. This indicates that applied impact energies don't give the significant deformation to the specimens resulting almost same amount of permanent deformation within the specimen. However, when the smaller contact area is used, the residual strain in the specimen tends to increase due to the fact that smaller contact area gives large deformation to the specimens at the higher applied impact energy.

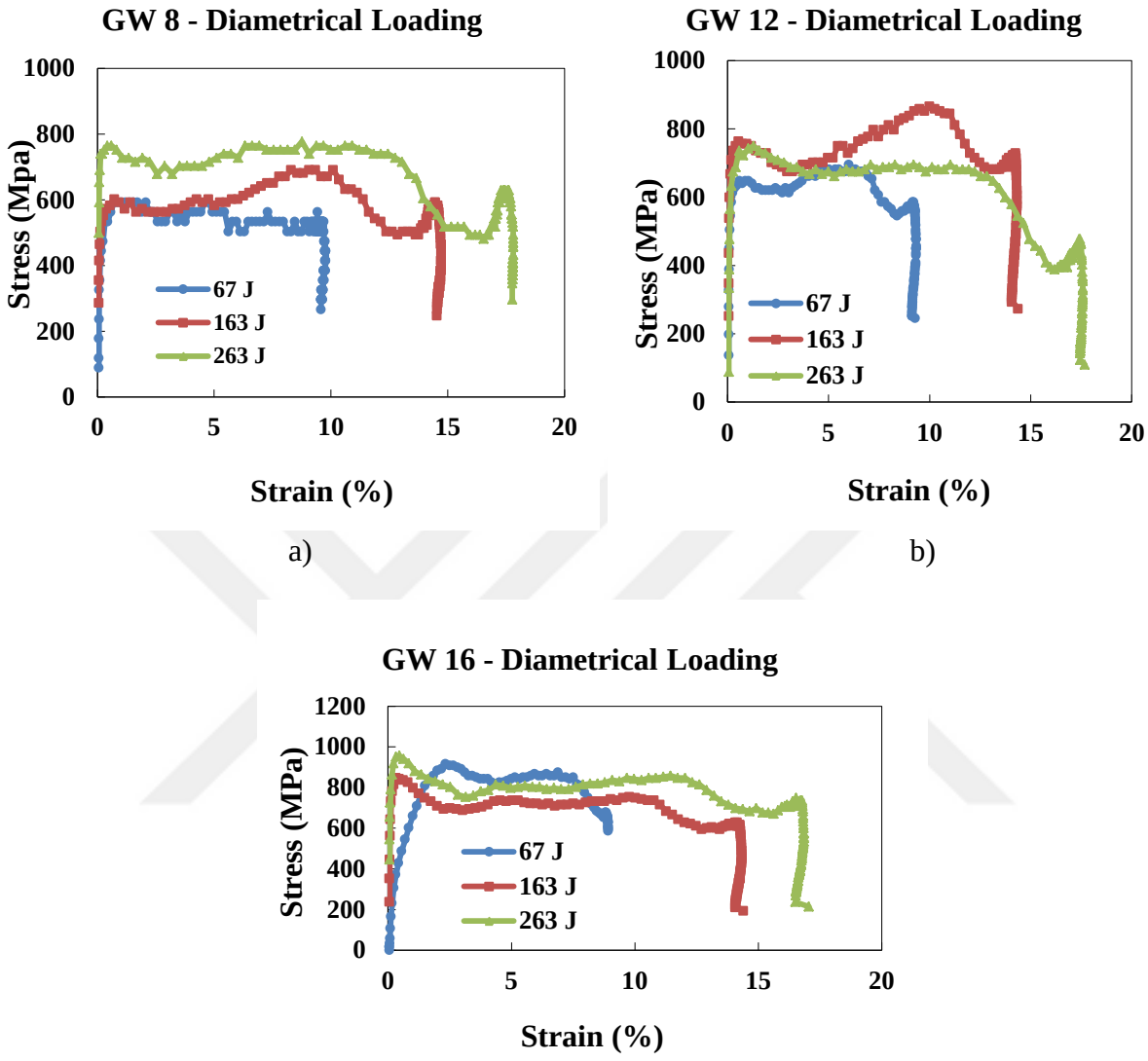

Figure 4.27 Stress - strain plot with varying impact energies for diametrically loaded a) 8 ply, b) 12 ply, and c) 16 ply specimens.

Figure 4.27 shows that the diametrically loaded specimens exhibit significant ductility which means absorbed energy is spent in deformation accumulation within the specimen. Figure 4.27 indicates that the ultimate stress is slightly increased with increasing impact energies for the specimens having same thicknesses. In addition, the ultimate failure strain in the specimen

increase with increasing applied energy indicating greater deformation occurs at the higher applied impact energy. Figure 4.28 and 4.29 show the effect of impact energy on the elastic modulus and ultimate strength with experimental error for the diametrically loaded specimens having same thicknesses, respectively.

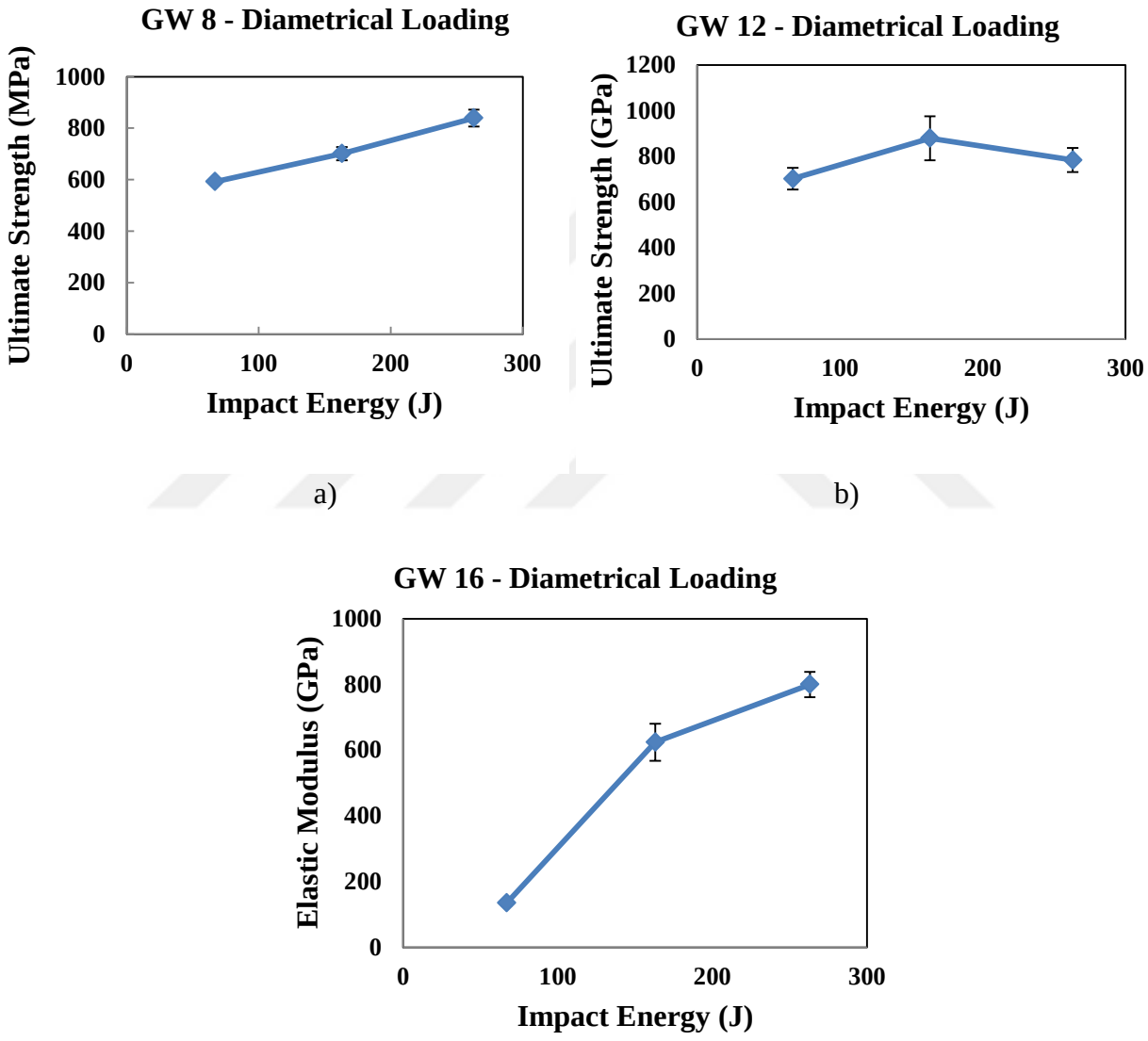

Figure 4.28 Effect of the impact energy on the elastic modulus with experimental error for the a) 8 ply, b) 12 ply, and c) 16 ply specimens subjected to diametrical loading.

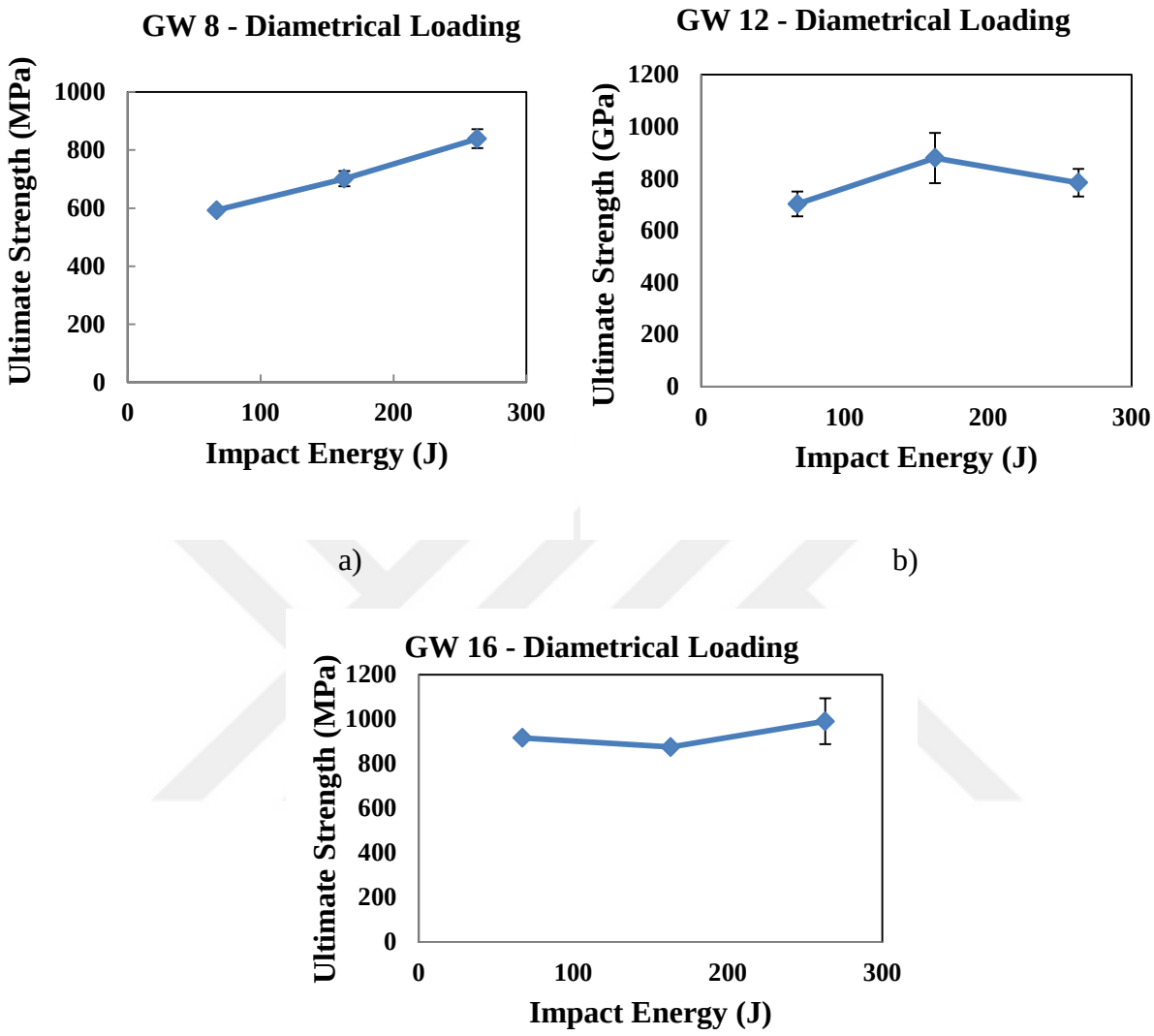

Figure 4.29 Effect of the impact energy on the ultimate strength with experimental error for the a) 8 ply, b) 12 ply, and c) 16 ply specimens subjected to diametrical loading.

4.2.3 Effect of Impact Energy on Strain Rate

Figure 4.30 and 4.31 show the effect of impact energy on strain rate – strain behavior for the specimens having same thicknesses and subjected to the transverse loading without using and with using 0.5 ″ indentor, respectively. Figures 4.30 and 4.31 show that strain rate for the same thickness increases with the increase in impact energy because the energy absorbed and consequently the deformation rate are higher for the higher impact energy for transverse loading case.

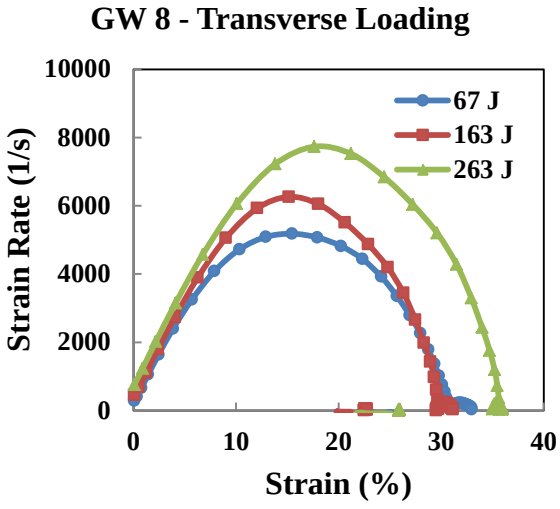

a)

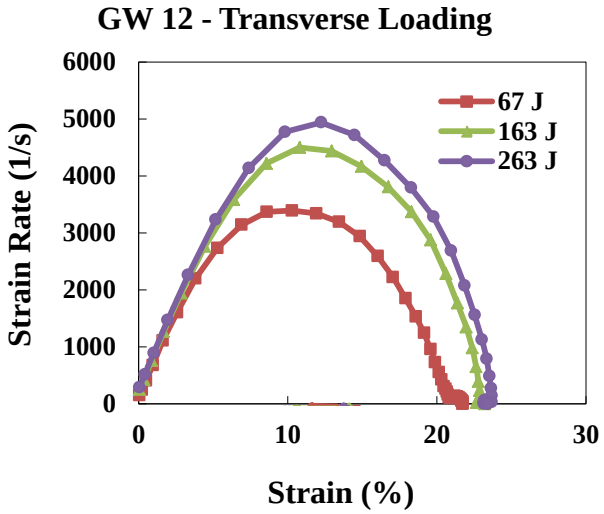

b)

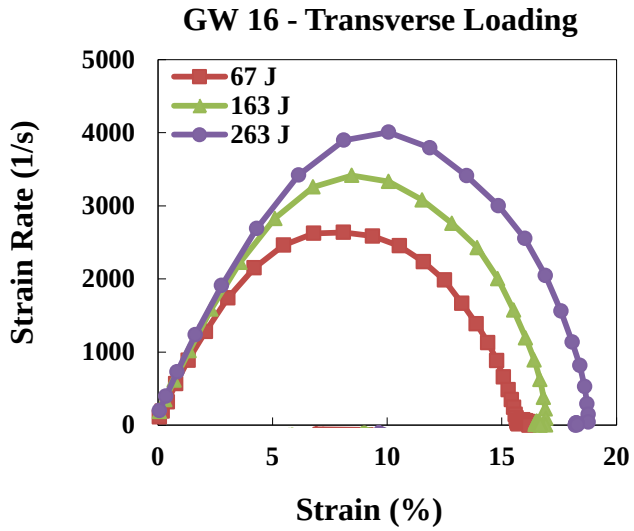

c)

Figure 4.30 Strain rate - strain plot with varying impact energies for transversely loaded a) 8 ply, b) 12 ply, and c) 16 ply specimens.

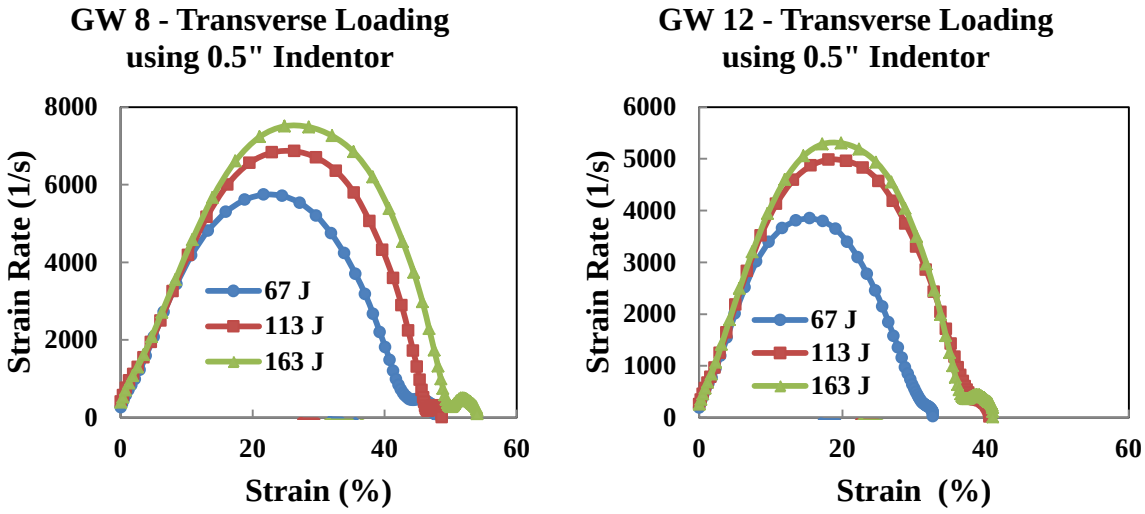

a) b)

Figure 4.31 Strain rate - strain plot with varying impact energies for transversely loaded a) 8 ply and b) 12 ply specimens using 0.5″ indentor.

Figure 4.32 and 4.33 show the effect of impact energy on the peak strain rate with experimental error for the transversely loaded specimens having same thicknesses without using and with using 0.5″ indentor, respectively.

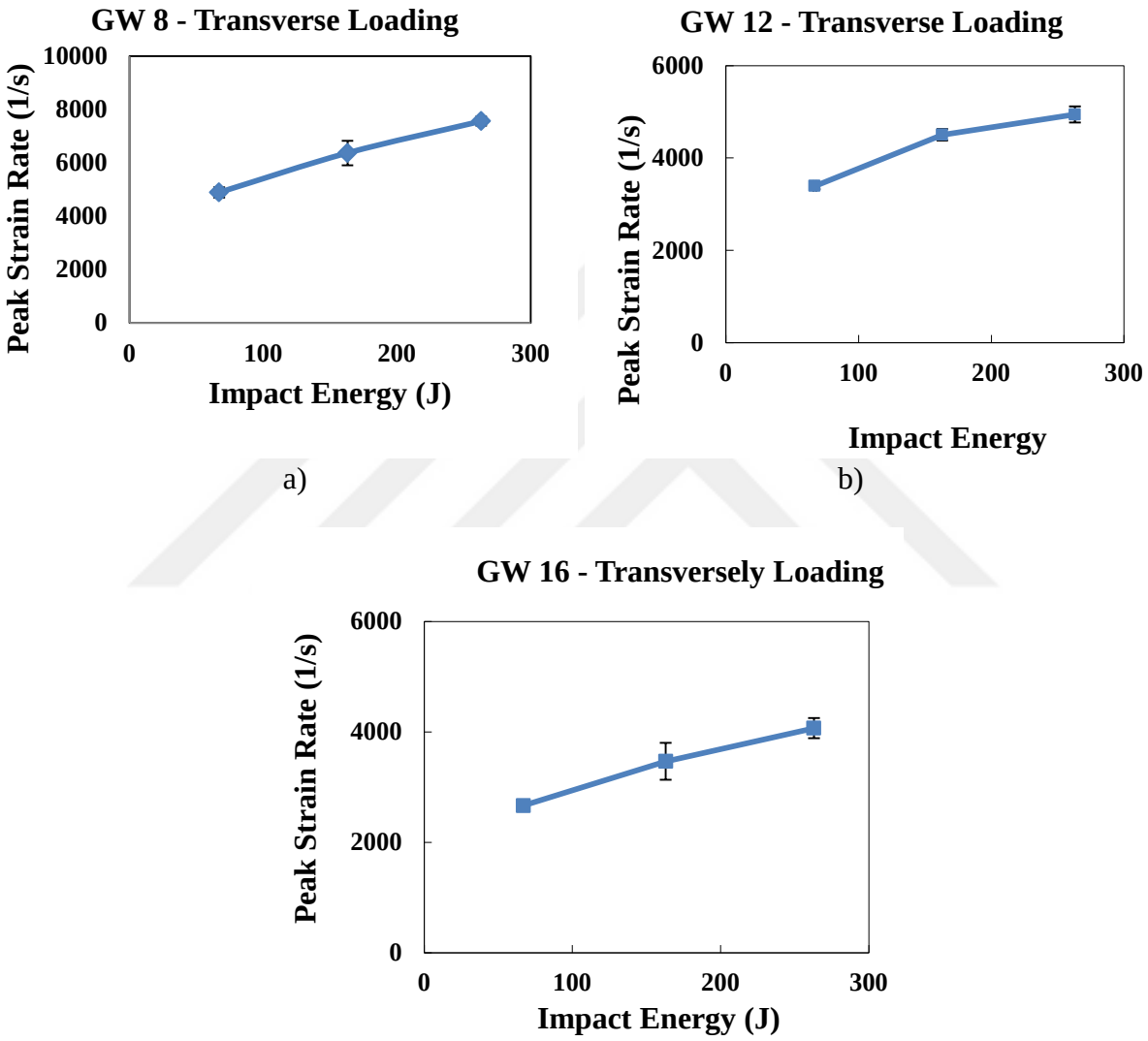

Figure 4.32 Effect of the impact energy on the peak strain rate with experimental error for the a) 8 ply, b) 12 ply, and c) 16 ply specimens subjected to transverse loading.

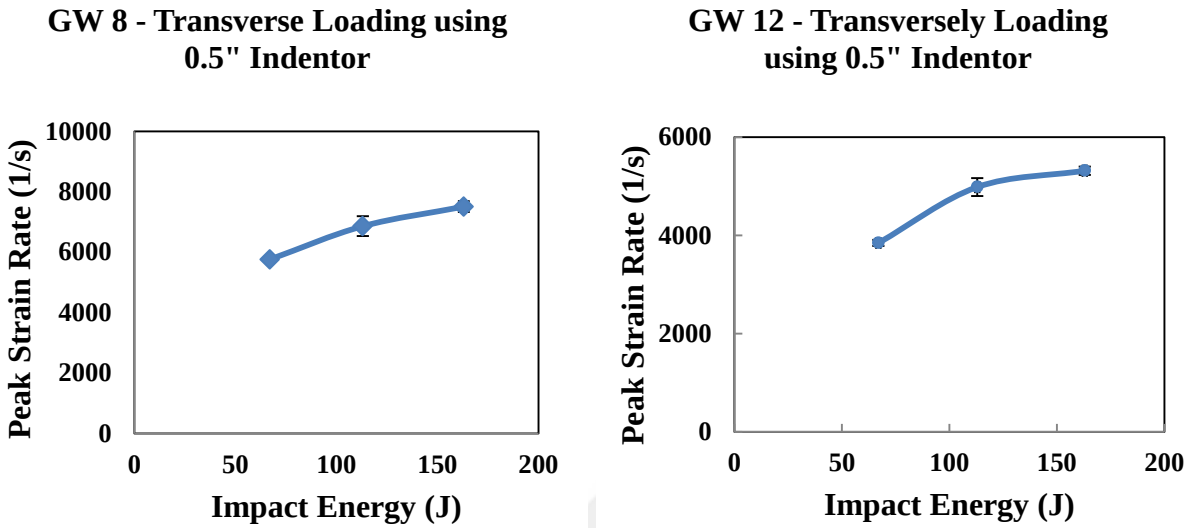

Figure 4.33 Effect of the impact energy on the peak strain rate with experimental error for the a) 8 ply and b) 12 ply specimens subjected to transverse loading using a 0.5″ indentor.

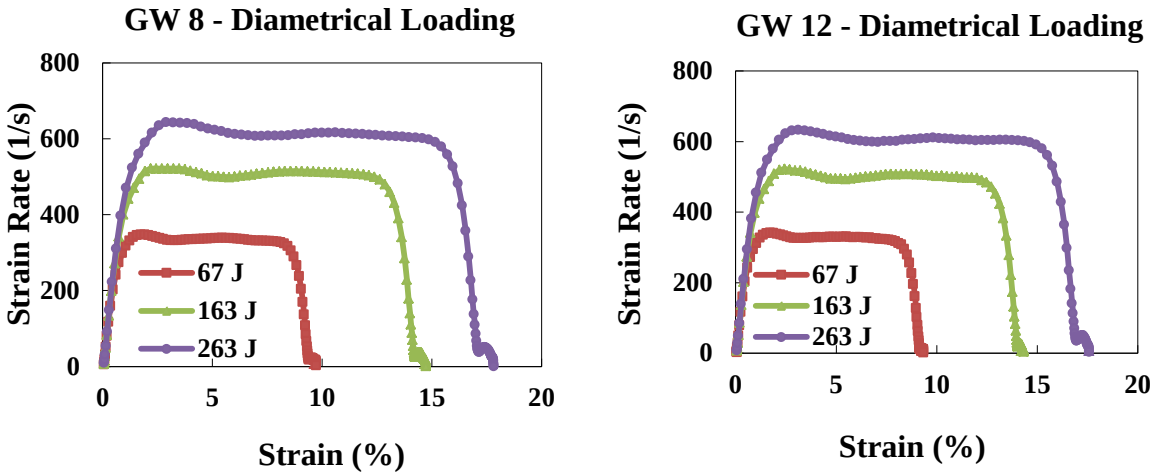

a) b)

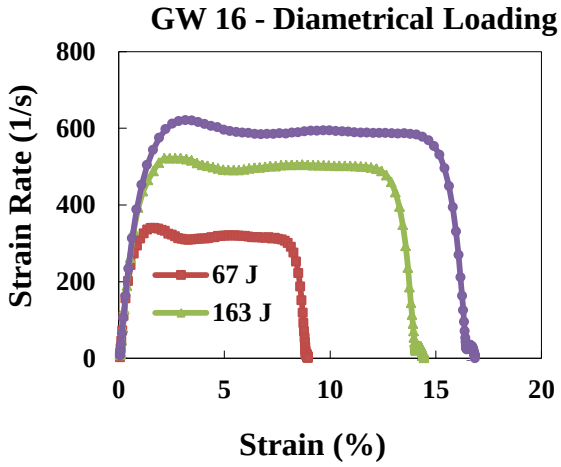

c)

Figure 4.34 Strain rate - strain plot with varying impact energies for diametrically loaded a) 8 ply, b) 12 ply, and c) 16 ply specimens.

Figure 4.34 shows the effect of impact energy on strain rate – strain behavior for the specimens having same thicknesses and subjected to the diametrical loading. As it is expected, with increasing impact energy, the maximum strain rate increases for the specimens having same thicknesses. Figure 35 shows the effect of impact energy on the peak strain rate with experimental error for the diametrically loaded specimens having same thicknesses.

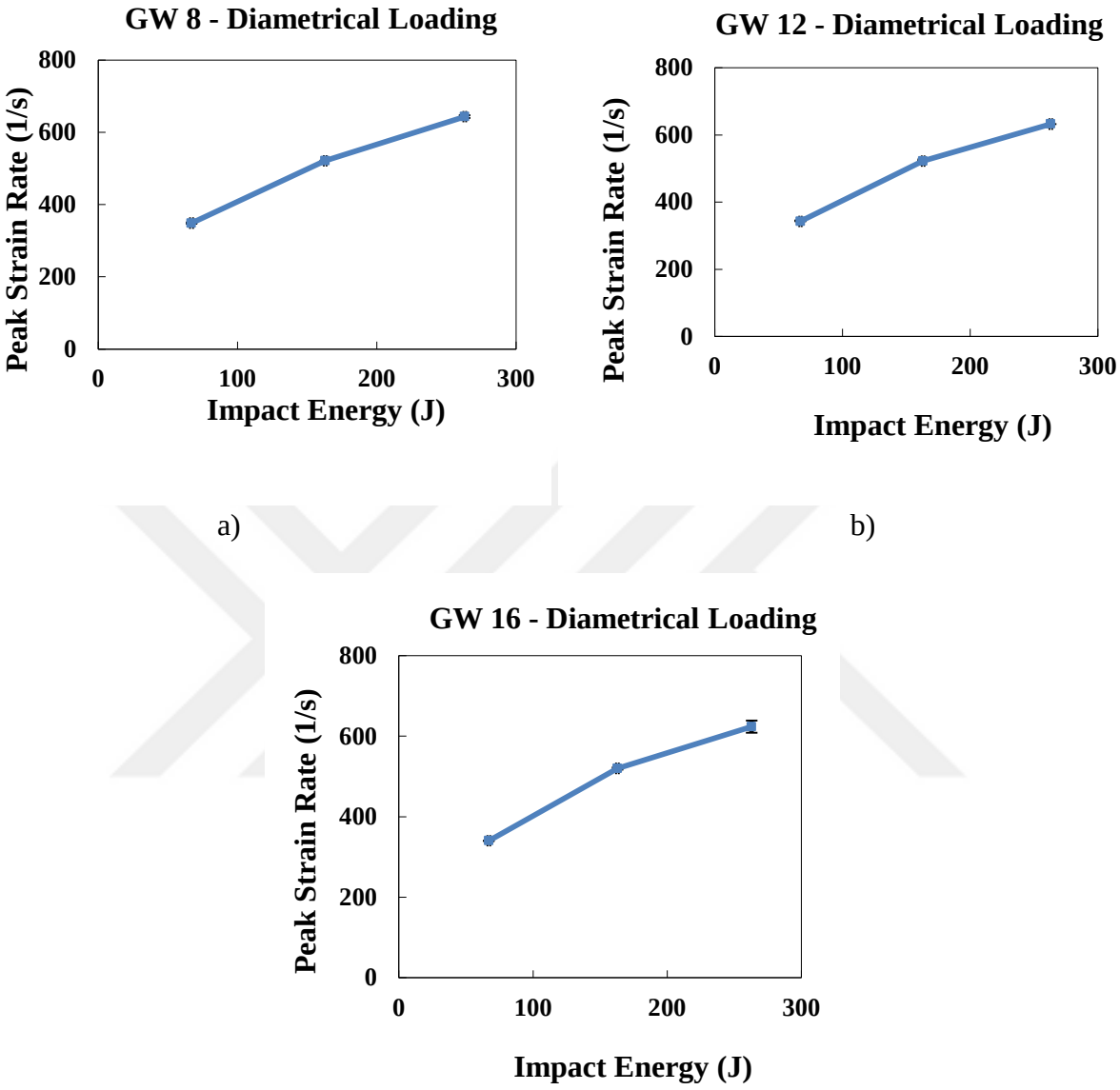

a) b)

c)

Figure 4.35 Effect of the impact energy on the peak strain rate with experimental error for the a) 8 ply, b) 12 ply, and c) 16 ply specimens subjected to diametrical loading.

4.3 EFFECT OF LOADING DIRECTION ON DAMAGE PARAMETERS

Typical results for specimens loaded transversely and diametrically are shown in Figures 3.5 and 3.6. Although transversely loaded specimens have no visible damage even at highest applied energy level of 263 J, visible damage can be observed even at lowest applied energy level of 67 J as shown in Figure 4.36 and 4.37. As it is seen, the visible failure level increases with increasing applied impact energy.

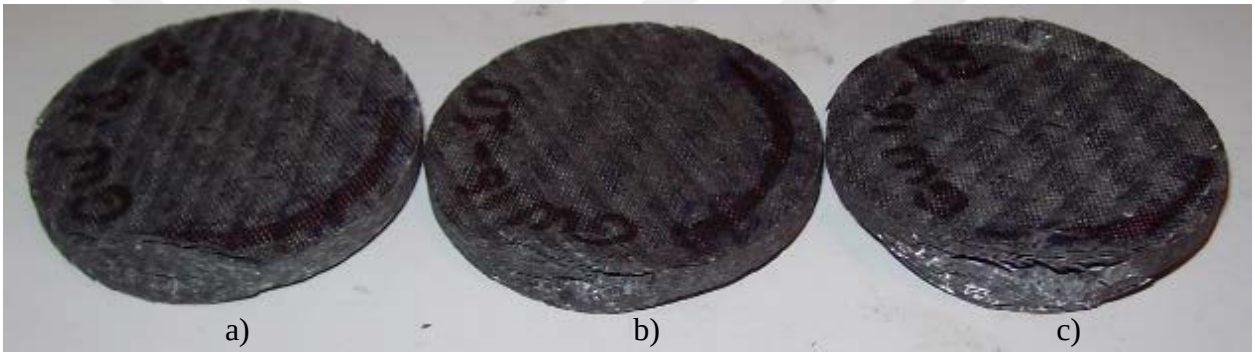

Figure 4.36 Diametrically loaded 16 ply graphite/epoxy composites at the applied impact energies of a) 67 J, b) 163 J, and c) 263 J.

Figure 4.37 Representative transversely loaded specimen showing no visible damage.

4.3.1 Effect of Loading Direction on the Energy Absorbed

Figures 4.38 – 4.40 show the effect of specimen geometry on the energy absorbed at same impact energies for the specimens having same thicknesses. It is clearly seen that the significant

amount of impact energy is absorbed in the case of transverse loading compared to the case of diametrical loading. This is due to the fact that no significant amount of energy is spent in the permanent damage process but only friction and heating consumes the applied impact energy for transverse loading case although the visible permanent damage occurs in the specimens subjected to the diametrical loading requiring significant energy consumption. Therefore, in the case of transverse loading, reflected wave is negligible allowing almost all incident wave transverse to the transmitted bar indicating that there is no significant damage, however, in the case of diametrical loading, reflected wave is quite significant and consequently the transmitted wave is almost zero indicating that there is a significant damage process as shown in Figure 2.2. As it is discussed earlier, reduction in the energy absorption is the indication of energy release for the diametrical loading case because of tensile stress the incident bar experiences after unloading stage.

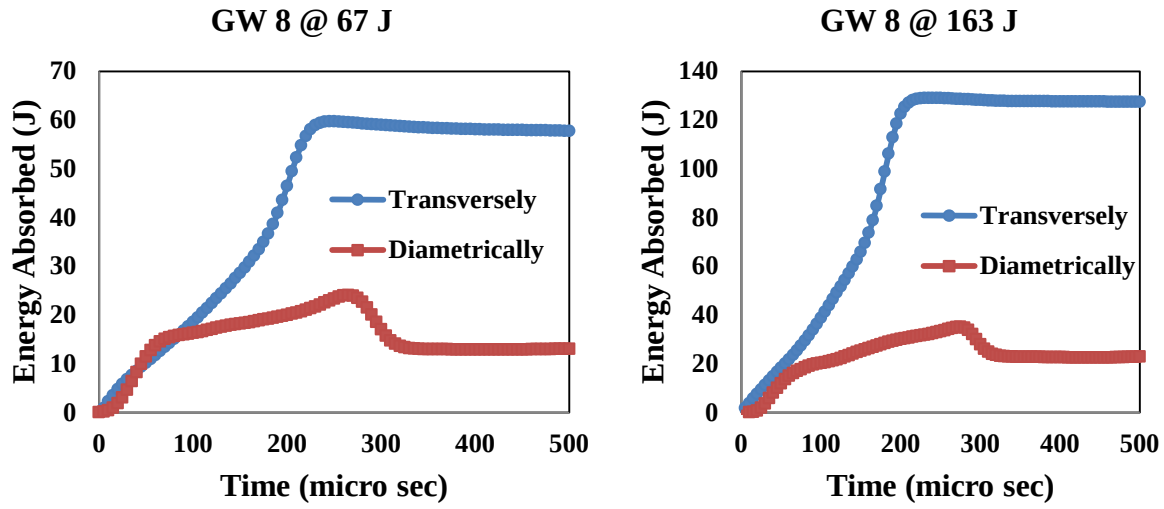

a) b)

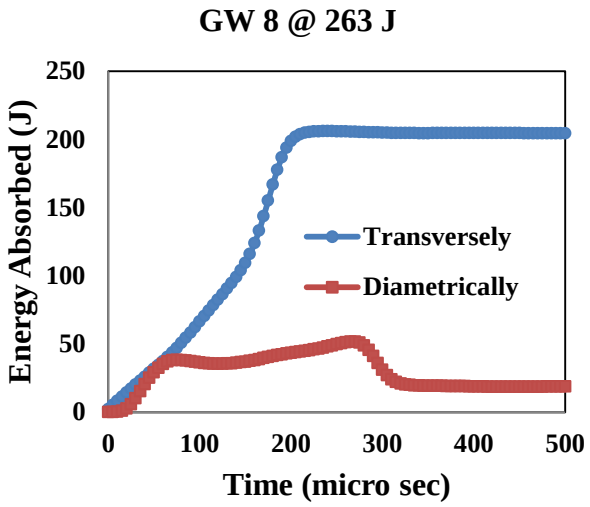

c)

Figure 4.38 Effect of the loading direction on the energy absorbed for 8 layers specimens at the same impact energy of a) 67 J, b) 163 J, and c) 263 J.

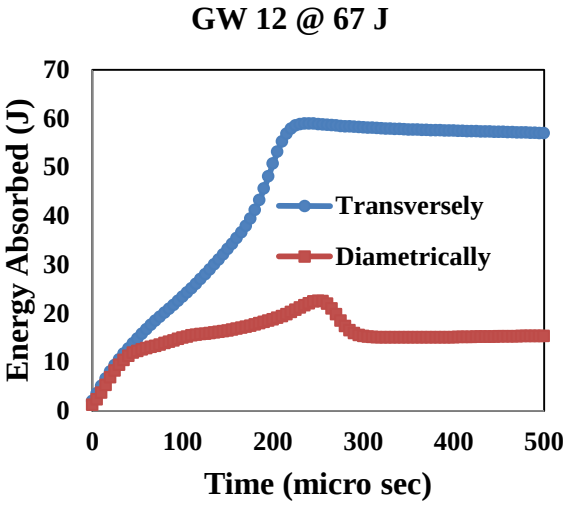

a)

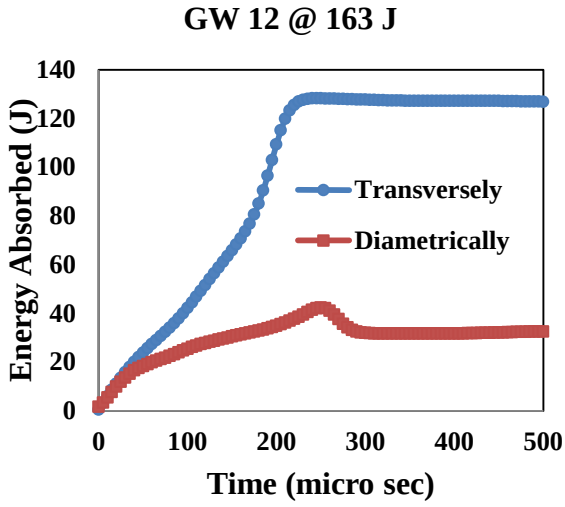

b)

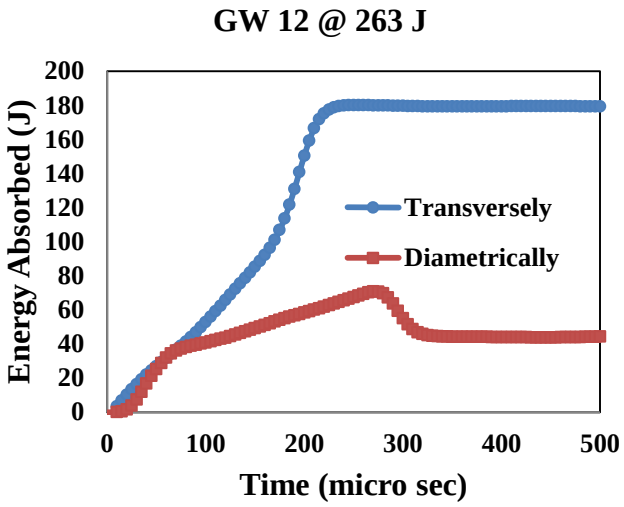

c)

Figure 4.39 Effect of the loading direction on the energy absorbed for 12 layers specimens at the same impact energy of a) 67 J, b) 163 J, and c) 263 J.

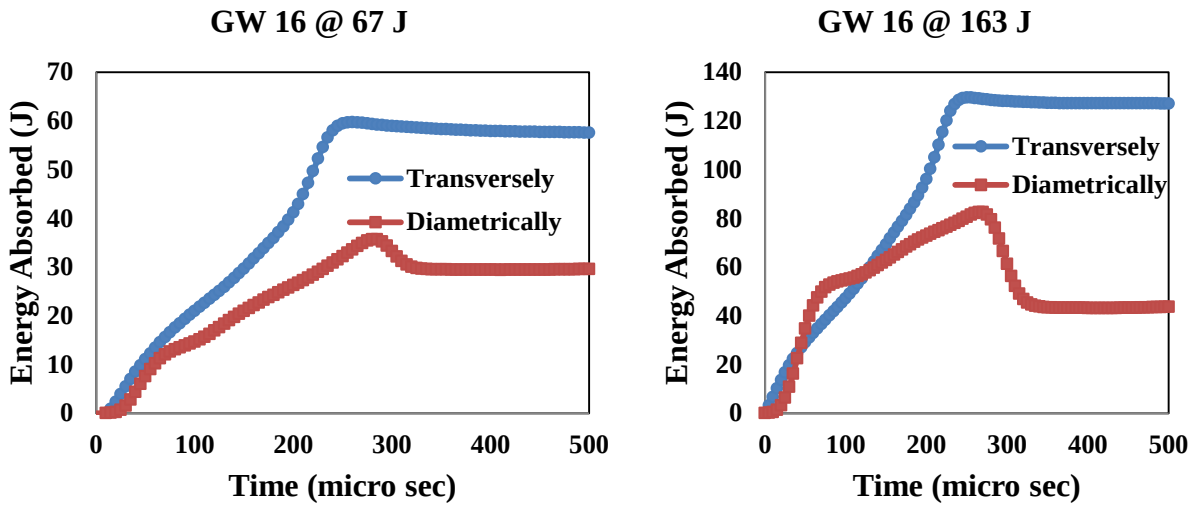

a) b)

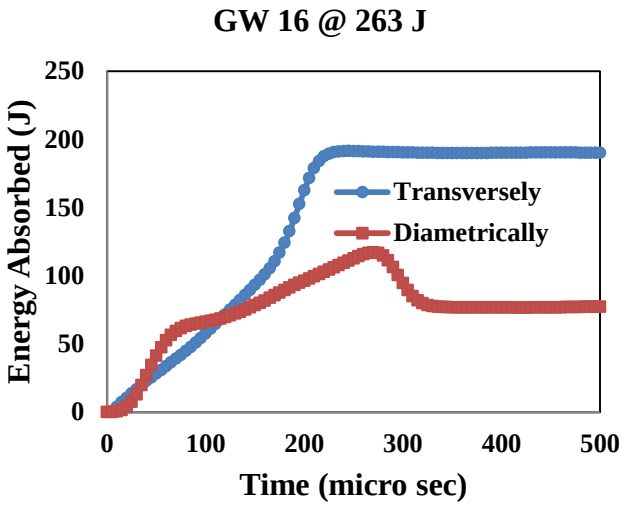

c)

Figure 4.40 Effect of the loading direction on the energy absorbed for 16 layers specimens at the same impact energy of a) 67 J, b) 163 J, and c) 263 J.

4.3.2 Effect of Loading Direction on Stress – Strain Behavior

The specimens subjected to transverse loading exhibit viscoplastic deformation while the specimens subjected to the diametrical loading exhibit completely plastic deformation. The nature of the boundary condition in the case of diametrical loading gives rise to change in the cross sectional area resulting stress concentration in the specimen as shown in Figure 3.7 – a. Stress is highly localized at the contact surface and therefore stress concentration has its highest value at the contact point. This means small portions of the specimen where the highly localized stresses occur absorb an excessive amount of energy before the main portion of the specimen can

be stressed appreciably and therefore before the main portion can be made to absorb an appreciable share of the energy delivered to the specimen. As a result, the small portion where the localized stress occurs is likely to be stressed above the yield stress of the material. Then the energy required to be absorbed may be great enough to cause plastic deformation. Hence, the greatest plastic deformation is observed in the contact surface of the specimen while main portion of the specimen is in overall integrity. Figure 4.41 shows the stress concentration in the diametrically loaded specimens.

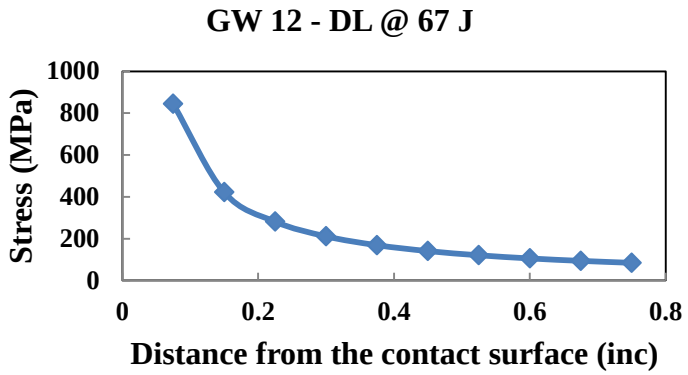

Figure 4.41 Stress concentration in the specimen with respect to the distance from contact surface.

4.3.3 Effect of Loading Direction on Strain Rate – Strain Behavior

Figures 4.42 – 4.44 show the effect of loading direction on strain rate – strain behavior for the specimens having same thicknesses at same impact energies. Even though high strain rate is observed in transversely loaded specimens, for diametrically loaded specimens the strain rate is substantially low in spite of the fact that visible damage occurs in the diametrical loading case. This behavior is due to the fact that transversely loaded specimens have significantly smaller initial length which is the main source that prevents fibers from being deformed. However,

longer initial length can make the deformation easier for fibers of diametrically loaded specimens. The flat region for the diametrical loading case corresponding to the maximum plastic deformation and damage accumulation cannot be observed for the transverse loading case because no significant damage occurs in this situation.

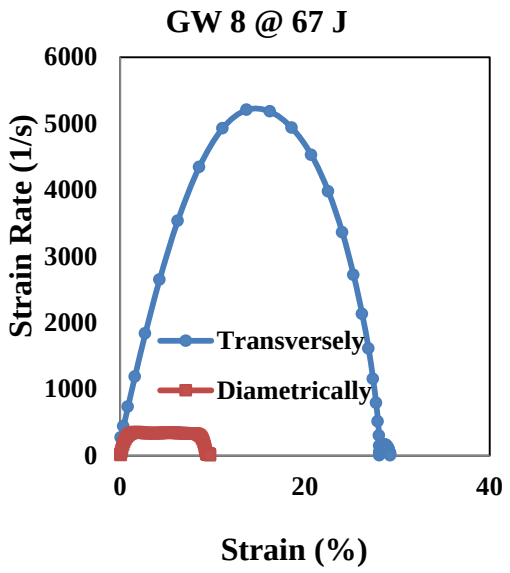

a)

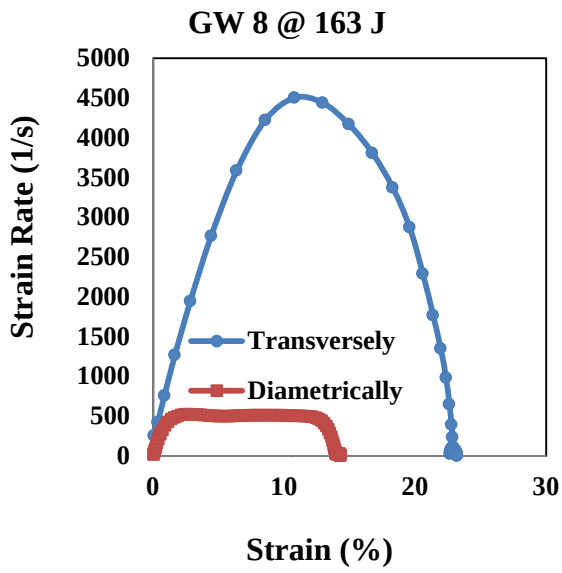

b)

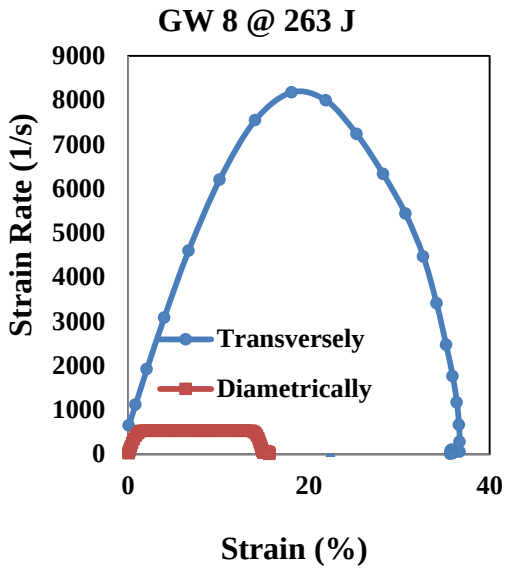

c)

Figure 4.42 Effect of the loading direction on strain rate behavior for 8 layers specimens at the same impact energy of a) 67 J, b) 163 J, and c) 263 J.

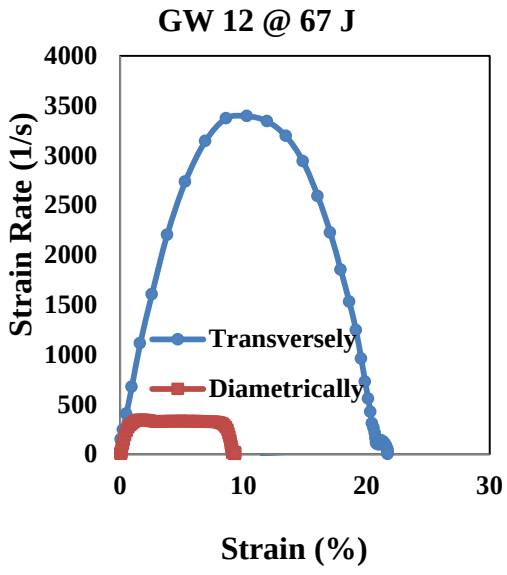

a)

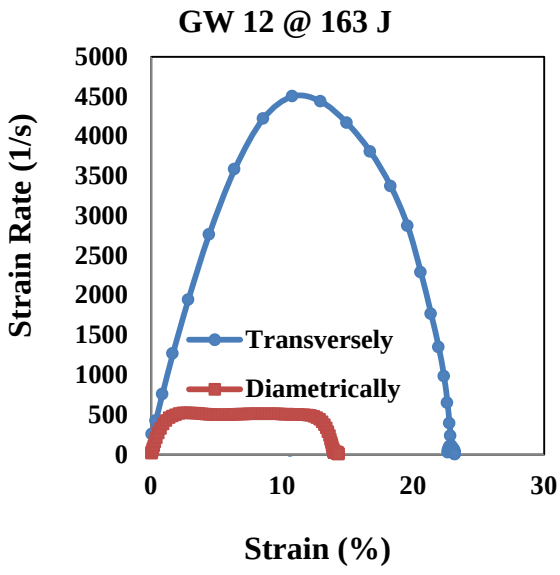

b)

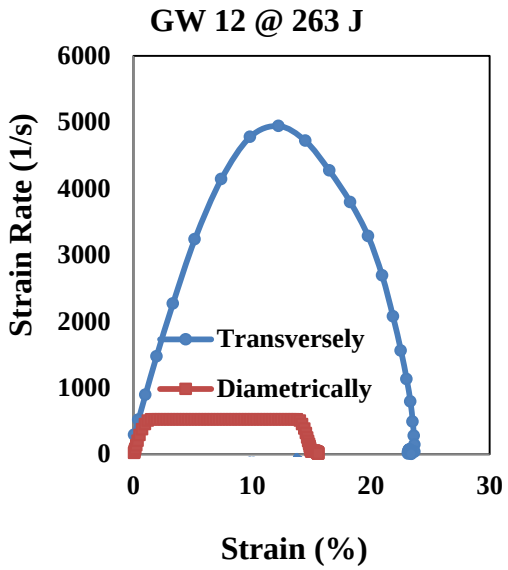

c)

Figure 4.43 Effect of the loading direction on strain rate behavior for 12 layers specimens at the same impact energy of a) 67 J, b) 163 J, and c) 263 J.

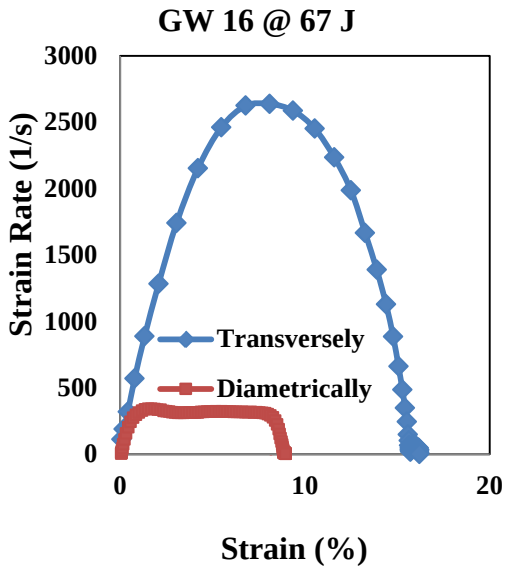

a)

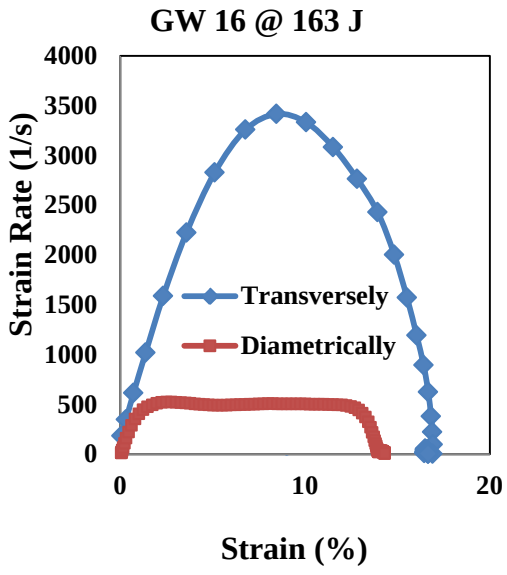

b)

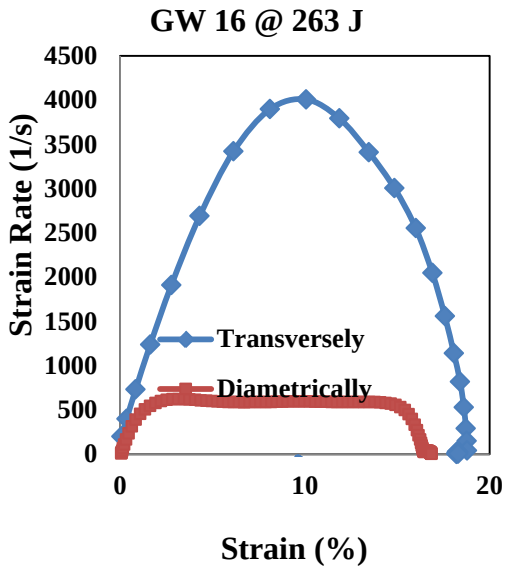

c)

Figure 4.44 Effect of the loading direction on strain rate behavior for 16 layers specimens at the same impact energy of a) 67 J, b) 163 J, and c) 263 J.

Figure 4.45 shows that use of the diameter of diametrically loaded specimens as the thickness satisfy the assumption of short specimen. In data reduction process, strain rate in equation 2.14 is calculated for short specimens assuming that $\varepsilon_t = \varepsilon_i + \varepsilon_r$. The question was if this assumption was satisfied in the case for the diametrical loading specimens using equation 2.11 and the diameter as the thickness (since the loading is diametrically applied). Comparison of the two in Figure 4.32 shows no appreciable difference in the results.

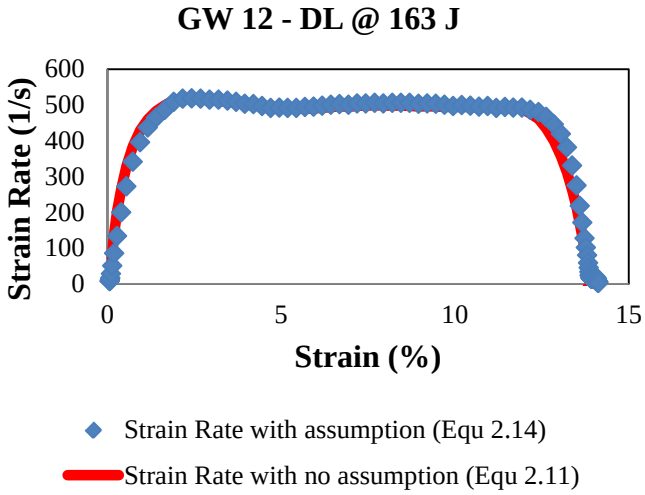

Figure 4.45 Showing diametrical loaded specimens can be count as short specimens.

4.4 EFFECT OF DIFFERENT CONTACT GEOMETRY ON THE DAMAGE PARAMTERES OF TRANSVERSELY LOADED SPECIMENS

4.4.1 Effect of Contact Geometry on the Energy Absorbed

Figure 4.46 and 4.47 show the effect of contact geometry on the energy absorbed at the same impact energies for 8 ply and 12 ply specimens, respectively. At each impact energy, it is observed that the specimens loaded with 0.5″ indentor have a tendency to show reduction in the energy absorbed after the peak energy absorbed while the specimens loaded without using indentor do not exhibit any significant reduction in the energy absorbed. This is because of the release of the strain energy stored during loading stage and this suggests that the plastic deformation of the specimens is higher when the indentor is used because strain energy release occurs when the materials experienced plastic deformation. Peak energy absorption and the

energy retained by the specimen tend to be higher when the smaller contact area is used. This is expected because more deformation occurs in the specimen for the same applied energy. It should be noted that the slope changes in the linear curve when the specimen is loaded using indentor. This is due to the fact that there is an impedance mismatch between indentor and the bars.

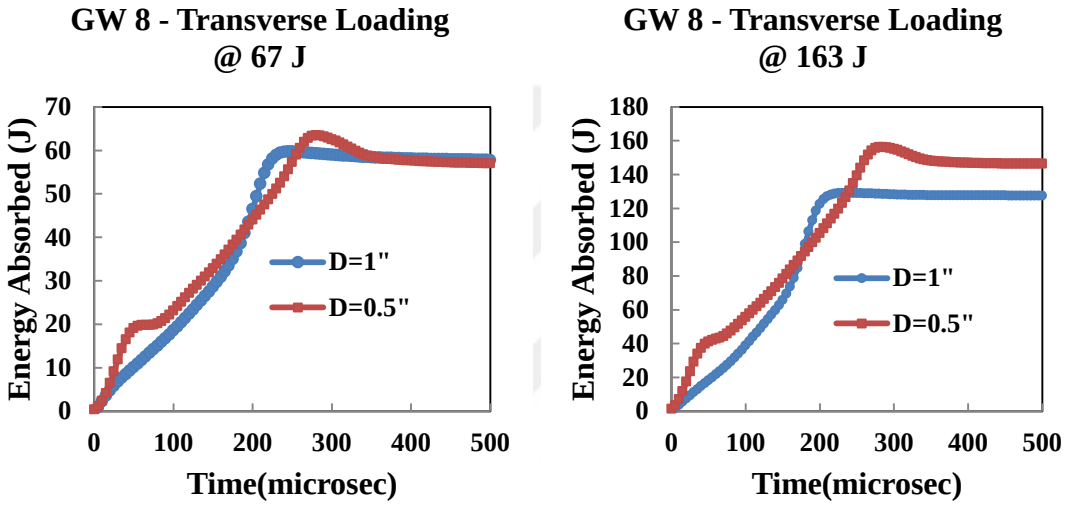

a) b)

Figure 4.46 Effect of the contact geometry the energy absorbed by transversely loaded 8 ply specimens for the same impact energies.

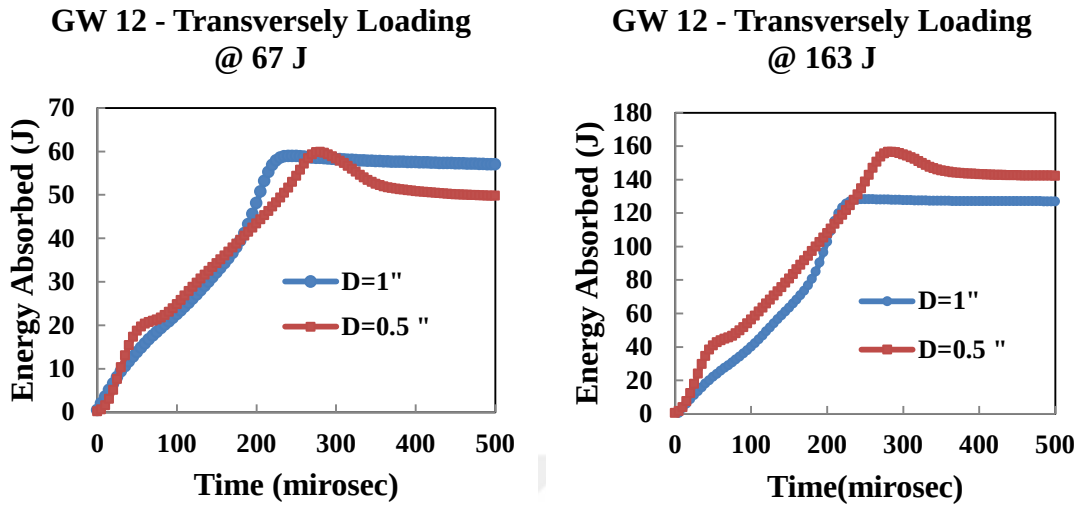

a) b)

Figure 4.47 Effect of the contact geometry the energy absorbed by transversely loaded 12 ply specimens for the same impact energies.

4.4.2 Effect of Contact Geometry on Stress – Strain Behavior

Figures 4.48 and 4.49 show the effect of contact geometry on the stress - strain behavior at the same impact energies for 8 ply and 12 ply specimens, respectively. As it is expected, the smaller contact area gives larger deformation to the specimens and the peak stress is slightly lower resulting in higher elastic modulus for the specimens loaded without using indentor.

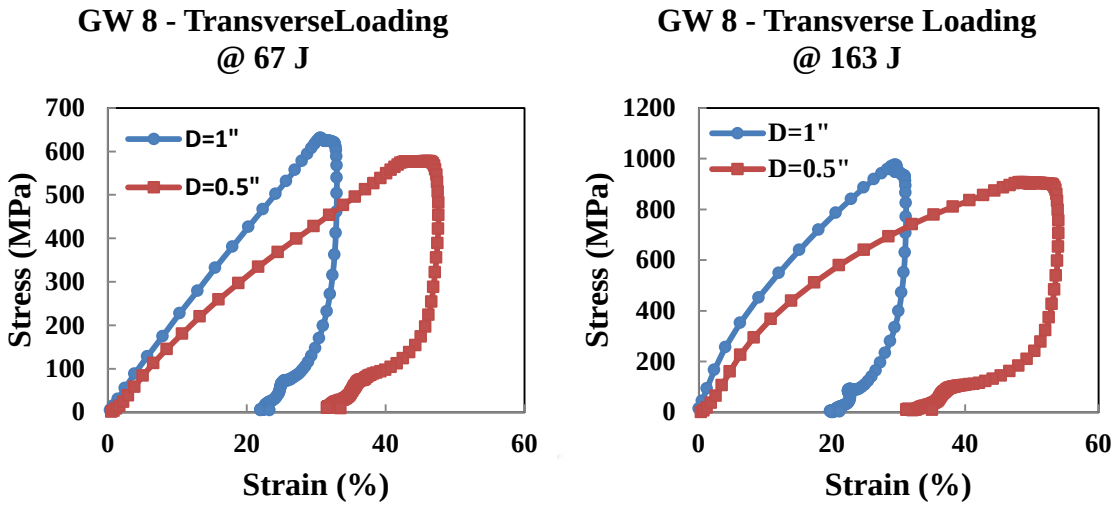

a) b)

Figure 4.48 Effect of the contact geometry on the stress – strain behavior of transversely loaded 8 ply specimens for the same impact energies.

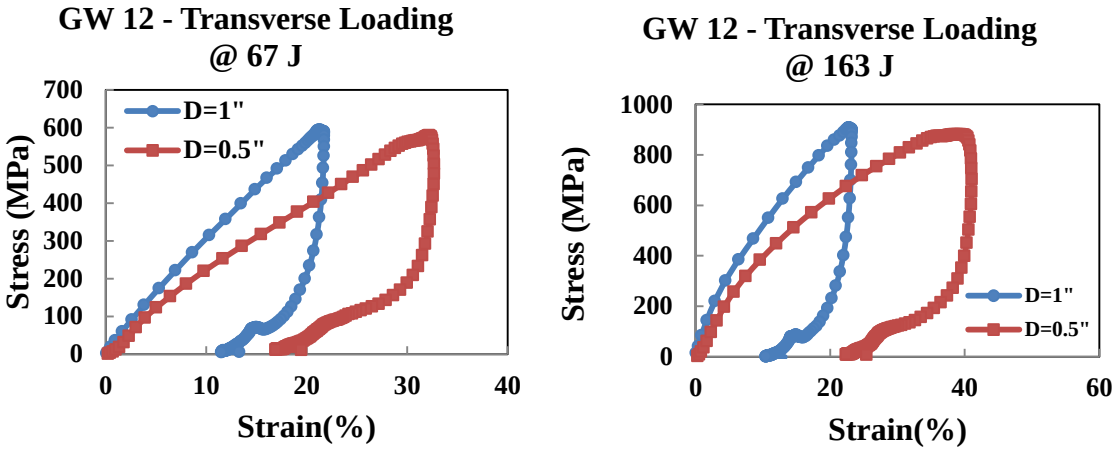

a) b)

Figure 4.49 Effect of the contact geometry on the stress – strain behavior of transversely loaded 12 ply specimens for the same impact energies.

4.4.3 Effect of Contact Geometry on Strain Rate – Strain Behavior

Figures 4.50 and 4.51 show the effect of contact geometry on the stress - strain behavior at the same impact energies for 8 ply and 12 ply specimens, respectively. It is clearly seen that smaller contact area gives higher deformation rate to the transversely loaded specimens since greater deformation and, consequently higher reflection occurs when the indentor is used.

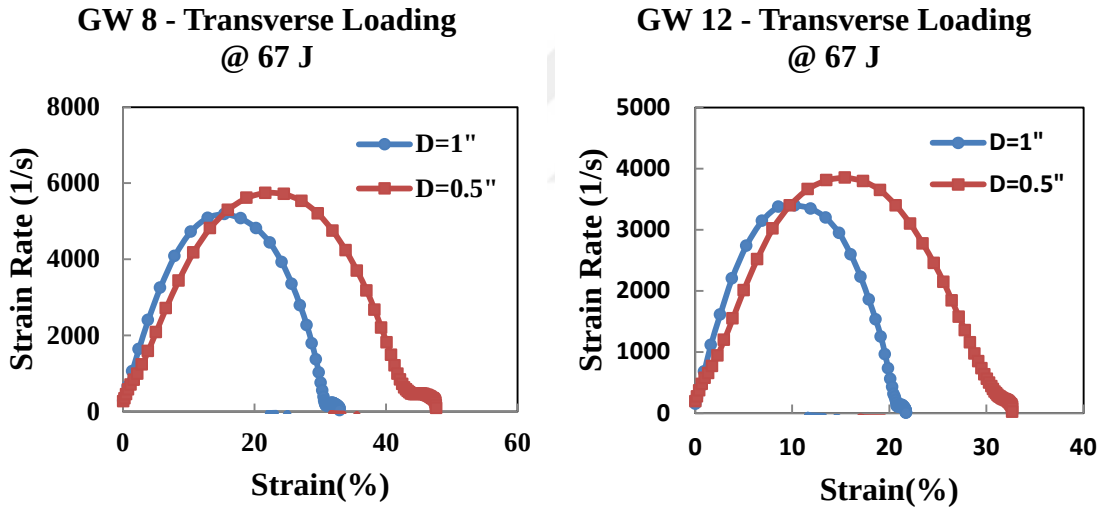

a) b)

Figure 4.50 Effect of the contact geometry on the stress – strain behavior of transversely loaded a) 8 ply and b) 12 ply specimens at 67 J of impact energy.

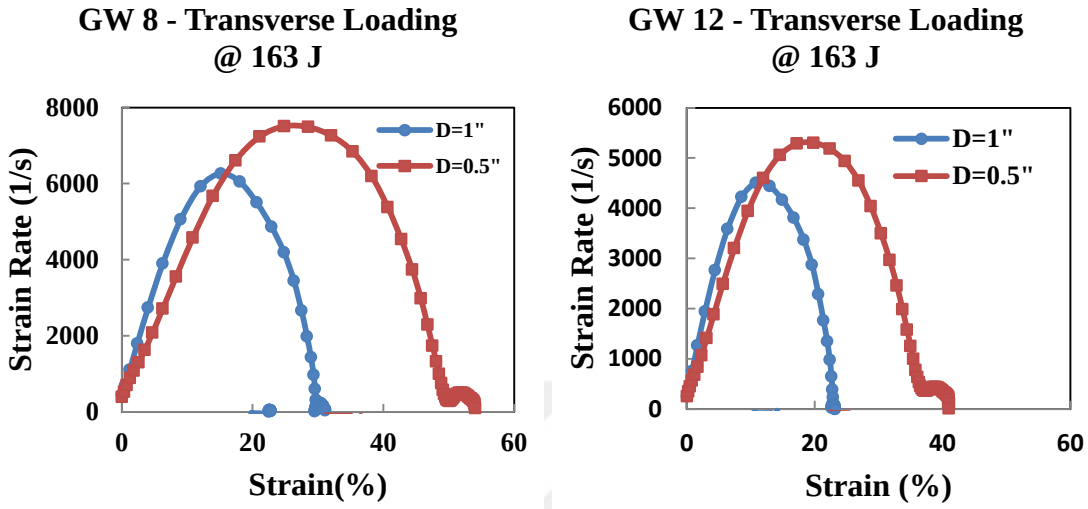

a) b)

Figure 4.51 Effect of the contact geometry on the strain rate – strain behavior of transversely loaded a) 8 ply and b) 12 ply specimens at 163 J of impact energy.

4.5 EFFECT OF FIBER DIRECTION ON DAMAGE PARAMETERS

Figure 4.52 – 4.54 show the effect of fiber direction on damage parameters for the diametrically loaded specimens. Results reveal that specimens exhibit higher peak energy absorption, ultimate strength along the fiber direction. Even though strain rate is same at two different directions, strain energy release is higher along the fiber direction. This suggests that the fibers are more likely tend to extent along the fiber direction as it is expected because the nature of the intersection of two fibers in the off direction prevents fibers to extend freely.

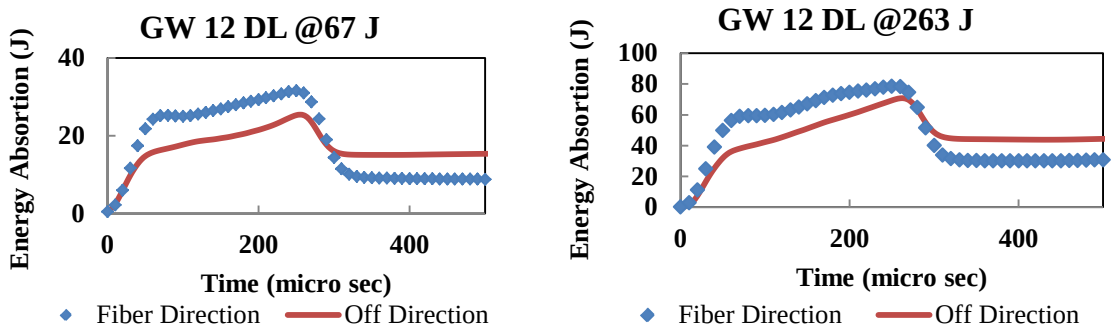

a) b)

Figure 4.52 Effect of fiber direction on energy absorption for diametrically loaded specimens at a) 67 J and b) 263 J.

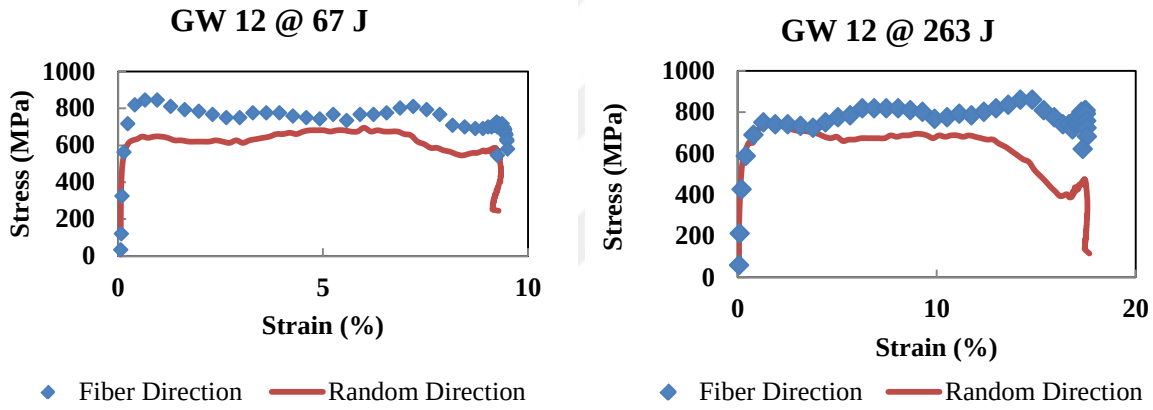

a) b)

Figure 4.53 Effect of fiber direction on stress - strain behavior of diametrically loaded specimens at a) 67 J and b) 263 J.

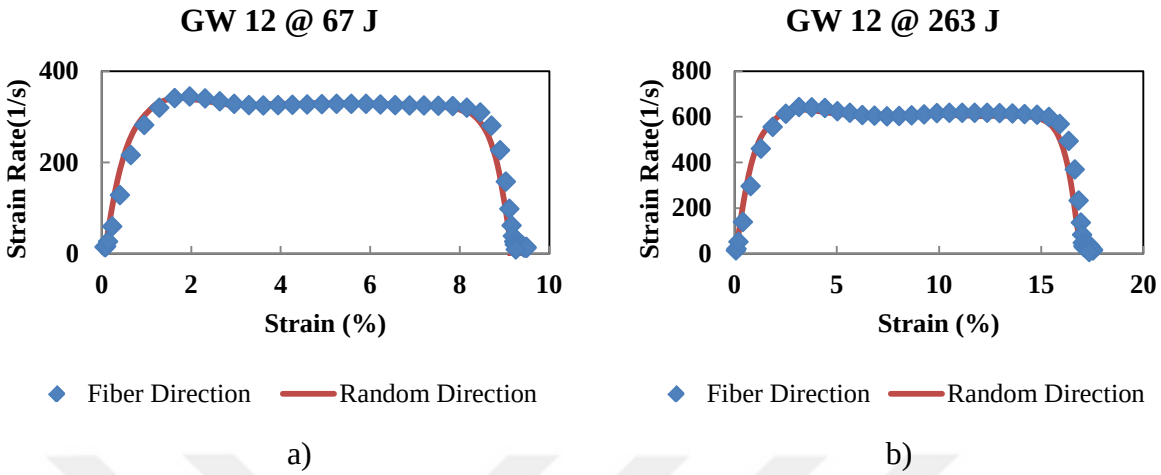

Figure 4.54 Effect of fiber direction on strain rate - strain behavior of diametrically loaded specimens at a) 67 J and b) 263 J.

5.0 SURFACE ANALYSIS

5.1 RAMAN

5.1.1 Background

Raman spectroscopy is an analytical technique that yields information about the molecular structure of materials based on the observation of scattered light spectra. Raman spectroscopy is sensitive to molecular interactions in materials such as Kevlar, graphite, and carbon used as reinforcement in composites [22 - 24]. These studies have also shown that Raman spectroscopy is applicable for strain measurement.

Raman spectroscopy is basically the measurement of the intensity and frequency of photons inelastically (with different frequency than the incident light) scattered from molecules, where the energy of the photon is shifted from the incident energy due to change from vibrational energy of the molecule. When a composite is irradiated with a laser beam, strong Raman scattering occurs due to the inherent vibration modes of atomic bonds in the crystal fiber within the composite. If the energy is transferred from a molecule to the photon, light of higher energy (lower wavelength) will be scattered by the material referred to as anti – stokes scattering.

If the energy of the incident photon is transferred from the photon to the molecule, light of the lower energy (higher wavelength) will be scattered by the material referred to stokes scattering. The amount of energy between the incident photon and Raman scattered photon gives the energy of vibration of a scattering molecule. A plot of intensity of scattered light versus energy difference gives the Raman spectrum. The frequency shifts are dependent upon the specific molecular geometry which means that frequency shifts also depend on the externally applied load since loading changes the molecular geometry that are different in all substances. The peak frequency shifts to a lower value under tension due to increasing bond length between atoms and to a higher value under compression due to decreasing bond length between atoms and therefore the level of stress or strain of the fiber through the shift of the peak frequency can be measured. This relationship between vibrational frequency and applied load can be useful to obtain stress strain distribution of the fibers [22 – 24]. Once stress and strain distribution is found, then one can measure the failure mechanisms of the fibers embedded in the composites since each failure mechanism occurs at different energy levels. Thus, in this study Raman spectroscopy will be used as a measurement tool for determining failure mechanism of the graphite/epoxy composites subjected to the impact loading.

5.1.2 Raman Results

In this study, Raman spectra were obtained using 632.8 nm line of He-Ne laser as the excitation wavelength. The incident laser was focused into 2 μm spot on the damaged portion of the composites by a microscope. The 180º backscattered light was collected by the same microscope and then focused into the monochromator spectrometer. Finally, a CCD (charged coupled device) was used as a photon detecting system for obtaining Raman spectra which was recorded on a personal computer.

5.1.2.1 Raman Spectra of Transversely Loaded Specimens

The Raman laser spot was focused on three different regions for the transversely loaded specimens as shown in Figure 5.1. The Raman analysis of the transversely loaded specimens subjected to three different impact energies was compared with the Raman analysis of undamaged specimens.

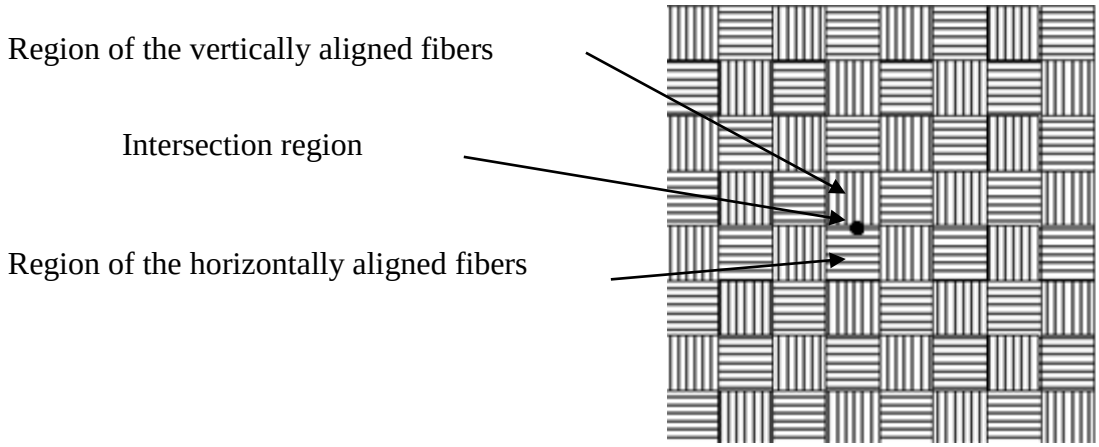

Figure 5.1 Schematic representation of the three regions used to measure Raman spectrum of the transversely loaded specimens.

Figure 5.2 shows Raman spectrums measured in the region of intersection of horizontal and vertical fibers, vertical fibers, and horizontal fibers, at the various impact energies for transversely loaded 16 ply graphite/epoxy composites. Figure 5.3 gives the relationship between Raman shift and impact energy in the region of horizontal fibers, intersection of horizontal and vertical fibers, and vertical fibers for transversely loaded 16 ply graphite/epoxy composites. Results indicate that generally impact on the surface of the transversely loaded specimens almost does not effect on the Raman shift at various energies even though it would be expected for the Raman shift to give higher value. This suggests that fibers loaded in the transverse direction are not effected by the impact loading significantly. Results also indicate that Raman shift does not show any significant dependence on the fiber directions due to the fact that both horizontally and vertically fibers are perpendicular to the Raman laser beam.

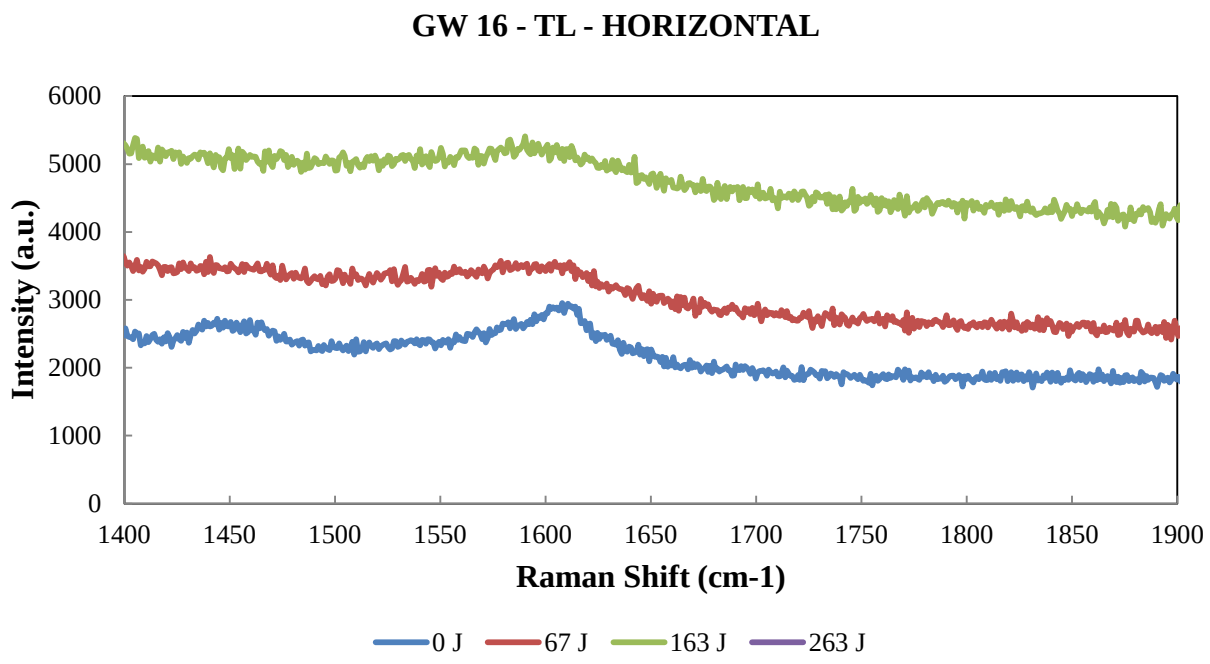

a)

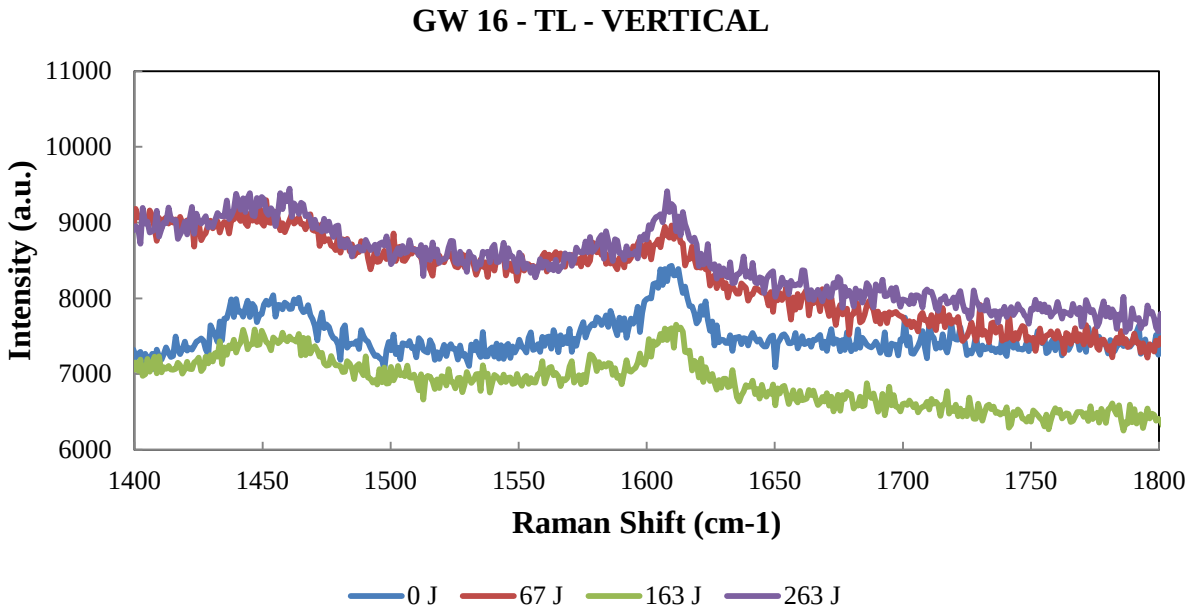

b)

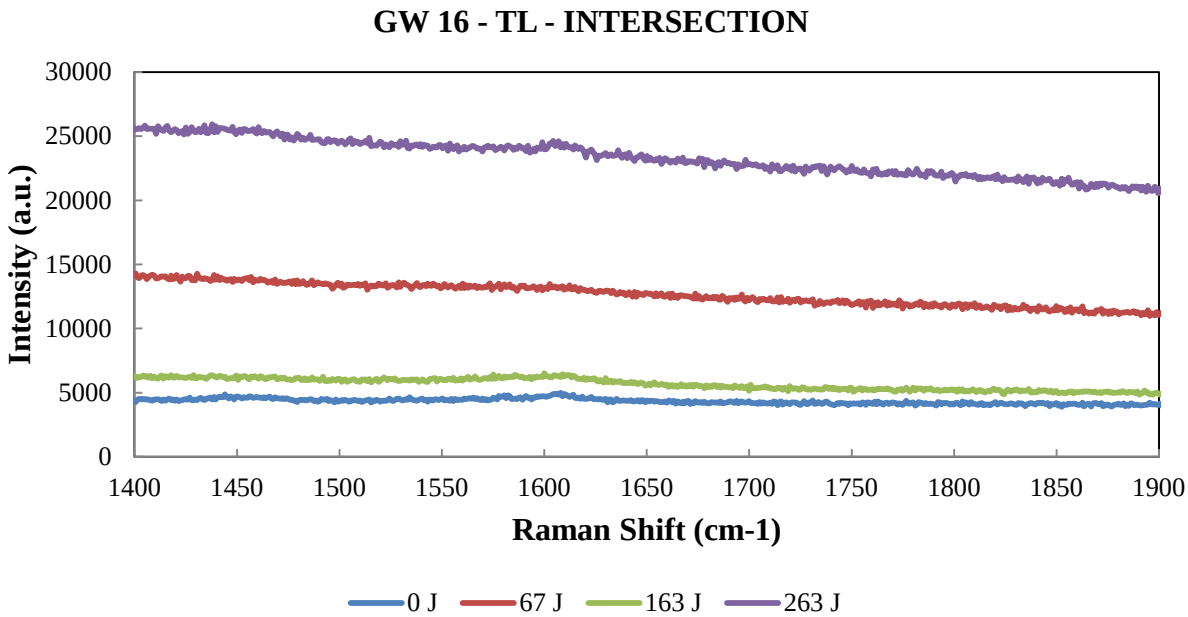

c)

Figure 5.2 Raman Spectrum of 16 ply transversely loaded specimen in the regions of a) horizontal fibers, b) vertical fibers, and c) intersection of horizontal and vertical fibers at various impact energies.

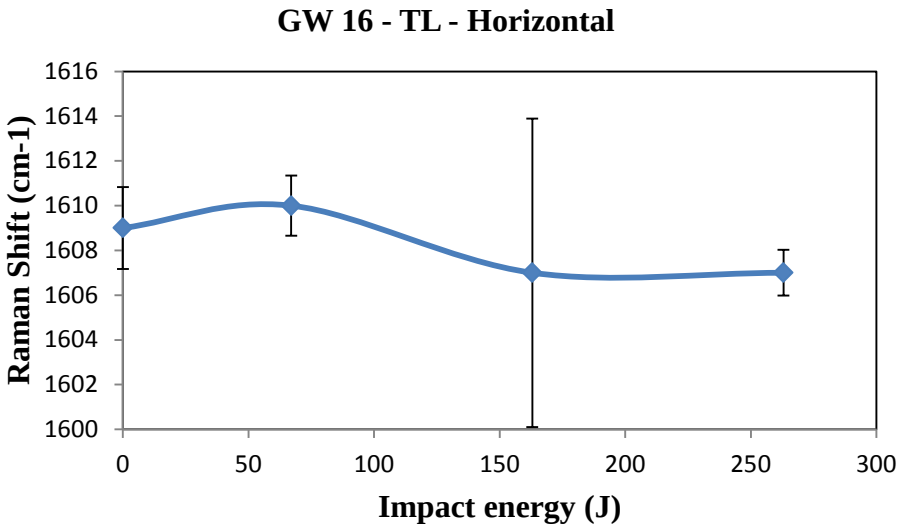
GW 16 - TL - Horizontal
Raman Shift (cm-1)
1616
1614
1612
1610
1608
1606
1604
1602
1600
0
50
100
150
200
250
300
Impact energy (J)

a)

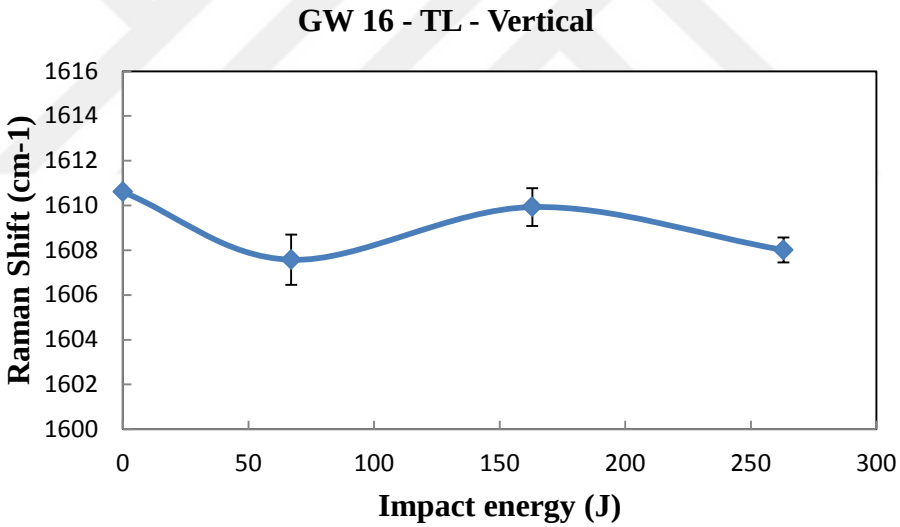
GW 16 - TL - Vertical
Raman Shift (cm-1)
1616
1614
1612
1610
1608
1606
1604
1602
1600
0
50
100
150
200
250
300
Impact energy (J)

b)

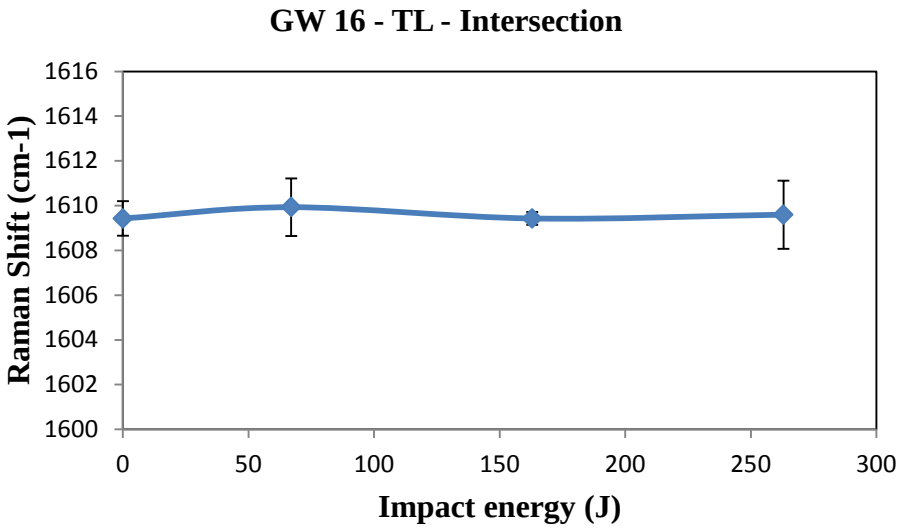

c)

Figure 5.3 Relationship between the Raman Shift and impact energy for the 16 ply transversely loaded specimens in the region of a) horizontal fiber, b) vertical fibers, and c) intersection of horizontal and vertical fibers.

5.1.2.2 Raman Spectra of Diametrically Loaded Specimens

The Raman laser spot as focused on three different regions for the diametrically loaded specimens as shown in Figure 5.4. The Raman analysis of the diametrically loaded specimens subjected to three different impact energies was compared with the Raman analysis of undamaged specimens.

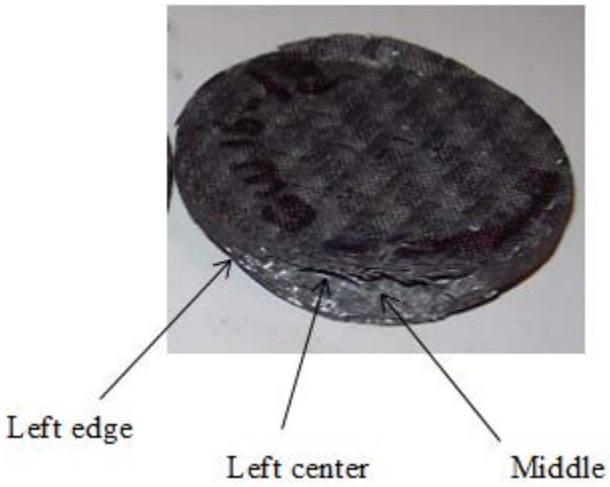

Figure 5.4 Schematic representation of the three regions used to measure Raman spectrum of the diametrically loaded specimens.

Figure 5.5 shows the Raman spectrums measured in the middle, left edge, and left center of the impacted regions at the various impact energies for diametrically loaded 16 ply graphite/epoxy composites. Figure 5.6 gives the relationship between Raman shift and impact energy in the middle, left edge, and left center of the fractured region for diametrically loaded 16 ply graphite/epoxy composites. Results show that Raman shift of the damaged specimens gives larger value than that of the undamaged specimens as opposed to the transverse loading case. It is expected because at the contact surface fibers of the diametrically loaded specimens are exposed to very intense impact loading absorbing significant amount of initial energy by being deformed and consequently resulting in shorter bond length between the neighboring atoms and hence showing higher Raman shit. However, the increase rate in the Raman shift for the diametrically loaded specimens is not proportional to the increasing applied impact energy due to the fact that the each individual fiber might be exposed to different impact energy for the same impact energy and the beam spot might focus the fibers which are exposed to lower energy or beam spot is focused to the fibers that have different orientation.

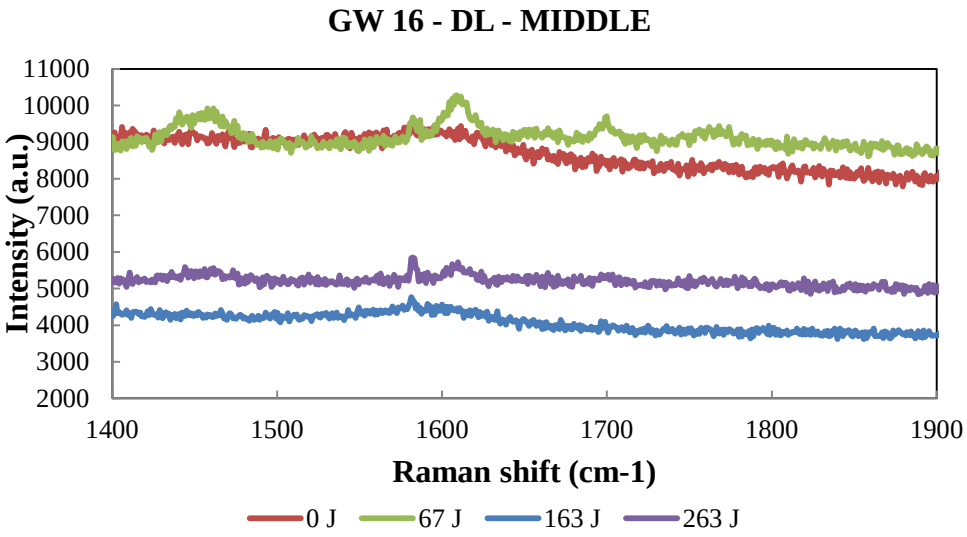
GW 16 - DL - MIDDLE
11000
10000
9000
8000
7000
6000
5000
4000
3000
2000
Intensity (a.u.)
1400
1500
1600
1700
1800
1900
Raman shift (cm-1)
0 J
67 J
163 J
263 J

a)

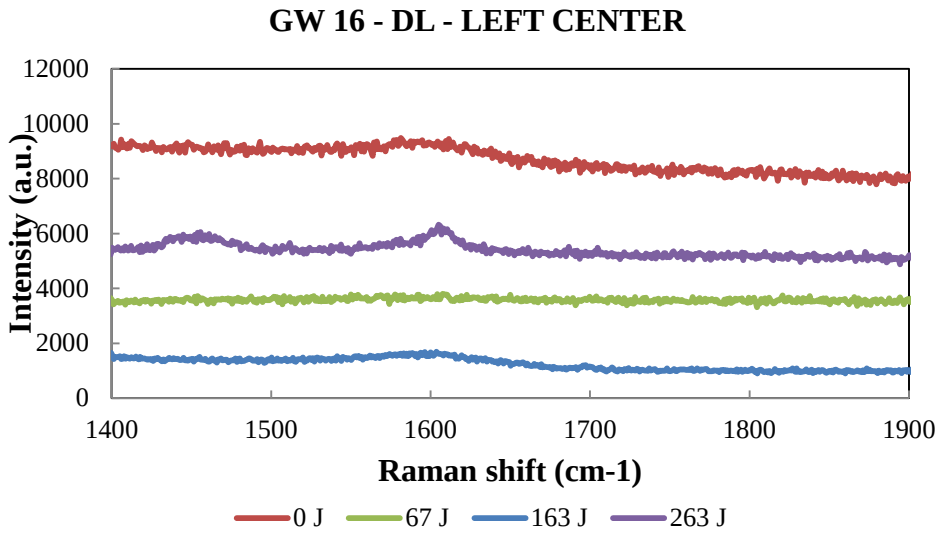
GW 16 - DL - LEFT CENTER
12000
10000
8000
6000
4000
2000
0
Intensity (a.u.)
1400
1500
1600
1700
1800
1900
Raman shift (cm-1)
0 J
67 J
163 J
263 J

b)

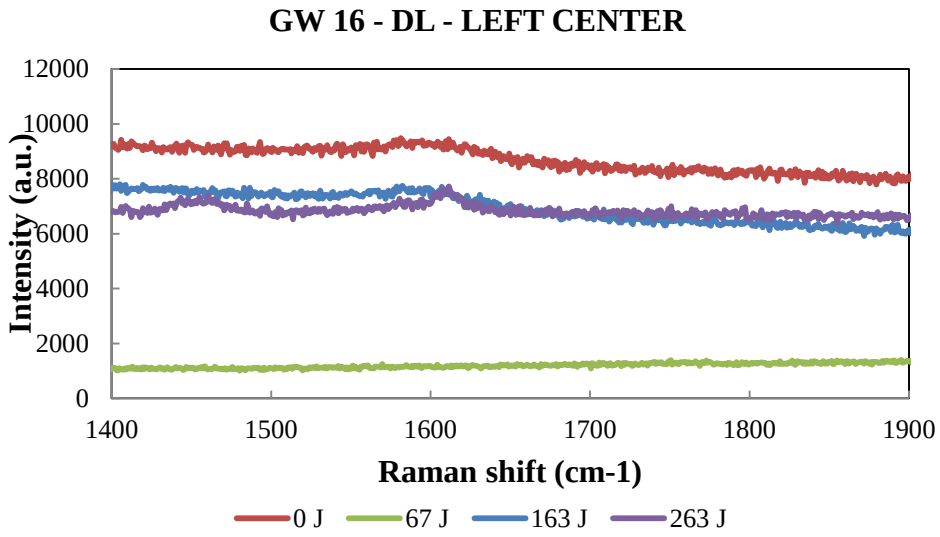

c)

Figure 5.5 Raman Spectrum of 16 ply diametrically loaded specimen in the a) middle, b) left center, and c) left edge of the impacted region at various impact energies.

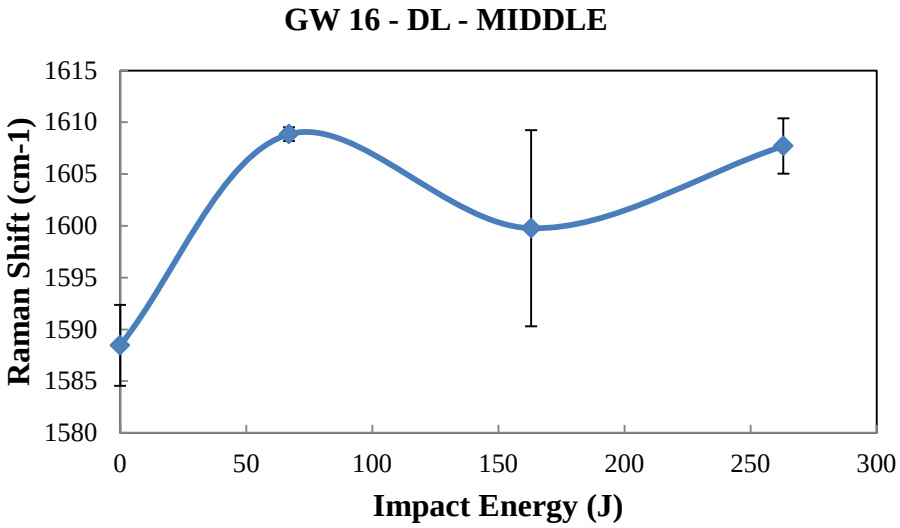

a)

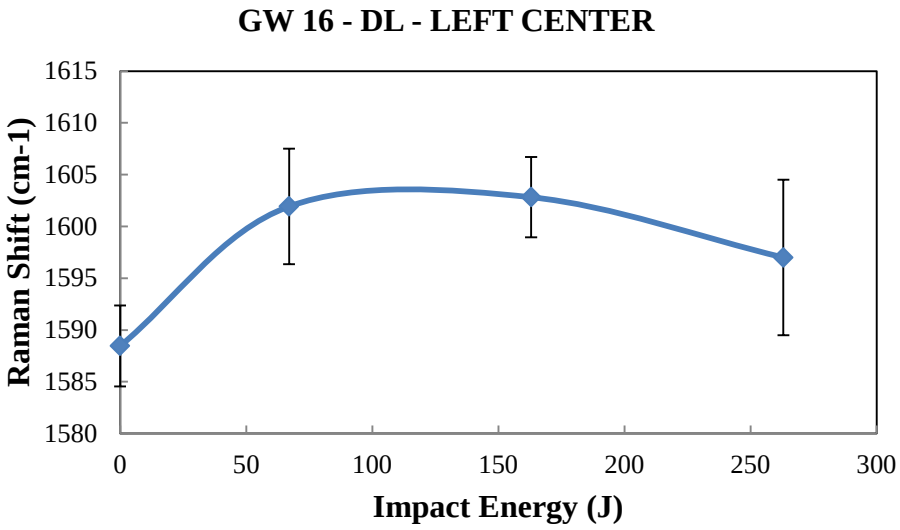

b)

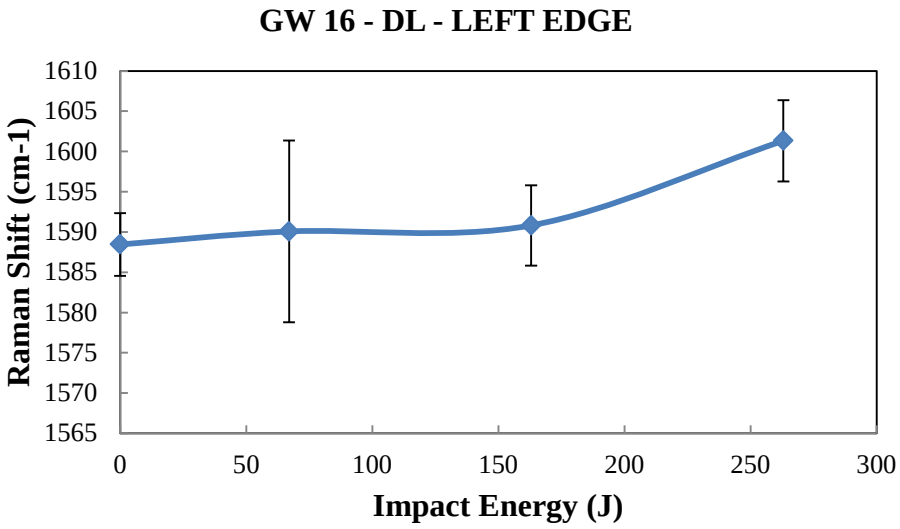

c)

Figure 5.6 Relationship between the Raman Shift and imp[act energy for the 16 ply diametrically loaded specimens in the a) middle, b) left center, and c) left edge of the impacted region at various impact energies.

It should be noted that different fiber orientation gives different Raman shift as it is expected. In the case of diametrical loading, the average Raman shift is 1588 cm^{-1} although the average Raman shift is 1610 cm^{-1}. This can be attributed to the fact that the length between neighboring atoms depends on the fiber orientation that cause different atomic vibrational modes.

5.2 DETERMINATION OF SURFACE MORPHOLOGY BY SEM

5.2.1 Background

The scanning electron microscope (SEM) is a type of electron microscope that images the sample surface by scanning it with a high-energy beam of electrons in a raster scan pattern. The electrons interact with the atoms that make up the sample producing signals that contain information about the sample's surface topography and composition.

SEM techniques have been successfully used for determining fractured surface of the composite specimens. The technique can be used to determine the cracks in the fibers, matrix, and fiber/matrix interface. Sivashanker et al [9] was able to observe microbuckling of the fibers within the composites subjected to the high strain rate by SEM. Using SEM, I. W. Hall and M. Guden [10] observed longitudinal splitting and kinking caused by microbuckling of the fibers for the unidirectionally reinforced graphite/epoxy composites subjected to high strain rate using

compression split Hopkinson Bar. In this study, SEM technique will be used to characterize the fracture surface morphology of impacted graphite/epoxy composites.

5.2.2 SEM Results

Figure 5.7 shows the comparison of SEM images of 16 ply transversely loaded specimens and diametrically loaded specimens at 67J, 163 J, and 263 J impact energies. SEM images indicate that a catastrophic failure as a result of fiber/matrix detachment and fiber breakages occurs destroying overall integrity of the impacted region for diametrically loaded specimens (d – f) which is visibly seen in the figure 4.24 while failure for the transversely loaded occurs in the different region of the composite's surface as a result of fiber breakages and fiber/matrix detachment which is not visibly seen in the figure 4.25. It should also be noted that the failure is in only at the top layer at 67 J, although the number of the layer in which failure occurs increase with increasing applied energy for the transversely loaded specimen.

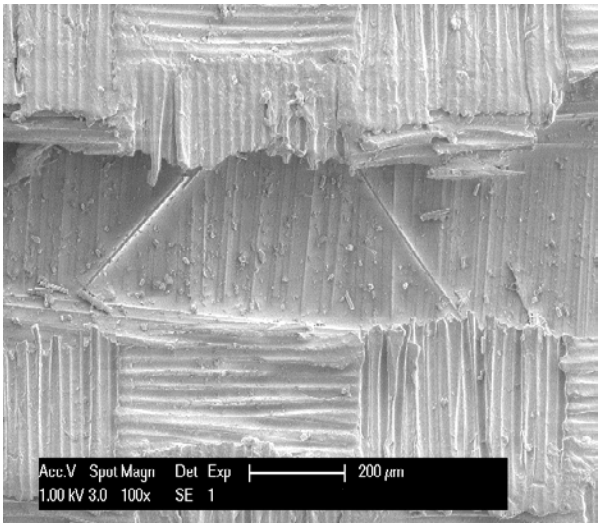

a)

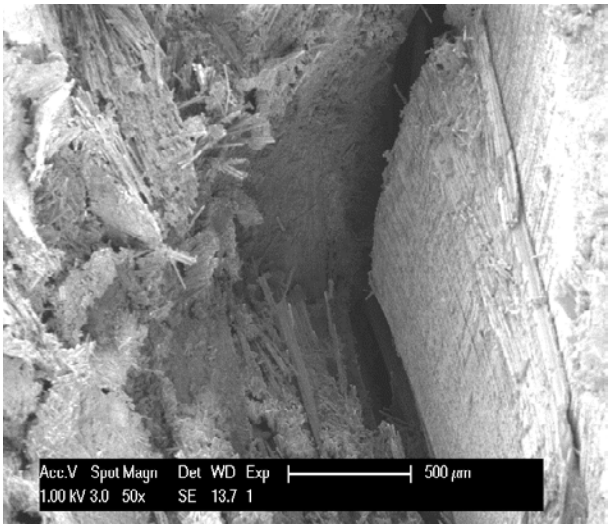

d)

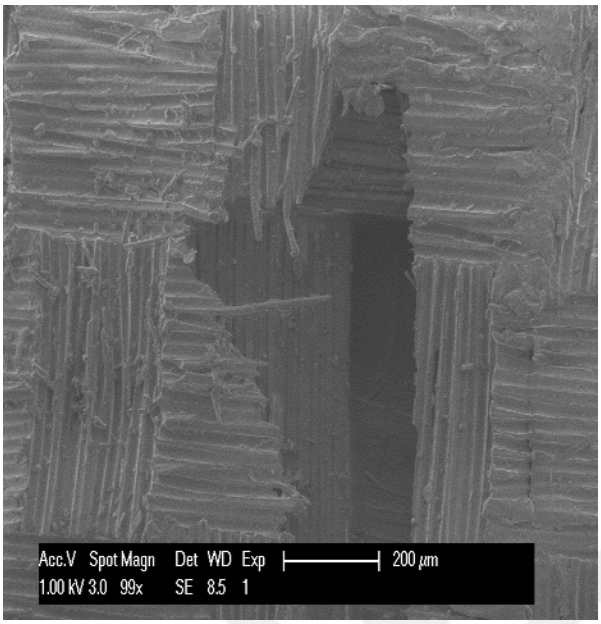

b)

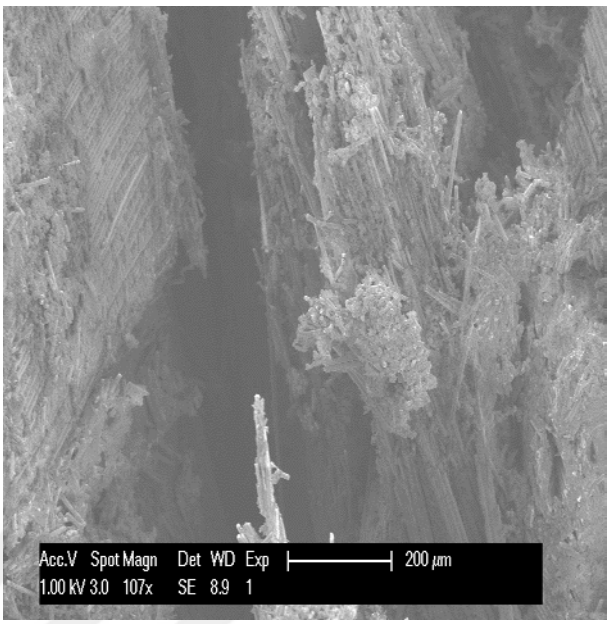

e)

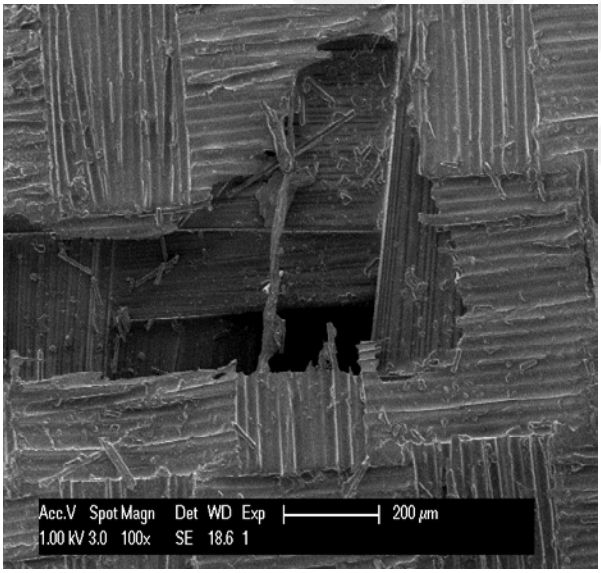

c)

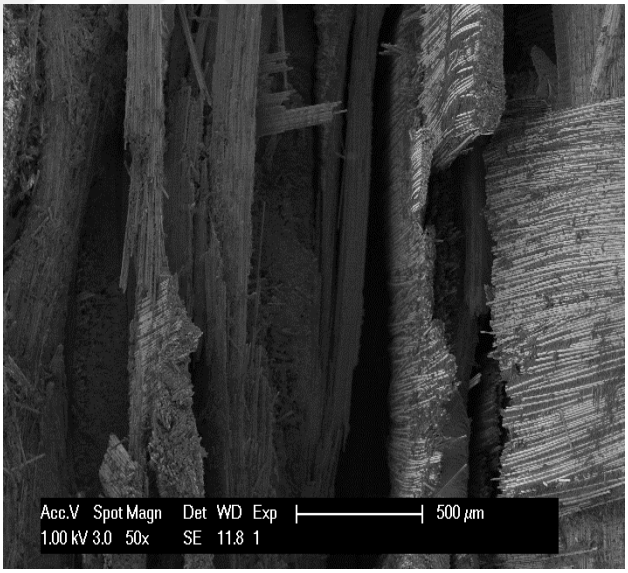

f)

Figure 5.7 Comparison of SEM photographs of (a - c) transversely loaded specimens and (d - e) diametrically loaded specimens at 67 J, 163 J, and 263 J impact energies, respectively.

Figure 5.8 – 10 show the comparison of different deformed region of diametrically loaded specimens at the impact energies of 67 J and 263 J. The results indicate that fiber breakages and fiber/matrix detachment are dominantly observed both in the middle part and center region of the deformed region of diametrically loaded specimens while in the edge of the deformed region, matrix detachment is more dominant and fiber breakages less dominant. It is also observed that intensity of the matrix cracks increase with increasing applied impact energy resulting increase in the length of the crack region as it can be seen in Figure 4.24.

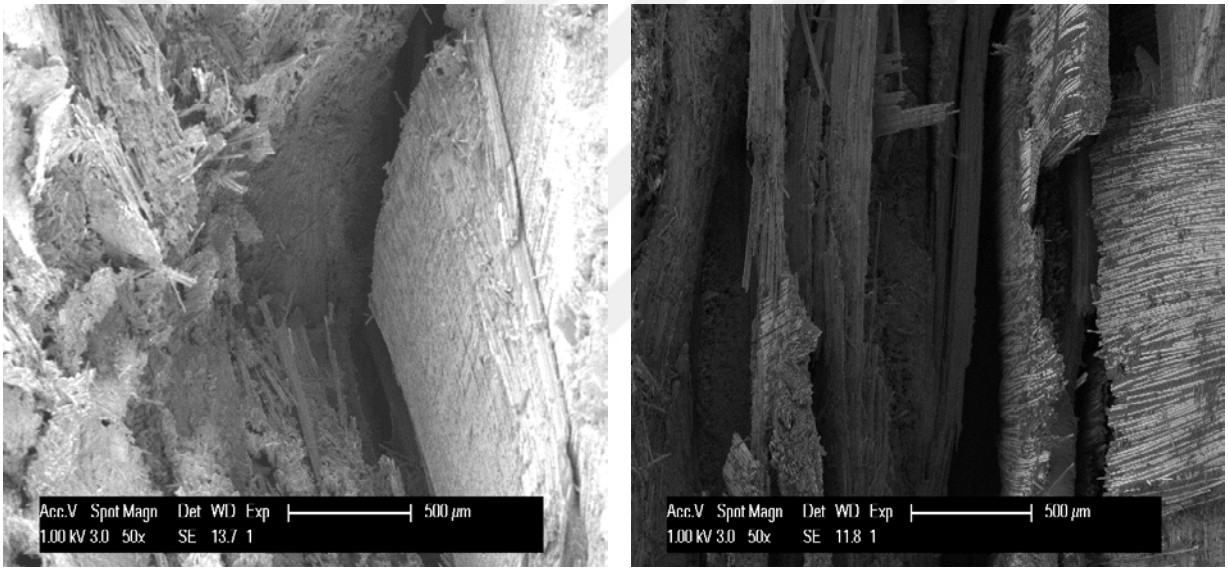

a) b)

Figure 5.8 Comparison of SEM images of middle part of the deformed region for diametrically loaded specimens at the impact energies of a) 67 J and b) 263 J.

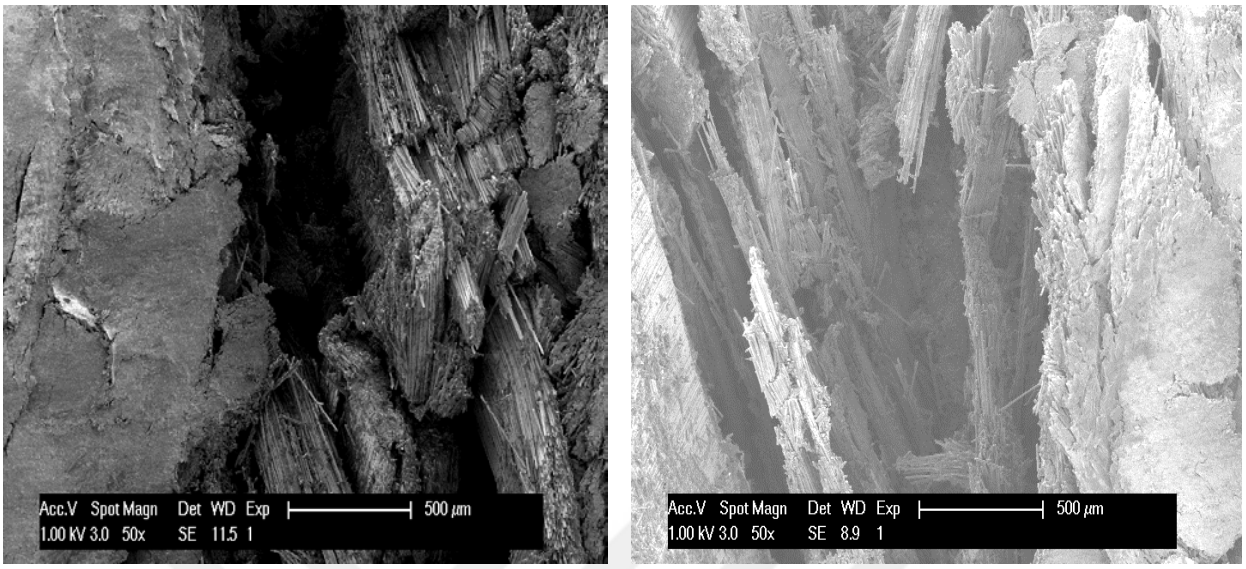

a) b)

Figure 5.9 Comparison of SEM images of left center part of the deformed region for diametrically loaded specimens at the impact energies of a) 67 J and b) 263 J.

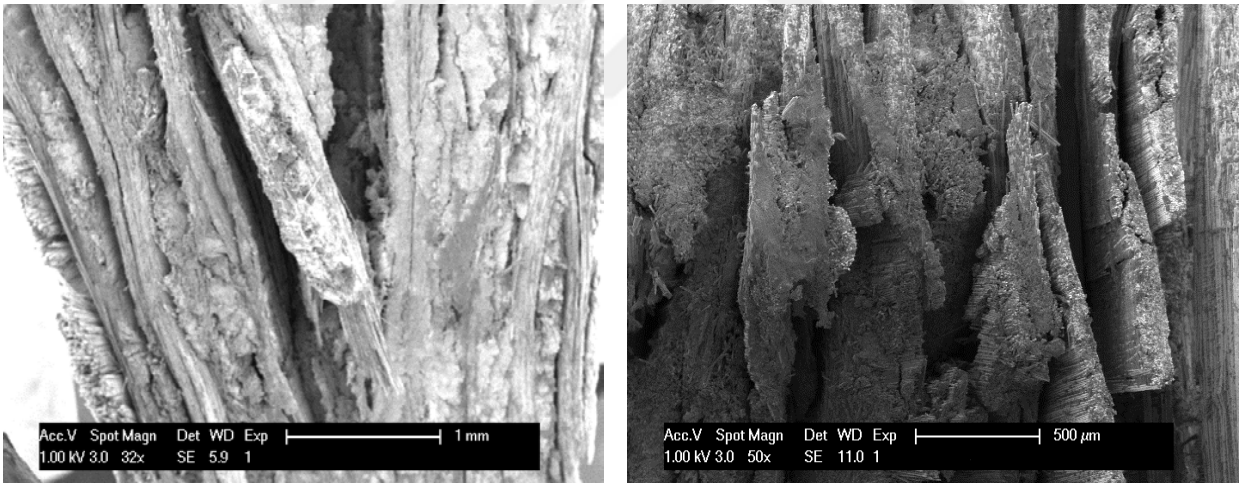

a) b)

Figure 5.10 Comparison of SEM images of left edge part of the deformed region for the diametrically loaded at the impact energies of a) 67 J and b) 263 J.

5.2.3 Comparison of Raman and SEM

Figure 5.11 – 13 show the comparison of Raman and SEM results obtained from the middle part of the deformed region of diametrically loaded specimen. Results show that the Raman peak is shifted to higher value for the fiber exposed to compressive impact energy as it is expected. However, as it was stated previously in this work, the shift does not proportionally increase with increasing applied energy due to the fact that the each individual fiber might be exposed to different impact energy for the same impact energy and the beam spot might focus the fibers which are exposed to lower energy or beam spot might focused to the fibers that have different orientation.

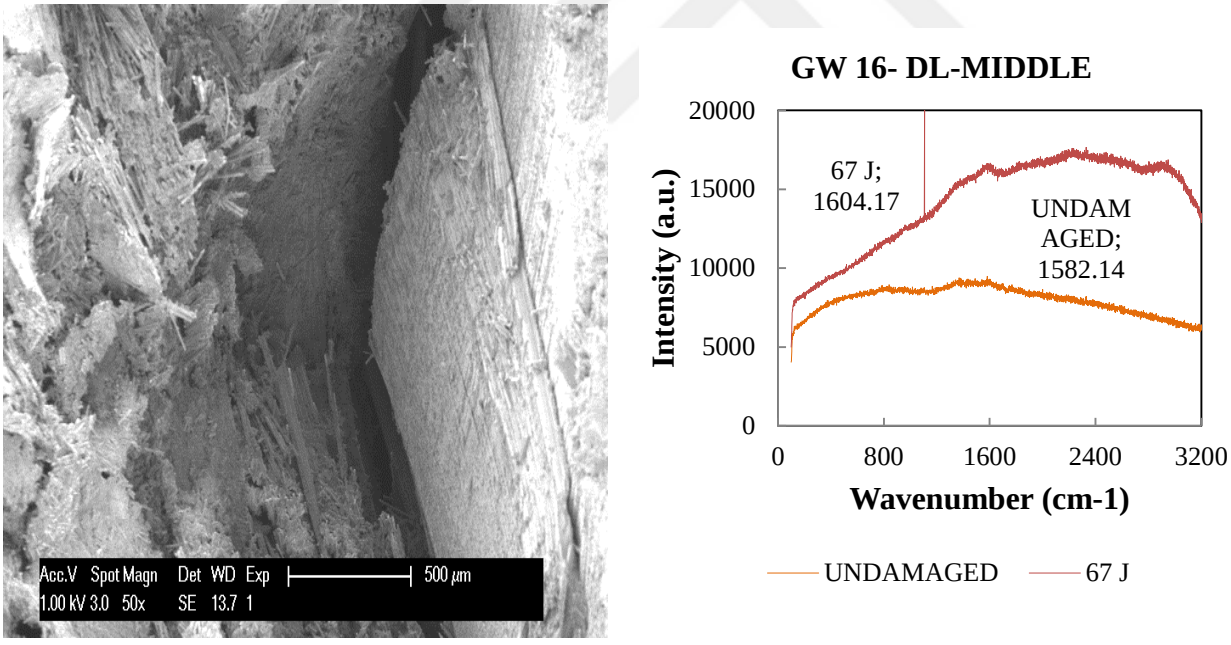

a) b)

Figure 5.11 Comparison of a) SEM and b) Raman for diametrically loaded specimens at 67 J.

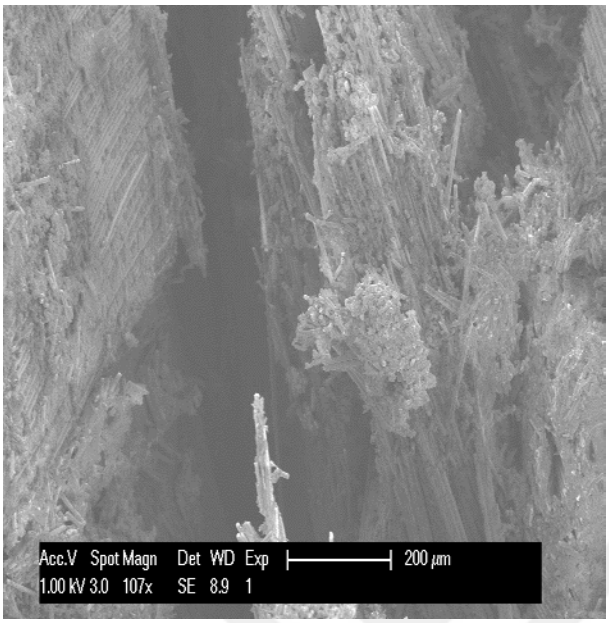

a)

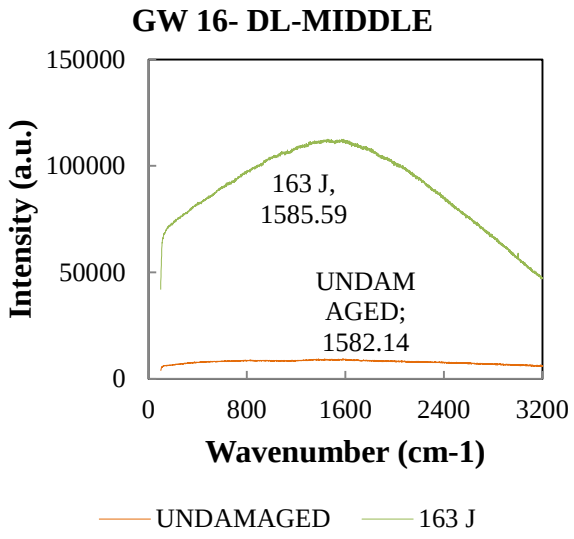

b)

Figure 5.12 Comparison of a) SEM and b) Raman for diametrically loaded specimen at 163 J.

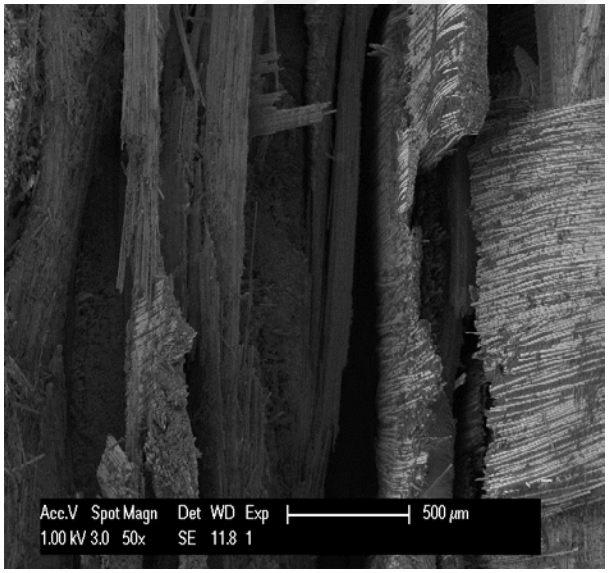

a)

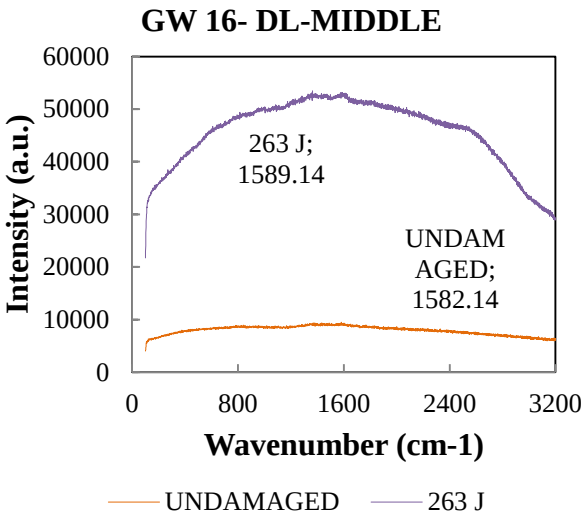

b)

Figure 5.13 Comparison of a) SEM and b) Raman for diametrically loaded specimen at 263 J.

6.0 DISCUSSIONS

6.1 EFFECT OF THICKNESS ON THE DAMAGE PARAMETERS

In investigating the effect of thickness on the damage parameters, the data clearly show that the variation of thickness does affect the energy absorption history and the stress – strain and strain rate – strain behaviors as was hypothesized. The stress – strain and strain rate behaviors of woven composite materials depends on thickness because the thinner specimens show more deformation than that of the thicker specimens.

Specimen thickness has almost no effect on the energy absorbed for the specimens subjected to the transverse loading because no visible damage occurs in transversely loaded specimens. This can be understood from the nature of waveforms in Figure 2.2 - a showing that almost all incident waves transmitted to the transmitted bar since no significant energy is spent in the deformation process. Unlikely in the diametrical loading case, in which visible damage occurs, the energy absorbed increases with increasing thickness due to the fact that more energy is spent in the damage process of thinner specimens which indicates that thicker specimens have greater compressive strength than that of the thinner specimens. Hence, in Figure 2.2 – b, the transmitted wave is almost zero and reflected wave is significantly higher.

For the same thickness, the energy absorption increases with increasing applied energy as it is expected because the stress that the material experiences increases with increasing applied

energy for both transversely and diametrically loaded specimens. However, the amplitude of the energy absorption is greater for the transverse loading case since no significant energy is spent in damage process as opposed to the diametrical loading case. For the same thickness, the strain rate increases with increasing applied impact energy as expected for both the transversely and diametrically loaded specimens.

Diametrically loaded specimen exhibits strain energy release when the incident bar experiences tensile force while transversely loaded specimens do not show any strain energy release because no tensile force is observed in incident bar.

6.2 EFFECT OF IMPACT ENERGY ON DAMAGE PARAMETERS

In the investigation of the effect of impact energy on damage parameters, the data show that impact energy do affect specimen energy absorption history, stress – strain, strain rate – strain behaviors, and Raman spectrum of graphite fibers. The data clearly support the stated hypotheses and show that the level of energy absorbed depends on the impact energy because of higher stain rate, specimen vibration, fiber breakage, and matrix cracking resulting in increased deformation level of the specimens. The increased specimen vibration also explains the observed shift in Raman peak spectrum. For the same thickness and with increasing applied impact energy, the ultimate strength increases for transverse loading case as expected because higher applied energy means higher stress than transversely loaded specimens can withstand. Although the same trend is observed in the diametrical loading case, the effect of the applied energy is not

significant compared to the diametrical loading case since deformation process prevents specimen from experiencing more stress.

For the same applied impact energy, the ultimate strength has almost no dependency on thickness for transversely loaded specimens due to the fact that all specimens experience same stress because no significant deformation on the specimen surface occurs. On the other hand, ultimate strength increases with increasing thickness for the diametrical loading case, in which visible damage occurs, due to the fact that it is difficult to deform thicker specimens than thinner specimens. In other words, the energy spent in the deformation process is higher and therefore the ultimate stress is lower for the thinner specimens than that of the thicker specimens. The data also show that for the same applied impact energy, elastic modulus increases with increasing thickness for both diametrically and transversely loaded specimens as it is expected.

For the same applied impact energy, strain rate increases as thickness decreases since thinner specimens undergo greater deformation than the thinker specimens for the transverse loading case. The same trend is slightly observed in the case of the diametrical loading because deformation rate is almost the same within the specimens. Even though high strain rate is observed in transversely loaded specimens, for diametrically loaded specimens the strain rate is substantially lower. This behavior is due to the fact that transversely loaded specimens have significantly smaller initial length than that of the diametrically loaded specimens and this is the main reason why the fibers of transversely loaded specimens cannot be deformed easily.

6.3 EFFECT OF LOADING DIRECTION ON COMPRESSIVE DAMAGE BEHAVIORS

To investigate the effect of the loading configuration on the compressive damage behaviors, the research questions were whether loading direction affect the energy absorption history, the stress – strain, and strain rate – strain behavior, and the Raman spectrum of graphite fibers. The data supported the stated hypotheses with mixed results: The level of energy absorbed by the woven composite materials depends on the loading configuration. The transversely loaded specimen showed higher energy absorption but without appreciable incipient damage. Most of the expendable energy was transmitted through the specimen to the system with damage. This is because transverse loading did not allow enough space to get deformed in contrast to diametrically loaded specimen that get easily deformed resulting in a significant portion of the applied energy consumed in the deformation process. Stress-strain behavior depends mainly in the transmitted incident compressive wave and since transverse and diametrical loading transmit the incident compressive wave differently, one would expect the stress-strain behaviors to be different. Transversely loaded specimens did not exhibit significant deformation unlike in the case of diametrical loading. Strain rate – strain behavior depends on the reflected incident compressive wave which in turn depends on such things as surface damage and impedance mismatch between interfaces. In the case of transversely loaded specimen, most of the incident wave is transmitted without dispersion. The reflected wave “thins” out such that there is no plateau region in the strain rate curve. The plateau region in the strain rate of diametrically loaded specimens is the indication of damage accumulation which is not observed for the transverse loading case because no important damage occurs in this case. This is in complete

contrast to specimens loaded diametrically which exhibit more deformation than that of the transversely loaded specimens.

The specimens subjected to diametrical loading exhibit very high strength at the contact surface as it is expected because of the highly localized impact loading at the contact surface. Also minimum strength in the diametrically loaded specimens is in the middle of the specimen because of the largest area of this region. The permanent deformation in the diametrically loaded specimens and no visible damage in the transversely loaded specimens at all level of impact energies explain the effect of the loading direction.

6.4 EFFECT OF CONTACT GEOMETRY ON COMPRESSIVE DAMAGE BEHAVIOR

In investigating the effect of the contact geometry on the compressive damage behavior of the woven graphite/epoxy composites subjected to high strain rate loading in transverse and diametrical directions, the basic research question on the effect of contact geometry energy absorption history and stress – strain and strain rate – strain behaviors are fully answered.

The data support the stated hypotheses and clearly shows that different contact areas result in different amount of deformation on the surface of the composites which affects the energy absorption; the specimens loaded using smaller contact area exhibit more deformation resulting in lower strength and higher strain rate than the specimens loaded in larger contact area.

For the same applied energy, it is observed that the specimens loaded with 0.5″ indentor have a tendency to show reduction in the energy absorbed after the peak energy absorbed while

the specimens loaded without using indentor do not exhibit any reduction in the energy absorbed. This is because of the release of the strain energy stored during loading stage and this can be attributed to the damage formation is higher within the specimen for the specimens loaded with 0.5″ indentor.

For the same applied impact energy, the smaller contact area gives larger deformation to the specimens and consequently the peak stress is slightly lower for the specimens loaded using indentor. This results higher elastic modulus for the specimens loaded without using indentor.

For the same impact energy and same thickness, smaller contact area gives higher strain rate to the transversely loaded specimens because the effect of the compressive wave in the specimen's surface is higher due to the smaller area of the indentor.

6.5 CHARACTERIZATION OF SURFACE MORPHOLOGY

To investigate the characterization of the surface morphology of the woven graphite/epoxy polymer composites subjected to the high strain rate loading in transverse and diametrical directions, the questions were whether there is a correlation between SEM and Raman surface morphologies of deformed region of loaded specimen and whether SEM and Raman results can differentiate between matrix and fiber dominated failures; and transverse and diametrical compressive failures. It was hypothesized that Raman peak for graphite will be higher for the impacted woven composite materials due to decreasing bond length and will be different for the transversely and diametrically loaded specimens because the atom vibration also depends on the

fiber orientation. It was predicted that that surface micro – structure of SEM images will exhibit higher damage density with increasing applied energy for both transversely and diametrically loaded specimens.

The results answer the research questions and clearly support the hypotheses: The Raman peak is shifted to higher value when the diametrically loaded specimens are subjected to the compressive applied although Raman peak is almost constant in the case of transverse loading. This is because higher energy concentration at the deformed region which Raman laser beam is focused on effects the microstructure of the fibers extensively which is not seen in the case of transverse loading. Raman shift does not increase proportionally to increasing applied energy in the case of diametrical loading. This might be due to the fact that the beam spot of Raman laser is focused to the fibers having different orientation or the fibers that Raman laser is focused to might be exposed to different applied energy for the same impact energy. In other words, the loading may not uniformly be distributed to each individual fiber. The reason why Raman shift Surface morphology by SEM indicates that with increasing applied energy the deformation rate increases for both diametrically and transverse specimens. The intensity of matrix crack formation increases with increasing applied energy as it is expected.

7.0 CONCLUSION

High strain compressive impact testing has been carried out using Split Hopkinson Pressure Bar for woven graphite/epoxy composites transversely and diametrically at the impact energies of 67 J, 113J, 163 J, and 263 J. The following conclusions can be drawn from high strain rate experimental data.

Thickness effect has been observed on the stress – strain and strain rate – strain behavior of the both transversely and diametrically loaded specimens. As it is hypothesized, thicker specimens have shown better elastic modulus and lower strain rate. However, no thickness effect has been observed on the energy absorption history for transversely loaded specimens even though energy absorption increases with increasing thickness for diametrically loaded specimens. This is because no damage occurs in the transversely loaded specimens.

The effect of the impact energy has been found on the damage parameters. Energy absorption, elastic modulus, ultimate strength, and the strain rate increase with increasing applied energy as it is hypothesized. This can be seen from the SEM images as the intensity of the matrix cracks in diametrically loaded specimens.

The most crucial findings in this work are the effects of the specimen loading configurations on the high strain rate damage parameters. No visible damage was observed on the transversely loaded specimens. This is due to the fact that the specimen was sandwiched between the two bars such that the fibers in the transversely loaded specimens have not enough

space to flex and deform as opposed to the diametrical loading case. Also, the nature of the boundary condition in the case of diametrical loading gives rise to change in the cross sectional area resulting stress concentration in the specimen. Stress is highly localized at the contact surface and therefore stress concentration has its highest value at the contact point. This means small portions of the specimen where the highly localized stresses occur absorb an excessive amount of energy before the main portion of the specimen can be stressed appreciably and therefore before the main portion can be made to absorb an appreciable share of the energy delivered to the specimen. As a result, the small portion where the localized stress occurs is likely to be stressed above the yield stress of the material. Then the energy required to be absorbed may be great enough to cause plastic deformation. Hence, the greatest plastic deformation is observed in the contact surface of the specimen while main portion of the specimen is in overall integrity. The difference in loading configurations explains the main reason for different behaviors:

1. Most of the expendable energy for specimen damage returns to the system in the transverse loading case, with no visible incipient damage, while some portion of the energy absorption is consumed in the deformation process for the diametrical loading case.
2. Significantly higher elastic modulus in the transversely loaded specimens compared to the diametrically loaded specimens
3. Higher strain rate in the transversely loaded specimens compared to the diametrically loaded specimens.

Smaller contact geometry gives larger deformation to the transversely loaded specimens resulting in lower elastic modulus, lower ultimate strength, lower energy absorption because of the energy release, and higher strain rate for the same thickness and impact energy.

.

APPENDIX

DYNAMIC PROPERTIES OF DIAMETRICALLY AND TRANSVERSELY LOADED SPECIMENS

Table A.1 Dynamic properties of 8 ply transversely loaded plain weave graphite/epoxy laminates tested at 67 J

Dynamic Properties of 8 ply transversely loaded plain weave graphite/epoxy laminates tested at 67 J								
Sample ID	**Peak Stress (MPa)**	**Strain at Peak Stress**	**Yield Stress (MPa)**	**Strain at Yield Stress**	**Peak Energy (J)**	**Residual Energy (J)**	**Strain Energy (J)**	**Modulus at Yield Stress (GPa)**
GW 8 - 1	123.6655	0.2271	18.45	0.0133	58.073	56.0209	2.0523	1.387218
GW 8 - 2	124.64698	0.2764	17.077	0.0336	60.78	58.6282	2.1516	0.508244
GW 8 - 3	123.6655	0.2731	18.05	0.0186	60.393	58.1654	2.2279	0.9704301
Average	123.99266	0.2589	17.859	0.0218	59.749	57.6048	2.1439	0.9552974

Table A.2 Dynamic properties of 8 ply transversely loaded plain weave graphite/epoxy laminates tested at 163 J

Dynamic Properties of 8 ply transversely loaded plain weave graphite/epoxy laminates tested at 163 J								
Sample ID	**Peak Stress (MPa)**	**Strain at Peak Stress**	**Yield Stress (MPa)**	**Strain at Yield Stress**	**Peak Energy (J)**	**Residual Energy (J)**	**Strain Energy (J)**	**Modulus at Yield Stress (GPa)**
GW 8 - 4	193.15374	0.2805	25.91	0.0084	129.97	128.314	1.6574	3.0845238
GW 8 - 5	192.17227	0.2593	29.83	0.0155	128.19	126.6	1.586	1.9245161
GW 8 - 6	192.56486	0.3725	21.19	0.0146	129.01	127.27	1.7362	1.4513699
Average	192.63029	0.3041	25.643	0.0128	129.05	127.395	1.6599	2.1534699

Table A.3 Dynamic properties of 8 ply transversely loaded plain weave graphite/epoxy laminates tested at 263 J

Dynamic Properties of 8 ply transversely loaded plain weave graphite/epoxy laminates tested at 263 J								
Sample ID	**Peak Stress (MPa)**	**Strain at Peak Stress**	**Yield Stress (MPa)**	**Strain at Yield Stress**	**Peak Energy (J)**	**Residual Energy (J)**	**Strain Energy (J)**	**Modulus at Yield Stress (GPa)**
GW 8 - 7	234.76816	0.3396	42.59	0.0152	197.84	196.494	1.3504	2.8019737
GW 8 - 8	236.142224	0.3614	34.15	0.0145	211.55	209.645	1.9059	2.3551724
GW 8 - 9	232.41263	0.3283	35.33	0.0172	208.24	206.565	1.6748	2.0540698
Average	234.44101	0.3431	37.357	0.0156	205.88	204.234	1.6437	2.4037386

Table A.4 Dynamic properties of 8 ply diametrically loaded plain weave graphite/epoxy laminates tested at 67 J

Dynamic Properties of 8 ply diametrically loaded plain weave graphite/epoxy laminates tested at 67 J								
Sample ID	**Peak Stress (MPa)**	**Strain at Peak Stress**	**Yield Stress (MPa)**	**Strain at Yield Stress**	**Peak Energy (J)**	**Residual Energy (J)**	**Strain Energy (J)**	**Modulus at Yield Stress (GPa)**
GW 8 - 12	592.574	0.00715	355	0.0008	28.1185	14.91377	13.2048	443.75
Average	592.574	0.00715	355	0.0008	28.1185	14.91377	13.2048	443.75

Table A.5 Dynamic properties of 8 ply diametrically loaded plain weave graphite/epoxy laminates tested at 163 J

Dynamic Properties of 8 ply diametrically loaded plain weave graphite/epoxy laminates tested at 163 J								
Sample ID	**Peak Stress (MPa)**	**Strain at Peak Stress**	**Yield Stress (MPa)**	**Strain at Yield Stress**	**Peak Energy (J)**	**Residual Energy (J)**	**Strain Energy (J)**	**Modulus at Yield Stress (GPa)**
GW 8 - 16	711.089	0.0944	503	0.0007	36.2981	23.90263	12.3955	698.611111
GW 8 - 17	651.832	0.11	414.8	0.0009	31.9899	19.86866	12.1212	432.083333
GW 8 -18	740.718	0.1	533.94	0.0009	36.8871	24.83155	12.0556	568.021277
Average	701.213	0.1014	483.91	0.0008	35.058	22.86762	12.1907	566.238574

Table A.6 Dynamic properties of 8 ply diametrically loaded plain weave graphite/epoxy laminates tested at 263 J

Dynamic Properties of 8 ply diametrically loaded plain weave graphite/epoxy laminates tested at 263 J								
Sample ID	**Peak Stress (MPa)**	**Strain at Peak Stress**	**Yield Stress (MPa)**	**Strain at Yield Stress**	**Peak Energy (J)**	**Residual Energy (J)**	**Strain Energy (J)**	**Modulus at Yield Stress (GPa)**
GW 8 - 51	888.86	0.1	703	0.0009	49.7777	18.06341	31.7143	781.111111
GW 8 - 52	851.82	0.08	740	0.001	51.8241	19.38337	32.4407	740
GW 8 - 53	777.75	0.0027	703	0.00083	53.764	19.26045	34.5035	846.987952
Average	839.48	0.0609	715.333	0.00091	51.7886	18.90241	32.8862	789.366354

Table A.7 Dynamic properties of 8 ply transversely loaded plain weave graphite/epoxy laminates tested at 67 J using 0.5" indentor

Dynamic Properties of 8 ply transversely loaded plain weave graphite/epoxy laminates tested at 67 J using 0.5" indentor								
Sample ID	**Peak Stress (MPa)**	**Strain at Peak Stress**	**Yield Stress (MPa)**	**Strain at Yield Stress**	**Peak Energy (J)**	**Residual Energy (J)**	**Strain Energy (J)**	**Modulus at Yield Failure (GPa)**
GW 8 - 28	116.01	0.46	14.32	0.0335	64.226	56.4765	7.7501	0.42746
GW 8 - 29	116.20	0.46	17.27	0.0435	59.402	51.8383	7.5644	0.39701
GW 8 - 30	114.83	0.4527	13.54	0.0382	63.454	56.4529	7.0017	0.35445
Average	115.68	0.45756	15.0433	0.0384	62.361	54.9226	7.4387	0.39297

Table A.8 Dynamic properties of 8 ply transversely loaded plain weave graphite/epoxy laminates tested at 113 J using 0.5" indentor

Dynamic Properties of 8 ply transversely loaded plain weave graphite/epoxy laminates tested at 113 J using 0.5" indentor								
Sample ID	**Peak Stress (MPa)**	**Strain at Peak Stress**	**Yield Stress (MPa)**	**Strain at Yield Stress**	**Peak Energy (J)**	**Residual Energy (J)**	**Strain Energy (J)**	**Modulus at Yield Failure (GPa)**
GW 8 - 37	152.717	0.46	21.39	0.044	102.28	92.13865	10.145	0.48613
GW 8 - 38	153.698	0.47	21.39	0.045	102.50	92.54161	9.9643	0.47533
GW 8 - 39	156.054	0.4964	25.32	0.06	100.57	90.77534	9.8038	0.422
Average	154.156	0.47546	22.7	0.0496	101.79	91.81853	9.9712	0.46115

Table A.9 Dynamic properties of 8 ply transversely loaded plain weave graphite/epoxy laminates tested at 163 J using 0.5" indentor

Dynamic Properties of 8 ply transversely loaded plain weave graphite/epoxy laminates tested at 163 J using 0.5" indentor								
Sample ID	**Peak Stress (MPa)**	**Strain at Peak Stress**	**Yield Stress (MPa)**	**Strain at Yield Stress**	**Peak Energy (J)**	**Residual Energy (J)**	**Strain Energy (J)**	**Modulus at Yield Failure (GPa)**
GW 8 - 40	179.02	0.47	32.58	0.0456	152.308	141.6681	10.639	0.7144
GW 8 - 41	180.59	0.4923	29.34	0.046	157.592	147.1474	10.445	0.6378
GW 8 - 42	178.6	0.511	32.97	0.049	158.677	148.2571	10.419	0.6728
Average	179.41	0.4911	31.63	0.04687	156.192	145.6909	10.501	0.6750

Table A.10 Dynamic properties of 12 ply transversely loaded plain weave graphite/epoxy laminates tested at 67 J

Dynamic Properties of 12 ply transversely loaded plain weave graphite/epoxy laminates tested at 67 J								
Sample ID	**Peak Stress (MPa)**	**Strain at Peak Stress**	**Yield Stress (MPa)**	**Strain at Yield Stress**	**Peak Energy (J)**	**Residual Energy (J)**	**Strain Energy (J)**	**Modulus at Yield Stress (GPa)**
GW 12 - 1	118.75	0.1921	8.44	0.0034	59.103	57.4199	1.6832	2.482353
GW 12 - 2	116.79	0.2121	14.91	0.02	57.387	55.3552	2.0318	0.7455
GW 12 - 3	116.59	0.2334	12.56	0.019	60.410	57.6692	2.7409	0.661053
Average	117.38	0.21253	11.97	0.0141	58.966	56.8148	2.15	1.296302

Table A.11 Dynamic properties of 12 ply transversely loaded plain weave graphite/epoxy laminates tested at 163 J

Dynamic Properties of 12 ply transversely loaded plain weave graphite/epoxy laminates tested at 163 J								
Sample ID	**Peak Stress (MPa)**	**Strain at Peak Stress**	**Yield Stress (MPa)**	**Strain at Yield Stress**	**Peak Energy (J)**	**Residual Energy (J)**	**Strain Energy (J)**	**Modulus at Yield Stress (GPa)**
GW 12 - 5	179.020	0.2086	17.66	0.0079	124.545	123.033	1.51125	2.23544
GW 12 - 6	178.628	0.2451	15.7	0.0098	127.778	125.927	1.85022	1.60204
GW 12 - 7	181.179	0.2287	16.48	0.0081	132.303	131.002	1.30054	2.03456
Average	179.609	0.22746	16.6133	0.0086	128.208	126.654	1.55401	1.95735

Table A.12 Dynamic properties of 12 ply transversely loaded plain weave graphite/epoxy laminates tested at 263 J

Dynamic Properties of 12 ply transversely loaded plain weave graphite/epoxy laminates tested at 263 J								
Sample ID	**Peak Stress (MPa)**	**Strain at Peak Stress**	**Yield Stress (MPa)**	**Strain at Yield Stress**	**Peak Energy (J)**	**Residual Energy (J)**	**Strain Energy (J)**	**Modulus at Yield Stress (GPa)**
GW 12 - 8	213.37	0.211	24.73	0.0075	169.78	168.774	1.0114	3.29733
GW 12 - 9	224.36	0.243	30.61	0.01	186.86	185.894	0.9718	3.061
GW 12 - 10	222.20	0.247	32.78	0.0117	183.21	182.271	0.9422	2.80170
Average	219.98	0.234	29.3733	0.0097	179.95	178.980	0.9752	3.01780

Table A.13 Dynamic properties of 12 ply diametrically loaded plain weave graphite/epoxy laminates tested at 67 J

Dynamic Properties of 12 ply transversely loaded plain weave graphite/epoxy laminates tested at 67 J								
Sample ID	**Peak Stress (MPa)**	**Strain at Peak Stress**	**Yield Stress (MPa)**	**Strain at Yield Stress**	**Peak Energy (J)**	**Residual Energy (J)**	**Strain Energy (J)**	**Modulus at Yield Stress (GPa)**
GW 12 - 11	777.16	0.0541	511	0.0011	23.320	15.895	7.4253	444.347
GW 12 - 12	715.80	0.0403	613	0.0008	24.986	17.406	7.5803	688.764
GW 12 - 13	613.55	0.0508	388	0.0012	19.348	11.629	7.7191	323.333
Average	702.17	0.0484	504	0.0010	22.551	14.976	7.5749	485.481

Table A.14 Dynamic properties of 12 ply diametrically loaded plain weave graphite/epoxy laminates tested at 163 J

Dynamic Properties of 12 ply transversely loaded plain weave graphite/epoxy laminates tested at 163 J								
Sample ID	**Peak Stress (MPa)**	**Strain at Peak Stress**	**Yield Stress (MPa)**	**Strain at Yield Stress**	**Peak Energy (J)**	**Residual Energy (J)**	**Strain Energy (J)**	**Modulus at Yield Stress (GPa)**
GW 12 - 14	1063.	0.102	736	0.0010	54.618	36.9226	17.695	681.481
GW 12 - 15	838.5	0.1	756	0.0011	50.458	31.3079	19.150	646.153
GW 12 - 16	736.2	0.09	593	0.0013	48.379	28.0550	20.324	452.671
Average	879.4	0.0973	695	0.0011	51.151	32.0952	19.056	593.435

Table A.15 Dynamic properties of 12 ply diametrically loaded plain weave graphite/epoxy laminates tested at 263 J

Dynamic Properties of 12 ply transversely loaded plain weave graphite/epoxy laminates tested at 263 J								
Sample ID	**Peak Stress (MPa)**	**Strain at Peak Stress**	**Yield Stress (MPa)**	**Strain at Yield Stress**	**Peak Energy (J)**	**Residual Energy (J)**	**Strain Energy (J)**	**Modulus at Yield Stress (GPa)**
GW 12 - 17	695.35	0.0268	306	0.0016	60.386	28.708	31.67	183.233
GW 12 - 18	777.16	0.0173	368	0.0015	77.470	47.705	29.76	232.911
GW 12 - 19	879.42	0.0036	715	0.0009	74.620	57.074	17.54	794.444
Average	783.98	0.0159	463	0.0013	70.826	44.496	26.32	403.529

Table A.16 Dynamic properties of 12 ply transversely loaded plain weave graphite/epoxy laminates tested at 67 J using 0.5" indentor

Dynamic Properties of 12 ply transversely loaded plain weave graphite/epoxy laminates tested at 67 J using 0.5" indentor								
Sample ID	**Peak Stress (MPa)**	**Strain at Peak Stress**	**Yield Stress (MPa)**	**Strain at Yield Stress**	**Peak Energy (J)**	**Residual Energy (J)**	**Strain Energy (J)**	**Modulus at Yield Stress (GPa)**
GW 12 - 20	114.4	0.3237	12.56	0.0294	58.792	47.90	10.883	0.4272
GW 12 - 21	114.6	0.3159	14.91	0.0289	59.903	48.77	11.127	0.5159
GW 12 - 22	114.0	0.3269	14.13	0.0315	60.818	50.260	10.557	0.4485
Average	114.3	0.3221	13.866	0.0299	59.838	48.98	10.856	0.46

Table A.17 Dynamic properties of 12 ply transversely loaded plain weave graphite/epoxy laminates tested at 113 J using 0.5" indentor

Dynamic Properties of 12 ply transversely loaded plain weave graphite/epoxy laminates tested at 113 J using 0.5" indentor								
Sample ID	**Peak Stress (MPa)**	**Strain at Peak Stress**	**Yield Stress (MPa)**	**Strain at Yield Stress**	**Peak Energy (J)**	**Residual Energy (J)**	**Strain Energy (J)**	**Modulus at Yield Stress (GPa)**
GW 12 - 23	148.7	0.4077	18.84	0.0367	104.61	90.666	13.949	0.51335
GW 12 - 24	149.5	0.3698		0.03	105.51	90.606	14.910	0.66666
GW 12 - 25	150.3	0.4158	18	0.038	106.88	92.091	14.797	0.47368
Average	149.7	0.3977	18.94	0.0349	105.67	91.121	14.552	0.55123

Table A.18 Dynamic properties of 12 ply transversely loaded plain weave graphite/epoxy laminates tested at 163 J using 0.5" indentor

Dynamic Properties of 12 ply transversely loaded plain weave graphite/epoxy laminates tested at 163 J using 0.5" indentor								
Sample ID	**Peak Stress (MPa)**	**Strain at Peak Stress**	**Yield Stress (MPa)**	**Strain at Yield Stress**	**Peak Energy (J)**	**Residual Energy (J)**	**Strain Energy (J)**	**Modulus at Yield Stress (GPa)**
GW 12 - 26	173.13	0.37	33.3	0.0324	156.066	141.08	14.980	1.0277
GW 12 - 27	174.11	0.406	33.9	0.0381	160.539	145.10	15.433	0.8897
GW 12 - 28	175.29	0.387	37.68	0.0438	153.121	138.09	15.024	0.8602
Average	174.17	0.388	34.96	0.0381	156.575	141.42	15.146	0.9259

Table A.19 Dynamic properties of 16 ply transversely loaded plain weave graphite/epoxy laminates tested at 67 J

Dynamic Properties of 16 ply transversely loaded plain weave graphite/epoxy laminates tested at 67 J								
Sample ID	**Peak Stress (MPa)**	**Strain at Peak Stress**	**Yield Stress (MPa)**	**Strain at Yield Stress**	**Peak Energy (J)**	**Residual Energy (J)**	**Strain Energy (J)**	**Modulus at Yield Stress (GPa)**
GW 16 - 1	115.6	0.1578	13.74	0.0099	54.29	52.003	2.289	1.3878
GW 16 - 2	119.3	0.1467	11.38	0.0129	61.79	59.578	2.216	0.8821
GW 16 - 3	117.9	0.1705	10.4	0.01	63.01	60.100	2.919	1.04
Average	117.6	0.15833	11.84	0.01093	59.70	57.227	2.475	1.103

Table A.20 Dynamic properties of 16 ply transversely loaded plain weave graphite/epoxy laminates tested at 163 J

Dynamic Properties of 16 ply transversely loaded plain weave graphite/epoxy laminates tested at 163 J								
Sample ID	**Peak Stress (MPa)**	**Strain at Peak Stress**	**Yield Stress (MPa)**	**Strain at Yield Stress**	**Peak Energy (J)**	**Residual Energy (J)**	**Strain Energy (J)**	**Modulus at Yield Stress (GPa)**
GW 16 - 4	186.67	0.1443	20.8	0.0034	128.035	125.57	2.462	6.0115
GW 16 - 5	186.67	0.1447	24.14	0.0038	128.734	127.37	1.363	6.2864
GW 16 - 6	184.12	0.2184	18	0.01	129.398	126.9	2.461	1.2857
Average	185.82	0.1691	20.98	0.007	128.722	126.62	2.096	4.5279

Table A.21 Dynamic properties of 16 ply transversely loaded plain weave graphite/epoxy laminates tested at 263 J

Dynamic Properties of 16 ply transversely loaded plain weave graphite/epoxy laminates tested at 263 J								
Sample ID	**Peak Stress (MPa)**	**Strain at Peak Stress**	**Yield Stress (MPa)**	**Strain at Yield Stress**	**Peak Energy (J)**	**Residual Energy (J)**	**Strain Energy (J)**	**Modulus at Yield Stress (GPa)**
GW 16 - 4	224.36	0.17	28	0.0044	184.81	183.08	1.7306	6.3636
GW 16 - 5	228.09	0.20	23.94	0.0083	193.47	191.80	1.6750	2.8774
GW 16 - 6	229.86	0.180	25.71	0.006	195.69	194.27	1.4181	4.1467
Average	227.43	0.186	25.8833	0.0063	191.32	189.74	1.607	4.4626

Table A.22 Dynamic properties of 16 ply diametrically loaded plain weave graphite/epoxy laminates tested at 67 J

Dynamic Properties of 16 ply diametrically loaded plain weave graphite/epoxy laminates tested at 67 J								
Sample ID	**Peak Stress (MPa)**	**Strain at Peak Stress**	**Yield Stress (MPa)**	**Strain at Yield Stress**	**Peak Energy (J)**	**Residual Energy (J)**	**Strain Energy (J)**	**Modulus at Yield Stress (GPa)**
GW 16 - 12	924.4	0.0222	198	0.0013	36.29	29.415	6.880	144.5
GW 16 - 13	907.9	0.0229	198	0.0015	35.15	28.414	6.737	126.11
Average	916.1	0.0225	1.41	0.0014	35.72	28.914	6.808	135.32

Table A.23 Dynamic properties of 16 ply diametrically loaded plain weave graphite/epoxy laminates tested at 163 J

Dynamic Properties of 16 ply diametrically loaded plain weave graphite/epoxy laminates tested at 163 J								
Sample ID	**Peak Stress (MPa)**	**Strain at Peak Stress**	**Yield Stress (MPa)**	**Strain at Yield Stress**	**Peak Energy (J)**	**Residual Energy (J)**	**Strain Energy (J)**	**Modulus at Yield Stress (GPa)**
GW 16 - 16	874.8	0.0048	561	0.0009	103.81	46.0748	57.737	578.94
GW 16 - 24	874.8	0.0036	742	0.0013	62.718	42.3401	20.378	557.89
GW 16 - 25	874.8	0.0019	825	0.0011	81.721	41.3311	40.390	736.60
Average	874.8	0.0033	709.33	0.0011	82.750	43.2487	39.502	624.48

Table A.24 Dynamic properties of 16 ply diametrically loaded plain weave graphite/epoxy laminates tested at 263 J

Dynamic Properties of 16 ply diametrically loaded plain weave graphite/epoxy laminates tested at 263 J								
Sample ID	**Peak Stress (MPa)**	**Strain at Peak Stress**	**Yield Stress (MPa)**	**Strain at Yield Stress**	**Peak Energy (J)**	**Residual Energy (J)**	**Strain Energy (J)**	**Modulus at Yield Stress (GPa)**
GW 16 - 20	907.9	0.002	808	0.00103	110.64	70.51	40.125	784.46
GW 16 - 21	957.4	0.0055	594	0.0008	103.90	77.25	26.650	742.5
GW 16 - 23	1105.	0.0024	874	0.001	137.88	82.51	55.335	874
Average	990.4	0.0033	758.6	0.00094	117.47	76.77	40.703	800.32

BIBLIOGRAPHY

1) Daniel, Isaac M. and O. Ishai. Engineering Mechanics of Composite Materials. Oxford University Press, New York, 1994.

2) Mallick, P. K. Fiber Reinforced Composites. CRC Press, New York, Second Edition, 1993.

3) P. Morgan. Carbon Fibers and Their Composites. CRC Press, 2005.

4) Deborah D.L.Chung. Carbon Fiber Composites. Butterworth – Heinemann, 1994.

5) Woldenbert, E. and Vinson, J.R. Effects of Specimen Geometry in High Strain Rate Testing of Graphite/Epoxy Composites. Structural Dynamic and Materials Conference, pp. 927 – 934, 1997.

6) Nwosu S.N, Hosur M.V, S. Jeelani, U.K Vaidya, Ajit D. Kelkar. Survivability of Affordable Aircraft Composite Structures. Air Force Final Report, Vol. 1, April 2003.

7) H.M. Hasio, I.M. Daniel, R.D. Cordes. Strain Rate Effects on the Transverse Compressive and Shear Behavior of Unidirectional Composites. Journal of Composite Materials, Vol.33, pp. 1620 – 1642, 1999.

8) N.K.Naik, R.K.Venkateswara. High Strain Rate Behavior of Woven Fabric Composites under Compressive Loading. Materials Science and Engineering, A 474, pp. 301 – 311, 2008.

9) S.Sivashanker, S.O.Osiyemi, and Asim Bag. Compressive Failure of a Unidirectional Carbon Epoxy Composite at High Strain Rates. Metallurgical and Materials Transactions, A Vol 34A, pp. 1396 – 1400, 2001.

10) I. W. Hall, M. Guden. High Strain Rate Testing of a Unidirectionaly Reinforced Graphite/Epoxy Composite. Journal of Material Science Letters 20, 897 – 899, 2001.

11) M.Guden, U. yildirim, I.W. Hall. Effect of Strain Rate on the Compression Behavior of a Woven Glass Fiber/SC-15 Composite. Polymer Testing 23, 719 – 725, 2004.

12) S. Barre, T. Chotard, M. L. Benzeggagh. Comparative Study of Strain Rate Effects on Mechanical properties of Glass Fibre – reinforced Thermoset matrix Composites. Composites Part A 27A, 1169 – 1181, 1996.

13) N. K. Naik, P. Yernamma, N. M. Thoram, R.Gadipatri, V. R. Kavala. High Strain Rate Tensile Behavior of Woven fabric E glass/epoxy Composite, Polymer Testing 29, 14 – 22, 2010.

14) Bunsell, A.R., Bernard J. Fundamentals of Fiber Reinforced Composite Materials. Institute of Physic Publishing, London, UK, 2005.

15) M.V. Hosur, S. Jeelani, U. K. Vaidya, A. D. Kelkar. Characterization of Affordable Woven Carbon/Epoxy Composites Under Low Velocity Impact Loading. Air Force Research Labrotary, Volume 3, 2003.

16) R.H.Elleithy. The Hierarchical Structure and Flexure Behavior of Woven Carbon Fiber Epoxy Composite Polymer Composites, Vol. 21, No. 5, 2000.

17) D. Gay, S. V. Hoa, S. W. Tsai. Composite Materials – Design and Applications. CRC Press, 2002.

18) B. Song, W. Chen, T. Weerasooriya. Quasi-Static and Dynamic Compressive Behaviors of a S-2 Glass/SC15 Composite. Journal of Composite Materials, 37, 1723, 2003.

19) B. A. Gama, S. L. Lopatnikov, J. W. Gillespie Jr. Hopkinson Bar Experimental Technique: A Critical Review. Applied Mechanical Review, Vol. 57, No. 4, 2004.

20) M. M. Al – Mousawi, S. R. Reid, W. F. Deans. The Use of the Split Hopkinson Pressure Bar Techniques in High Strain Rate Materials Testing. Proc Instn Mech Engrs, Vol 211, Part C, 1996.

21) NWosu. High Strain Rate Perforation and Mixed Mode Delamination of Laminated Composites. Final Report, Dillard University, 1997.

22) C. Galiotis, D. N. Batchelder. Strain Dependences of the First and Second Order Raman Spectra of Carbon Fibers. Journal of Material Science letters 7, 545 – 547, 1988.

23) R. J. Young. Analysis of Composites Using Raman and Flourescence Microscopy – A Review. Journal of Microscopy, Vol. 185, 199 – 205, 1997.

24) N. Sato, N. Tatsuda, T. Kurauchi. Application of Laser Raman Spectroscopy to the Analysis of Stress Distribution of Fibers in Composites. Journal of Material Science Letters 11, 365 – 366, 1992.

25) Shivakumar, K. N., W. Elber. Prediction of Impact Force and Duration Due to Low – Velocity Impact on Circular Composite Laminate. Journal of Applied Mechanics, Vol. 52, 674 – 677, 1985.

26) Zukas, A. Jonas, H. W. Swift, L. B. Greszcuk. Impact Dynamics. Krieger Publishing Company, Florida, 1992.

27) Meyers, Marc Andre. Dynamic Behavior of Materials. John Wiley & Sons Inc., 1994.